AD NUMBER: AD0341046
CLASSIFICATION CHANGES
TO: Unclassified
FROM: Secret
AUTHORITY
DNA LTR 13 JAN 1983

[redacted]

AD 341046L

DEFENSE DOCUMENTATION CENTER

FOR

SCIENTIFIC AND TECHNICAL INFORMATION

CAMERON STATION, ALEXANDRIA, VIRGINIA

[redacted]

SECRET

WT-415

Copy No. 247 A

Operation

BUSTER - JANGLE

NEVADA PROVING GROUNDS
OCTOBER - NOVEMBER 1951

Project 10.10

BLAST MEASUREMENTS

LOS ALAMOS SCIENTIFIC LABORATORY
UNIVERSITY OF CALIFORNIA

SECRET
SECURITY INFORMATION

This document consists of 193 pages
No. 097 of 300 copies, Series A

BLAST MEASUREMENTS [a],
Operation Buster-Jangle

Edited by

E. J. ZADINA

and

F. B. PORZEL

Los Alamos Scientific Laboratory
Los Alamos, New Mexico

March 1952

3-4

CONTENTS

Part I — Beta-densitometer Feasibility Report

CONTENTS (Continued)

CONTENTS (Continued)

CONTENTS (Continued)

Part V — Resistor Method for Determination of Radius vs Time of a Nuclear Explosion in Soil, Operation Jangle Underground Shot

ILLUSTRATIONS

Part I — Beta-densitometer Feasibility Report

ILLUSTRATIONS (Continued)

ILLUSTRATIONS (Continued)

ILLUSTRATIONS (Continued)

ILLUSTRATIONS (Continued)

TABLES

Part I — Beta-densitometer Feasibility Report

Part III — Blast-wave-material Velocity Measurements

Part V — Resistor Method for Determination of Radius vs Time of a Nuclear Explosion in Soil, Operation Jangle Underground Shot

Part I

BETA-DENSITOMETER FEASIBILITY REPORT

by

Pedro R. FlorCruz

SECRET

ABSTRACT

The principal problem of the beta densitometer is to develop a detector-recording combination capable of discriminating between the flux from the beta source and the radiation from the nuclear bomb. Modifications to the Operation Greenhouse model of the densitometer were tested during Operation Buster. One modification was the combination of a mechanical modulator of the beta signal and a tuned amplifier designed to discriminate between the beta flux and the bomb radiation. Another modification consisted in raising the phototube (radiation detector) from below ground level into the air to test the feasibility of measurement away from ground surface. The field tests at Operation Buster showed that these modifications were extremely difficult owing to effect of a strong electromagnetic disturbance from the nuclear explosion, which is not yet well understood, on the amplifier and on the phototube and wiring used in air mounting. The recording system, mechanical parts, and a new system of source mounting and loading were all satisfactory. Electronic components of the system of a-c modulation require redesign. If the beta densitometer as an air-density-measuring instrument is desired for use in nuclear weapons tests, the main research effort must be directed to the improvement of the electronic components.

SECRET

PREFACE

The theory underlying the functioning of the beta densitometer and all developmental work up to and including the feasibility test at Operation Greenhouse is covered in detail in the two Los Alamos Scientific Laboratory reports listed in the reference section to Chap. 2, Part I.

This part of the Program 10.10 report covers the developmental work after Operation Greenhouse and the field tests during Operation Buster.

The experiment and modifications to be tested were performed under the technical direction of F. B. Porzel, who followed the subsequent development closely and whose constructive direction and assistance were invaluable.

Members of Los Alamos Blast Measurements Group, J-10, assisted in one way or another in the development and experimentation. LT John M. Smith, USN, took charge of the electronic and photographic components and assembled, tested, and fabricated some electrical units. Maj J. E. Whitener, USAF, calculated the effects of air flow around the football housing of the phototube on the air density along the beta path. CDR W. D. Baker, USN; Maj C. G. Young, USA; and R. W. Newman helped conduct small-charge tests. Maj Young also improved the characteristics of the tuned amplifier.

Credit is also due to the Equipment, Engineering, and Specifications Group, Group J-7, for their assistance in the design and fabrication of the mechanical components of the densitometer.

CHAPTER 1

INTRODUCTION

1.1 OBJECTIVE

One of the objectives of Program 10.10, Operation Buster, was to test further the feasibility of the beta densitometer as an instrument for measuring the air density in a blast wave as a function of time and, in particular, to test some modifications of the model used in Operation Greenhouse.

1.2 OPERATION GREENHOUSE MODEL OF THE BETA DENSITOMETER

The Operation Greenhouse model of the beta densitometer (Fig. 1.1) employed a d-c circuit.[1] The output of an RCA 5819 phototube which "sees" only background gamma radiation from the bomb is balanced against the output of another RCA 5819 phototube which sees both the beta flux and the background radiation. The change in the net output becomes a measure of the air density along the beta path.

At Greenhouse the phototubes, from which density vs time and gamma radiation vs time were successfully measured, were monitored separately, but the d-c system presented difficulties in balancing. No two phototubes have identical characteristics, and although this difficulty may be circumvented by altering the output impedance of one phototube, the procedure was found to be troublesome in practice. Furthermore, the balancing system required two instrument setups of exactly the same geometry. Consequently at Operation Greenhouse a compromise arrangement was made. The tubes were placed 8 in. apart. One was shielded by lucite thick enough to stop beta particles without appreciably stopping the gamma radiation. The effectiveness of this lucite shield is not clear. There is a possibility that the lucite alters the spectrum of secondary electrons from radiation in the background.

A system of chopping the beta source to provide a modulated a-c signal to be distinguished from the background d-c signal from gamma radiation showed obvious promise. This was the principal development tested at Operation Buster. Such a scheme, employing only one phototube, would not only eliminate the problem of balancing but would also result in a more compact instrument.

A density measurement away from ground surface with both the beta source and the receiver or the detector in the air was desired. From the Greenhouse results with the beta densitometer it was clear that dust loading of the shock wave could have a large effect on the density. Although measurement of dust loading effect on density is an excellent application for the beta densitometer, the measurement in free air was considered desirable, if feasible. Consequently another modification changed the beta radiation from a vertical to a horizontal path. When the path is vertical, dirt and stones sometimes accummulate on the foil covering the phototube hole and cause spurious measurements.

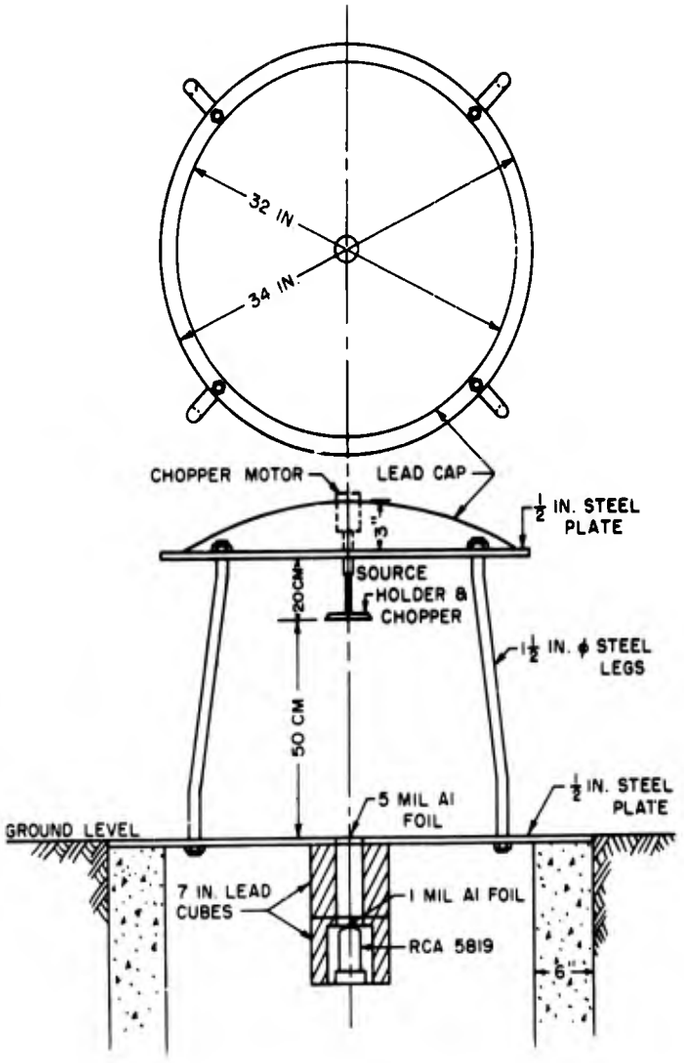

Fig. 1.1—Beta densitometer, Greenhouse model.

SECRET

1.3 THEORY OF OPERATION

The beta densitometer is an application of a behavior of beta particles, namely, that beta-particle attenuation in air is a function only of the amount of matter and therefore of the air density in their path, depending only to a slight extent on the Z number of the material.

If a detector which is sensitive only to the number of beta particles reaching it is placed in the path of the beta flux, it will be possible to obtain a measurement of the attenuation of the flux and, hence, of the change in air density between the detector and the source of beta particles. The best detector found so far (considering such factors as resolving time, sensitivity, ruggedness, size, availability, and cost) is the multiplier phototube. The phototube is sensitive to all radiation so that a means of separating the effect of the beta flux from that of the background radiation produced by the bomb is necessary.

The scheme selected at Operation Buster to accomplish the separation of the beta signal from background signal is the modulation of the beta signal and subsequent amplification of the modulated signal with a tuned amplifier. The amplitude of the modulated signal becomes a measure of the beta signal and of the components of the background radiation with frequencies within the plateau of the amplifier frequency response. The background radiation, which is assumed to be principally gamma rays, is expected to decay exponentially and should be negligible compared to the amplified beta signal. The amplitude of the beta signal, corrected for the statistical variation of the beta signal and for the air-flow effects around the densitometer, should therefore be a measure of the air density in the beta path. This method of separating beta signal from background was investigated prior to Operation Greenhouse but was not used there because the necessary mechanical components for modulating the beta signal were not developed in time for the test.[1]

REFERENCE

1. F. B. Porzel and Group J-7, Measurement of Air Density in a Shock Wave, Preoperation Report for Operation Greenhouse, Los Alamos Scientific Laboratory Report LAB-J-2160, January 1951 (not available).

CHAPTER 2

INSTRUMENTATION

2.1 MECHANICAL COMPONENTS AND BETA SOURCES

Figure 2.1 shows the schematic arrangement of the principal components of the beta densitometer used at Operation Buster.

The mechanical components consist of the source holder and chopper and a $\frac{1}{20}$-hp synchronous-capacitor motor, which is housed in a rectangular steel box (see Fig. 2.2). The chopper (Fig. 2.3) is a $\frac{3}{16}$-in. steel disk with six trapezoidal slots, mounted on a three-bearing steel shaft and coupled to the motor by means of a step-up pulley. By means of the pulley the motor, running at 3600 rpm, drives the chopper at 4000 rpm.

The choice and method of canning of the beta source have been described in previous reports.[1,2] A Sr^{90} beta source, as it comes already canned from Oak Ridge, Tenn., has the appearance of an aluminum disk $1\frac{1}{16}$ in. in diameter and $\frac{3}{32}$ in. thick. To protect the beta source from mechanical deterioration, each pellet was placed in a watertight brass case. The case has a replaceable window of 0.0015-in.-thick aluminum foil (see Fig. 2.4). Five 1-curie Sr^{90} beta sources were placed in brass cases. A sixth source, which arrived from Oak Ridge with defective foil and had to be recanned, did not fit the brass case and was not used.

The brass cases for the sources not only protected the sources from mechanical wear and weather but also facilitated their handling, especially in loading and unloading the source holder. The encased sources are kept in a rectangular steel cartridge. One end of the cartridge is open and has a lip which aligns the slot of the source holder with the top slot of the chopper (see Fig. 2.5). Then, a milled ring at the rear end of the chopper shaft is turned clockwise, causing the source holder to turn also. As a recess in the source holder becomes aligned under the cartridge, a source case drops into place. A lucite window near the open end of the loading cartridge indicates when all the sources have been loaded. The cartridge is then pulled out of the chopper slot, and the slot door is closed.

To unload the sources the bottom slot of the chopper is opened, and the lip of the cartridge is inserted into the slot. The chopper is again turned clockwise. As each source passes over the open end of the cartridge, it drops out of its recess and into the cartridge.

2.2 ELECTRONIC AND PHOTOGRAPHIC COMPONENTS

The recording apparatus consists of the following electronic and photographic components:

1. RCA 1P21 multiplier phototube in a lead "football" shield and a battery box (power source for phototube)
2. Tuned amplifier
3. Du Mont 304H oscilloscope
4. Fairchild 35-mm oscillorecord camera

The RCA 1P21 multiplier phototube which was used as a detector had an over-all length of $3\frac{11}{16}$ in. and a diameter of $1\frac{5}{16}$ in. The small size is an advantage in that a correspondingly

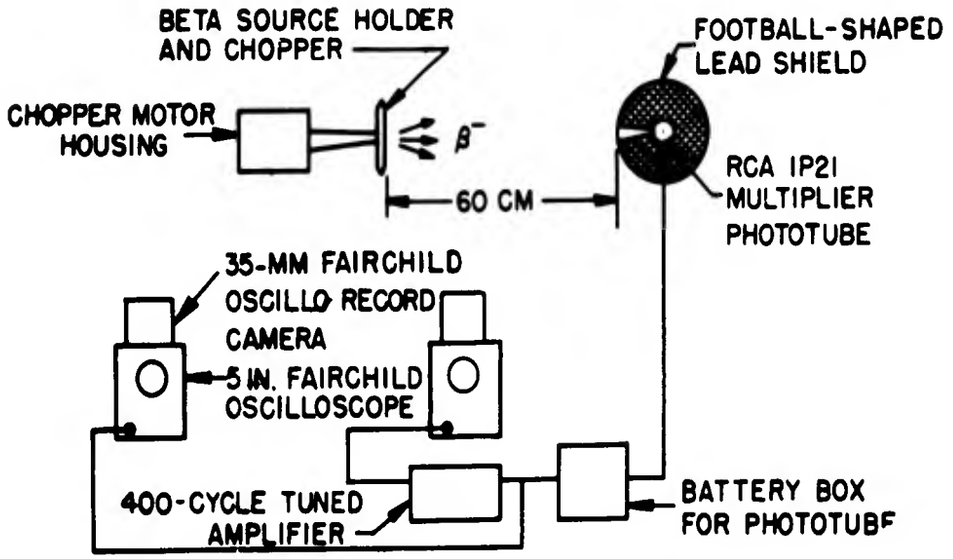

Fig. 2.1—Schematic arrangement of the beta densitometer, Operation Buster model. The multiplier phototube and the chopper were 5 ft above ground surface. The tuned amplifier, oscilloscope, and camera were in an underground shelter.

SECRET

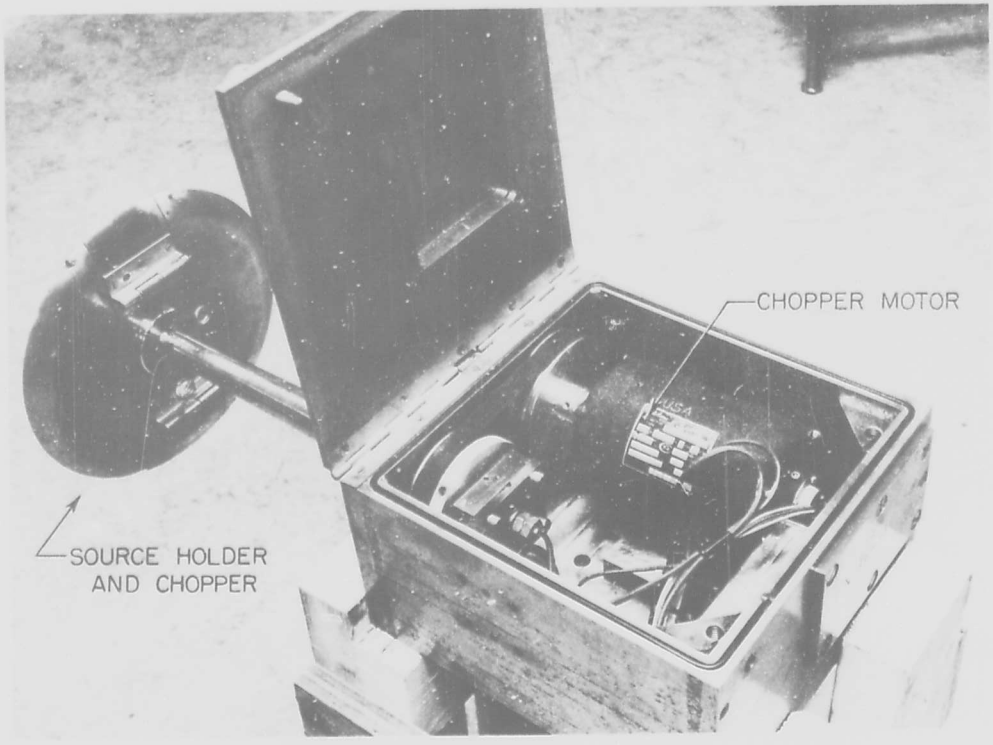

Fig. 2.2—Mechanical components of the beta densitometer.

Fig. 2.3—Source holder and chopper.

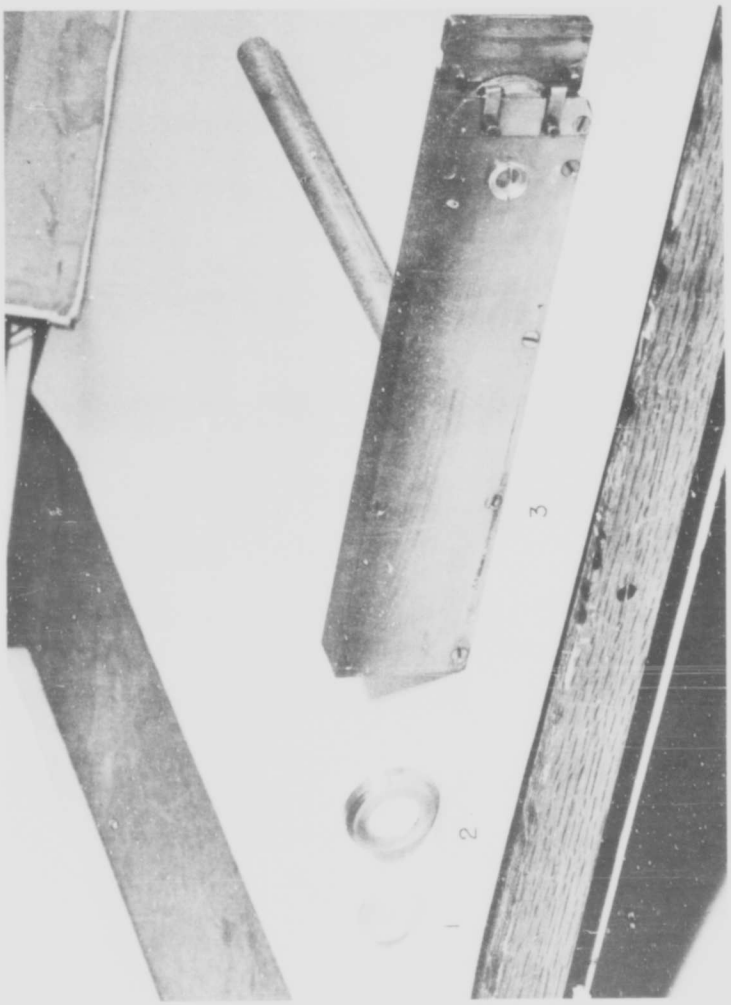

Fig. 2.4—Beta source for the densitometer. (1) Aluminum source carrier. (2) Brass source case with aluminum foil window. (3) Loading cartridge.

SECRET

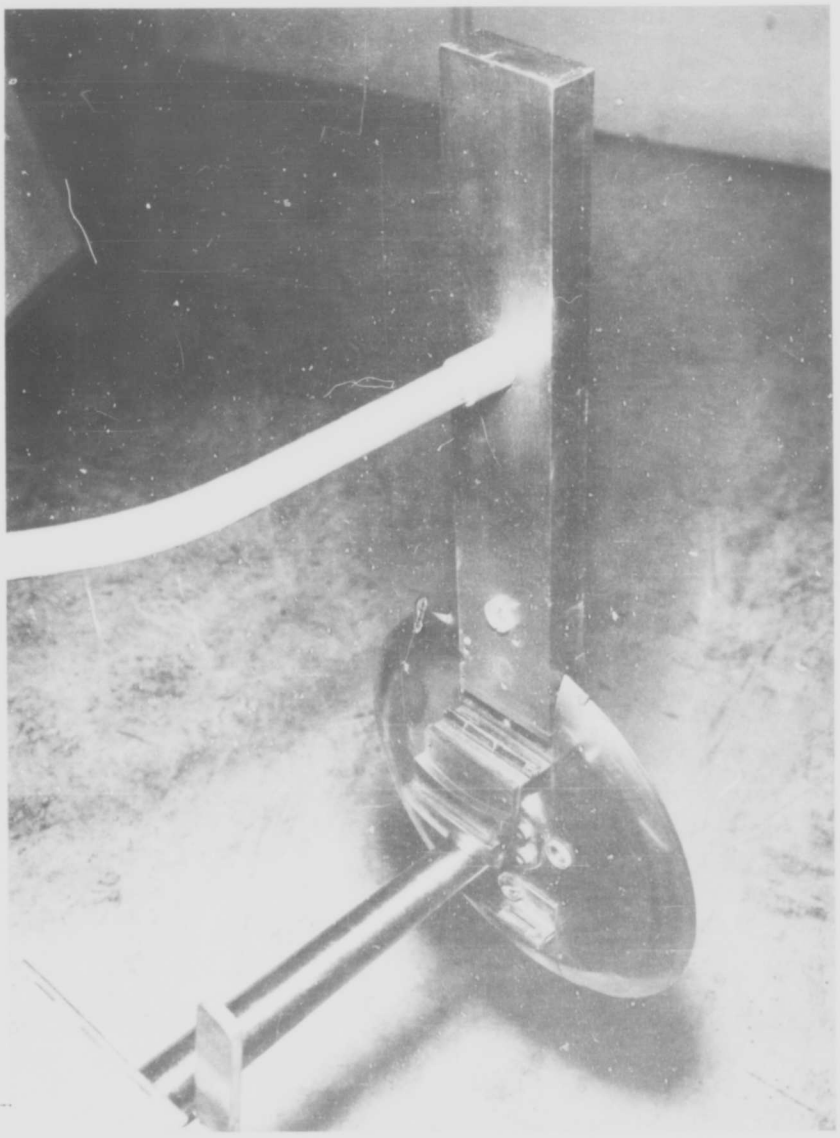

Fig. 2.5 — Method of loading beta sources.

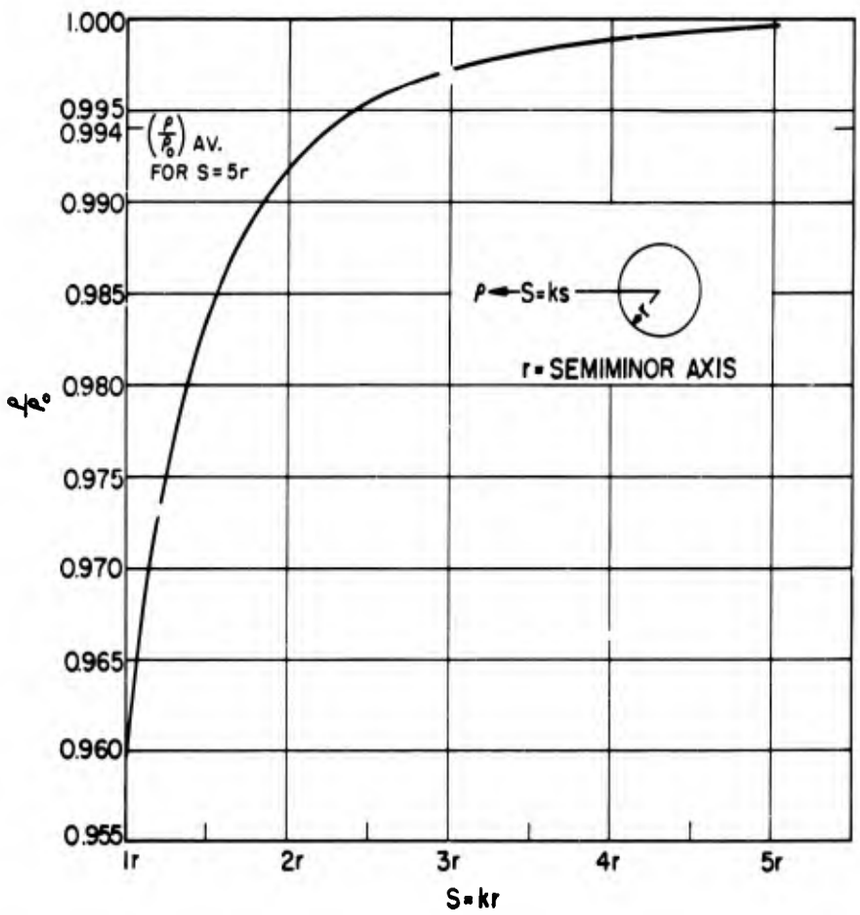

Fig. 2.6—Effect of the lead shield on air density.

SECRET

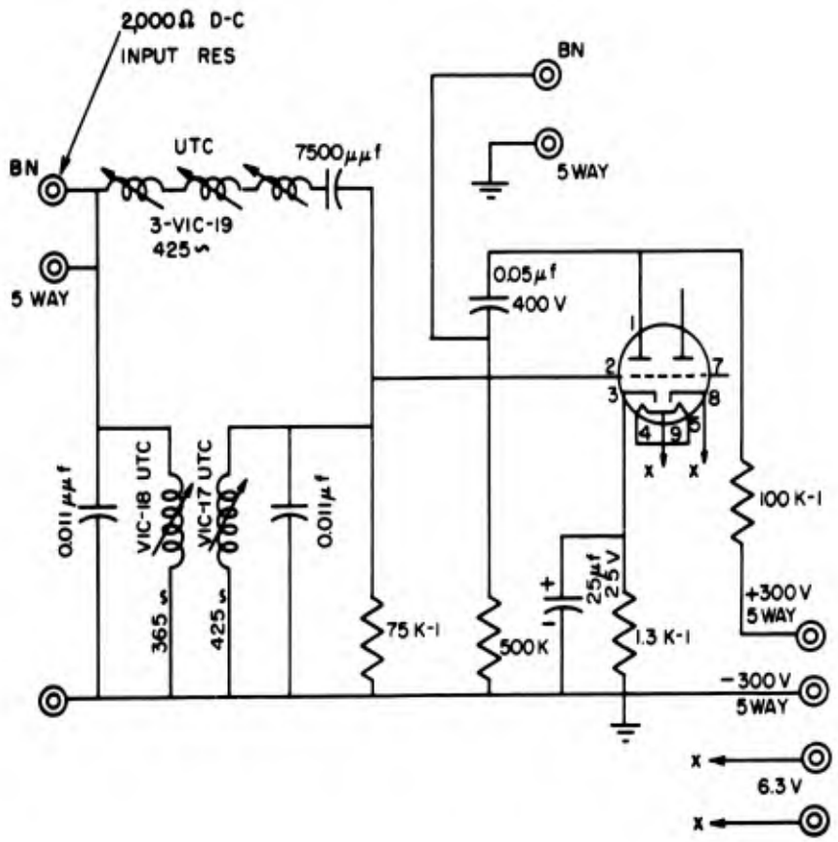

Fig. 2.7—Wiring diagram of the 400-cps tuned amplifier.

SECRET

small lead shield is required. To minimize air-flow effects, all parts exposed to the shock wave must be made as small as possible. The tube is mounted in a Mu metal can, which provides magnetic shielding and facilitates making the tube lighttight.

The football shape of the lead shield (Fig. 4.2) was chosen to minimize effects of air flow on air density. Figure 2.6 shows the variation of ρ/ρ_0 vs S, where S is the distance from the center of an ellipsoid of revolution with major axis equal to 1.66 times the minor axis, ρ_0 is the air density if the shield were absent, and ρ is the air density at a distance S from the center of the ellipsoid. For S = 5r the integrated average is $\rho/\rho_0 = 0.994$. Except for pointed ends, the lead shield has the shape of an ellipsoid of revolution whose major axis is 1.66 times the minor axis. The semiminor axis is 10 cm, and therefore for a beta-source-football distance of 50 cm the presence of the lead football shield introduces a negative error in ρ/ρ_0 of less than 0.6 per cent, when $u/c = \frac{1}{3}$ (u refers to material velocity and c to sound velocity behind the shock). This is the value of u/c in the region of 10 psi overpressure. As the path lengths increase the error decreases.

The wiring diagram of the 400-cps tuned amplifier is shown in Fig. 2.7.

Calibration of the beta densitometer is discussed in Ref. 2. Briefly, final calibration should be done in an air-pressure tank with a diameter of approximately 40 in. The minimum diameter of the calibration tank is determined by the amount of beta scattering from the tank walls. Some beta particles which would otherwise miss the phototube could be deflected by the tank walls to the phototube. Experiments were conducted prior to Operation Greenhouse to determine the radiation pattern from a beta source, which in turn determines the size of the calibration tank.

REFERENCES

1. F. B. Porzel and J. E. Whitener, Feasibility Report on Measurement of Density, Temperature, and Material Velocity in an Air Shock Produced by a Nuclear Explosion, Los Alamos Scientific Laboratory Report LAB-J-719, Nov. 25, 1949 (not available).
2. F. B. Porzel and Group J-7, Measurement of Air Density in a Shock Wave, Preoperation Report for Operation Greenhouse, Los Alamos Scientific Laboratory Report LAB-J-2160, January 1951 (not available).

CHAPTER 3

LABORATORY TESTS

Tests were made on beta-densitometer components in the laboratory prior to the field tests at the Nevada Proving Grounds to determine, as far as practicable, their characteristics and whether they would function as desired.

3.1 PHOTOTUBE TESTS

Tests were made on 931A and 1P21 phototubes to determine their sensitivity to shock and radiation and to determine their fatigue characteristics.

Each tube was placed in a Mu metal can, and the window was covered with 1-mil aluminum foil. Then each tube was exposed to a 0.1-curie Sr^{90} beta source at a distance of 7.0 cm. Exposure time varied from 1 to 12 hr, depending on how quickly the tube fatigued to a constant output. Fatigue ' ts were repeated on selected tubes to determine whether their characteristics vary after repeated exposures. Tube output was measured with a d-c microammeter.

These tests showed that (1) tubes vary considerably in sensitivity and fatigue characteristics, (2) the 1P21, on the average, is two to three times more sensitive than the 931A and has flatter fatigue characteristics, and (3) it was indicated that the 1P21 was superior to the 931A in stability against shock.

The fatigue characteristics of three 1P21 phototubes are shown in Fig. 3.1.

3.2 PHOTOTUBE LEAD-SHIELD ASSEMBLY

The effectiveness of the lead football for shielding the tube against gamma radiation was measured by exposing the tube, housed inside the football, to an 11-curie Co^{60} gamma source at a distance of 1 meter. The experimental arrangement is shown in Fig. 3.2. By means of interchangeable inserts, provision was made to change the size and shape of the collimating hole. Phototube output was measured with a d-c microammeter for several values of angle of incidence θ from 0 to 90°. This procedure was followed with each of three collimating holes: a rectangular slit, $\frac{3}{8}$ by $1\frac{1}{8}$ in.; a circular cylinder, $1\frac{1}{8}$ in. in diameter; and a rectangular frustum or tapered slit, $\frac{1}{2}$ by $1\frac{1}{8}$ in. at the phototube end and 1 by $\frac{1}{8}$ in. at the mouth of the hole. The theory underlying this procedure is explained in Ref. 1. To compare the sensitivity of the phototube to gamma radiation with its sensitivity to beta radiation, a 0.1-curie Sr^{90} source was placed 50 cm from the mouth of the hole at an angle of incidence of 90°.

Assuming that both gamma and beta fluxes were symmetrical about an axis from the source to the mouth of the hole, the test showed that the rectangular frustum was the best collimating hole from the standpoint of both maximum beta signal and minimum ratio of gamma-to-beta sensitivity. The results are tabulated in Table 3.1.

Phototube response to gamma radiation as a function of angle of incidence is shown in Fig. 3.3.

Table 3.1—TEST OF PHOTOTUBE SHIELD, RCA PHOTOTUBE 1P21

Type of collimating hole	Comparative phototube sensitivity to beta radiation	Comparative ratio of gamma-to-beta sensitivity
Rectangular slit	1.00	1.23
Circular cylinder	1.13	1.34
Rectangular frustum	1.32	1.00

3.3 THE 400-cps TUNED AMPLIFIER

The frequency response of the 400-cps tuned amplifier is shown in Fig. 3.4.

3.4 SMALL-CHARGE TESTS (Oct. 4 to 10, 1951)

Owing to difficulties hindering the fabrication of the components, especially of the source holder and the chopper, small-charge tests on the complete assembly could not be made until Oct. 4, 1951. The purpose of the small-charge tests was to determine whether the densitometer would function under conditions which were as similar as possible to the conditions following a bomb explosion. In particular, small-charge tests were necessary to determine

1. Ability of above-ground parts to withstand blast
2. Effect of shock on electronic and photographic equipment
3. Functional reliability of the complete assembly and whether the densitometer could indeed record air-density changes

The experimental arrangement is shown in Fig. 3.5. The chopper and football were set up on pipe mounts similar but inferior to those that were to be used at the Nevada Proving Grounds. Phototube and chopper motor cables were run inside the pipes and then underground to power terminals. Recording instruments were placed inside an underground shelter where firing was controlled.

The test procedure and results are outlined in Table 3.2. After procedure 6 in Table 3.2, more attempts were made to determine and eliminate the cause of the hash in film records. Tube and chopper mounts were steadied with braces and guy wires. Nonshielded cables were replaced with shielded ones. Shock mounting of recording instruments was improved. The amplifier was placed inside a steel chassis. Seven additional charges were fired. The hash in the film record was reduced but not sufficiently to make identification and measurement of density change easy and accurate.

Considering the steps that had been taken to eliminate erratic deflection of the oscilloscope beam, it appeared that the greatest remaining difficulty was in the amplifier. The shock mounting and electromagnetic shielding of the amplifier were improved. One of the tubes was replaced. The changes made the amplifier less sensitive to shock and stray electromagnetic fields. Unfortunately, time was not available for additional proof firing before the densitometer had to be shipped to the Nevada Proving Grounds.

REFERENCE

1. F. B. Porzel and Group J-7, Measurement of Air Density in a Shock Wave, Preoperation Report for Operation Greenhouse, Los Alamos Scientific Laboratory Report LAB-J-2160, January 1951 (not available).

Table 3.2—SMALL-CHARGE TESTS

Procedure No.	Description	Results	Conclusions
1	Close beta source; hit chopper, football, and battery box each in turn with a sledge-hammer; observe position of oscilloscope beam	Position of electron beam unchanged	Blast hitting chopper, football, and battery box has no effect on the position of the electron beam
2	Open beta source; hit chopper, football, and battery box each in turn with a sledge-hammer; observe position of oscilloscope beam	Position of electron beam unchanged	Blast hitting chopper, football, and battery box has no effect on the position of the electron beam
3	Close beta sources in holder; tape 0.1-curie Sr^{90} source to mouth of collimating hole; hit football and battery box each in turn with a sledge-hammer; observe position of electron beam	Position of electron beam unchanged	Blast hitting chopper, football, and battery box has no effect on the position of the electron beam
4	Open beta sources; tap oscilloscope and amplifier	Beam moved slightly when oscilloscope was tapped; considerably when amplifier was tapped	Oscilloscope and amplifier sensitive to shock
5	Shock-mount oscilloscope and amplifier with rubberized hair and foam rubber; set off 35 lb of composition B, 44 ft from densitometer; take film record of density change	Film trace showed too much "hash" that could not be reasonably attributed to density change	Some components of densitometer are sensitive to shock and/or electromagnetic disturbance produced by explosion
6	Cable from phototube to battery box wrapped in steel foil; set off charge and obtain film record	Hash slightly reduced, but much still appears in film record	Some components of densitometer are sensitive to shock and/or electromagnetic disturbance produced by explosion

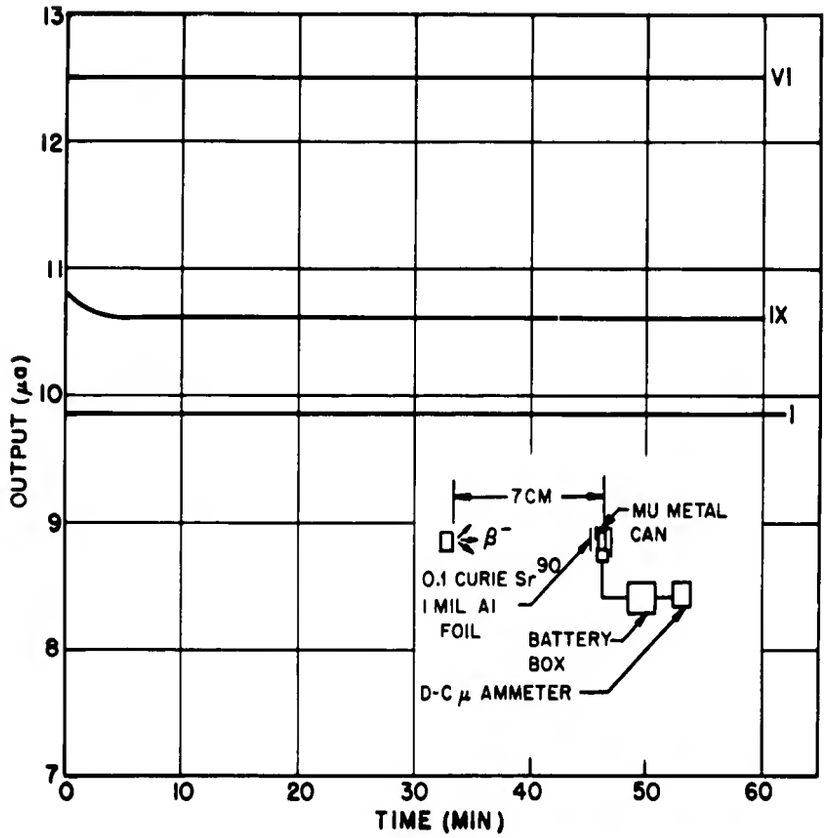

Fig. 3.1—Fatigue characteristics of 1P21 phototubes.

SECRET

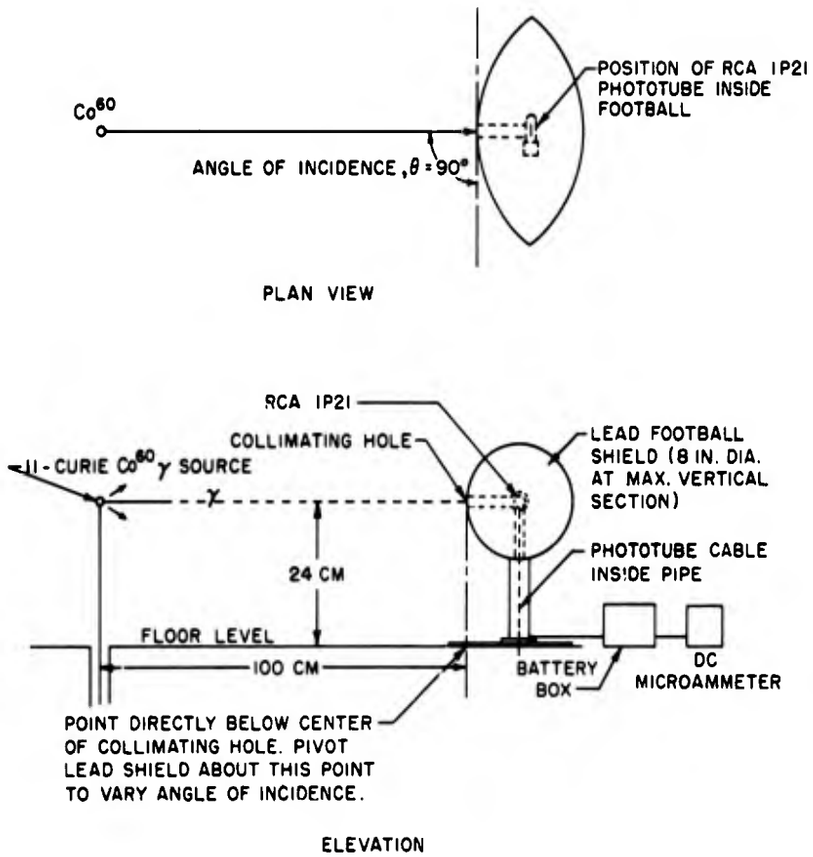

Fig. 3.2—Experimental arrangement for testing effectiveness of the lead-shield assembly.

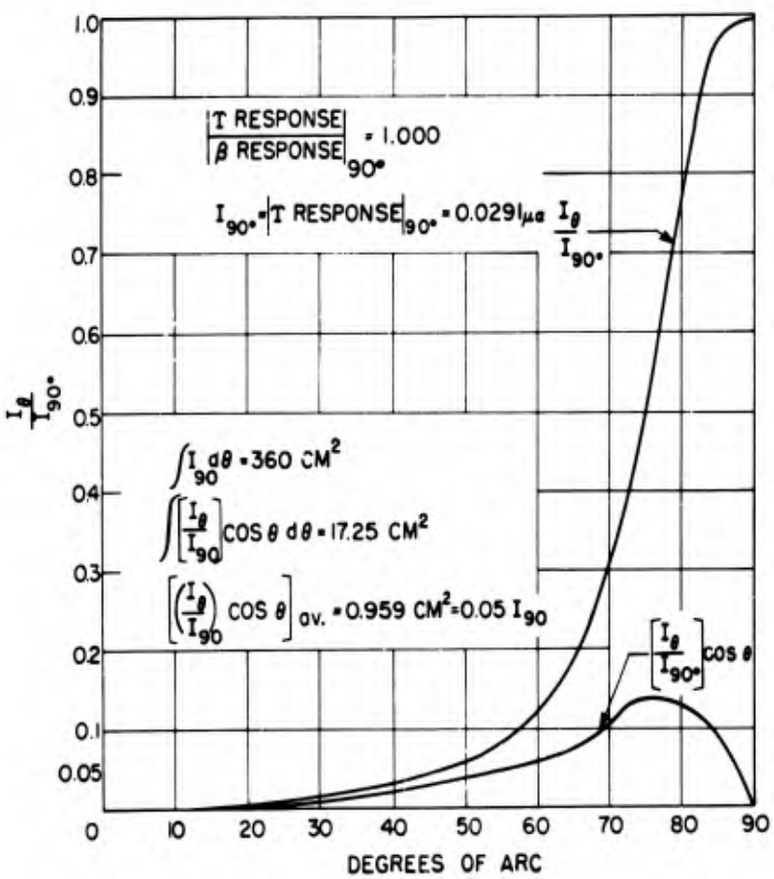

Fig. 3.3—Phototube-assembly response as a function of angle of incidence.

SECRET

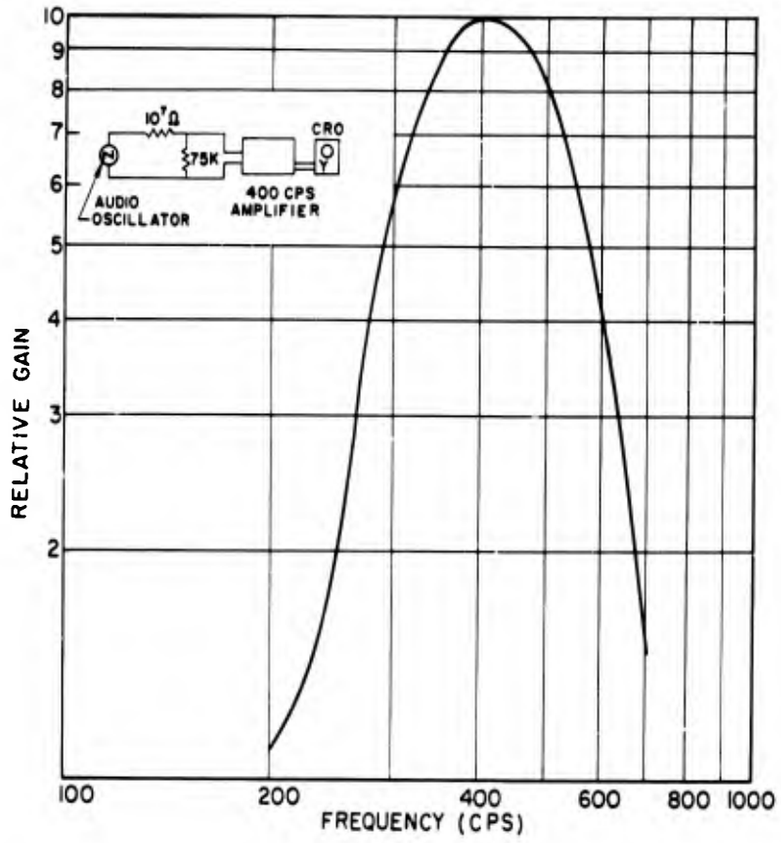

Fig. 3.4—Frequency response of the 400-cps tuned amplifier.

SECRET

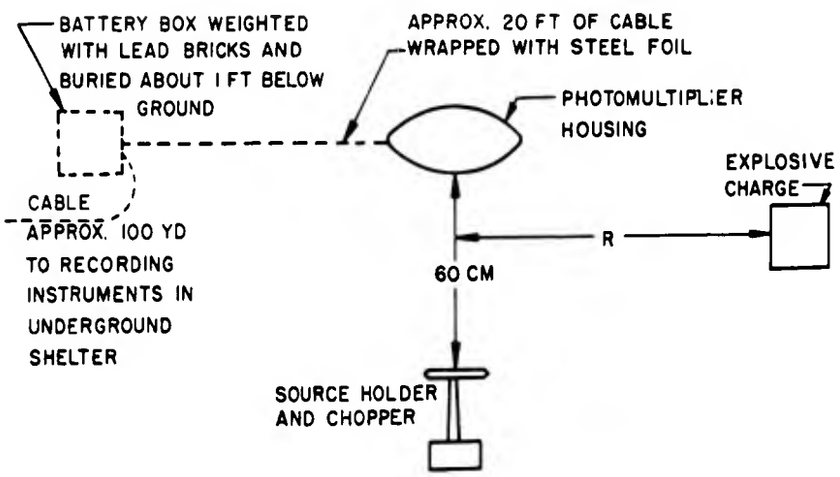

Fig. 3.5—Experimental arrangement for testing with small charges.

SECRET

CHAPTER 4

OPERATION BUSTER TEST

4.1 PURPOSE

The beta densitometer was set up for Operation Buster, Shots Baker, Charlie, and Dog, to test the feasibility of the densitometer for measuring the air density behind a blast wave produced by a nuclear explosion.

4.2 INSTRUMENTATION

The beta densitometer was set up at Station 620, 4000 ft north of ground zero and inside an asphalt-pav. l area. The location in a paved area was chosen in an attempt to eliminate the complicating effect that dust and flying rocks have on air density near the ground surface.

The instrument arrangement for Operation Buster shots was similar to the arrangement during the proof firing, but it was considerably improved with regard to shock mounting and shielding against background radiation. Significant improvements were

1. The mounts for the components exposed to blast (chopper and football) were much more rugged and steady (see Figs. 4.1 and 4.2).

2. Cables from the chopper motor to the power outlet and from the phototube to the battery box in the underground instrument shelter were run through separate steel pipes which provided shielding against thermal and electromagnetic radiation.

3. All recordi g instruments were housed inside a concrete shelter 12 ft below ground surface (see Fig. 4.3).

The instrument shelter and general instrument layout are sketched in Fig. 4.4; the wiring diagram is shown in Fig. 4.5.

To measure gamma radiation as a function of time, an oscilloscope was connected in parallel to the densitometer oscilloscope between the battery box and the tuned amplifier (Figs. 4.6 and 4.7). Thus the gamma-recording oscilloscope saw a small alternating beta signal riding on a unidirectional gamma signal.

The timing sequence in the operation of the densitometer was as follows:

The phototube was turned on the evening prior to shot day.

H−5 min: Oscilloscopes, amplifier filament, and camera electronic control were turned on.

H−5 sec: Camera motors and chopper motor were turned on.

H+1 min: All units except the phototube were turned off.

4.3 RESULTS

4.3.1 Buster-Able (Oct. 21, 1951)

It was not originally planned to test the densitometer on Buster-Able. However, as all

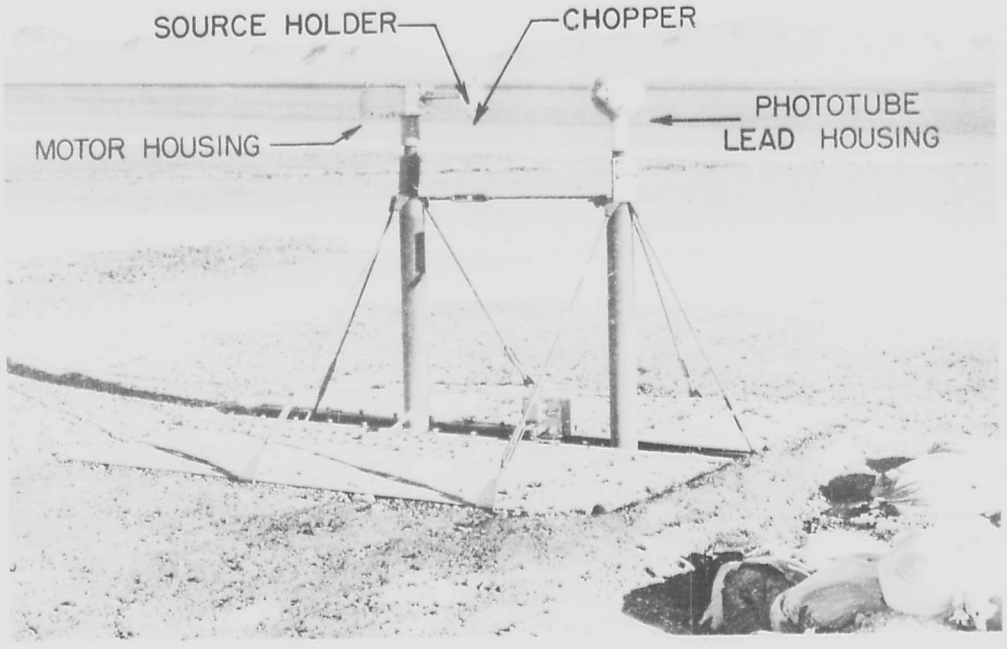

Fig. 4.1—Source holder and phototube housing. This picture was taken after Buster-Dog.

Fig. 4.2—Phototube lead housing. The collimating hole is covered with 2-mil aluminum foil.

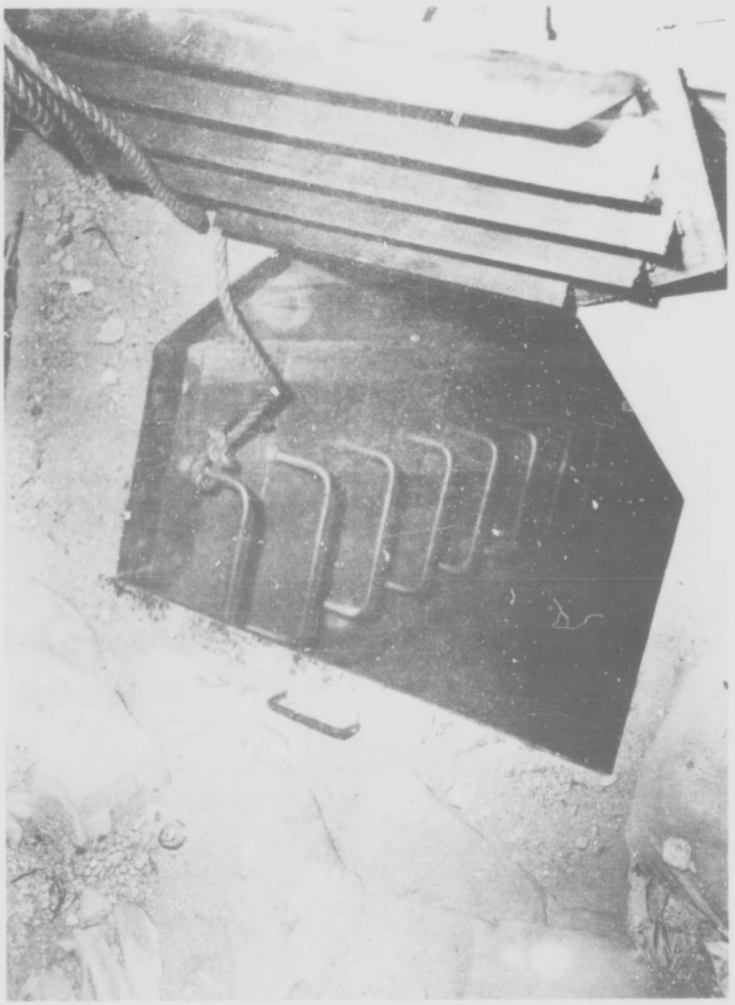

Fig. 4.3 — Entrance to underground instrument shelter, Station 620.

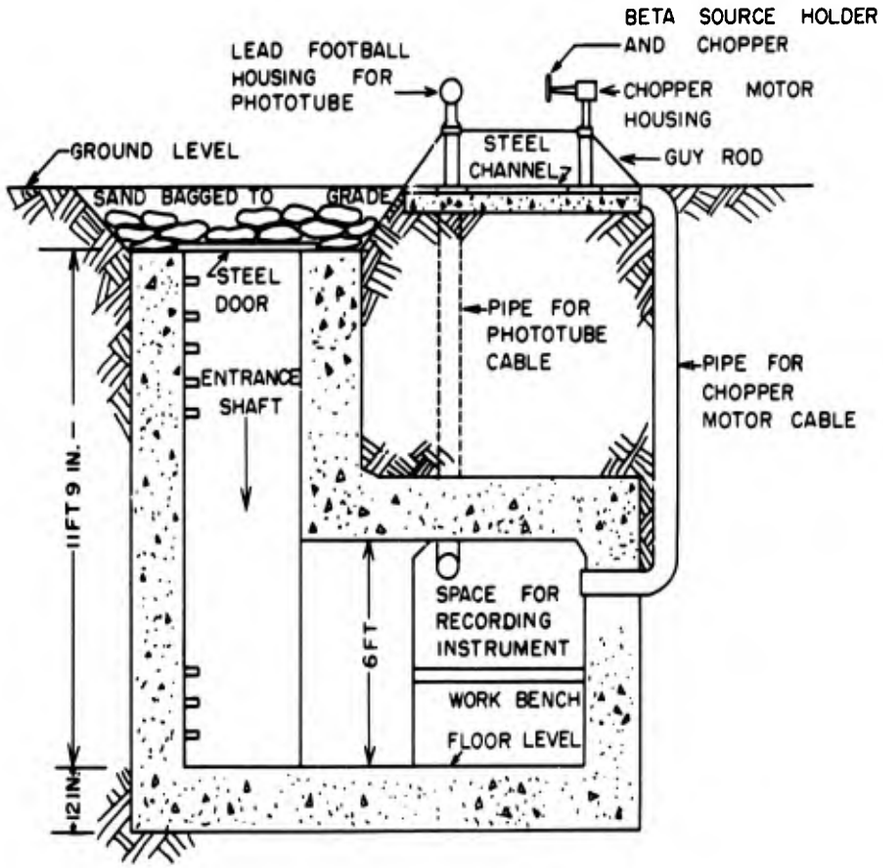

Fig. 4.4—Instrument shelter and general instrumentation layout of Station 620.

SECRET

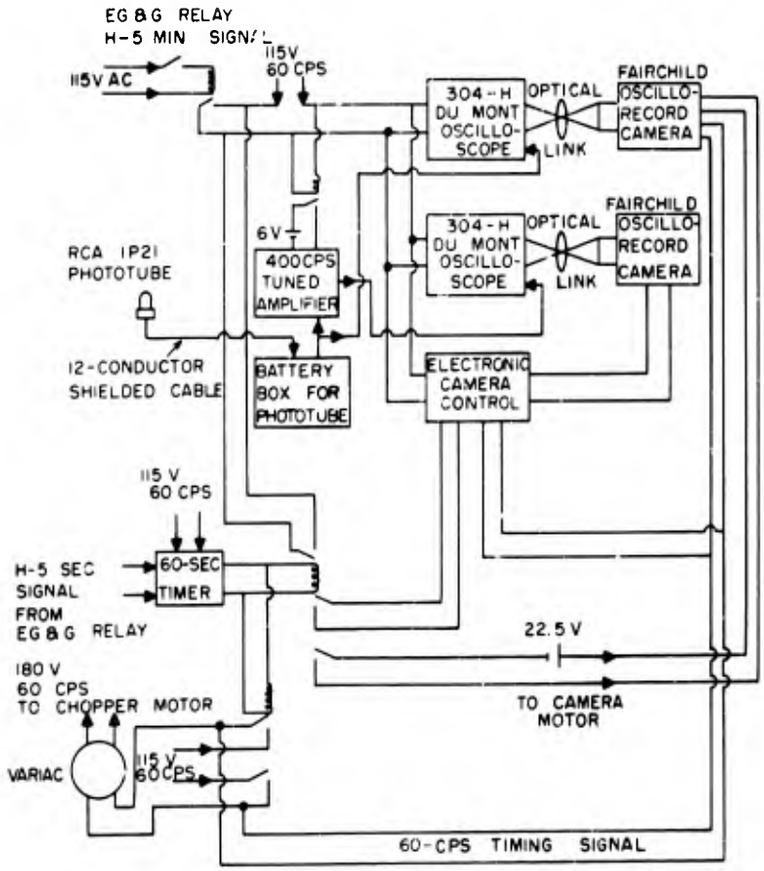

Fig. 4.5—Wiring diagram of the beta densitometer at Station 620.

SECRET

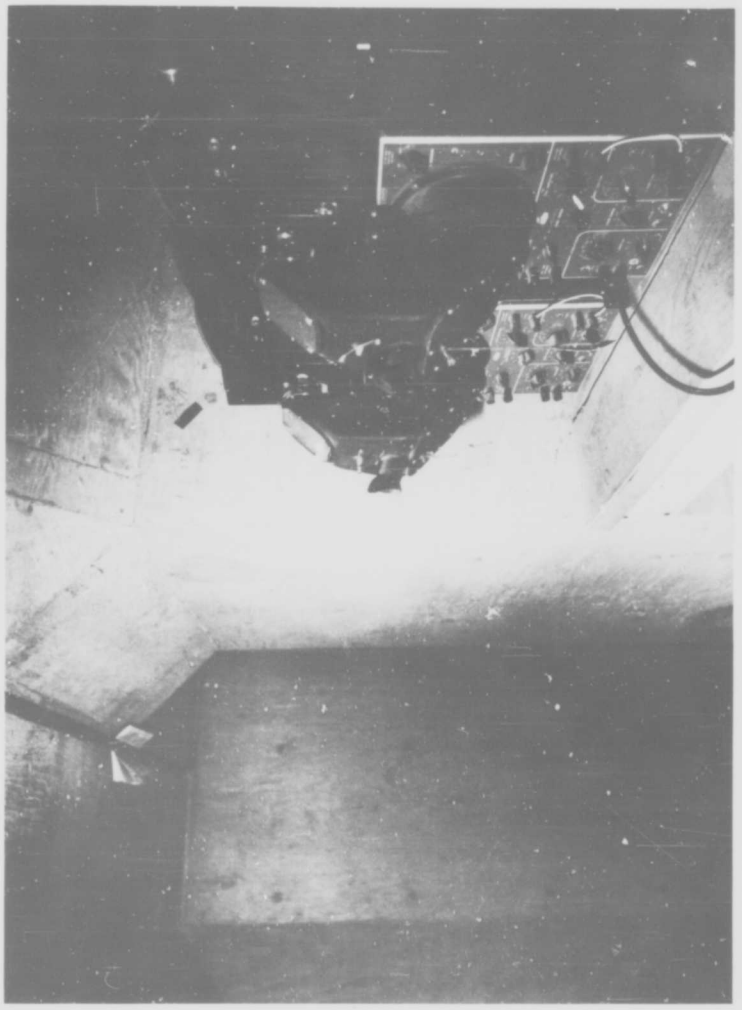

Fig. 4.6 — Underground instrument shelter at Station 620. The Du Mont 304H oscilloscopes and the 35-mm Fairchild cameras are shown.

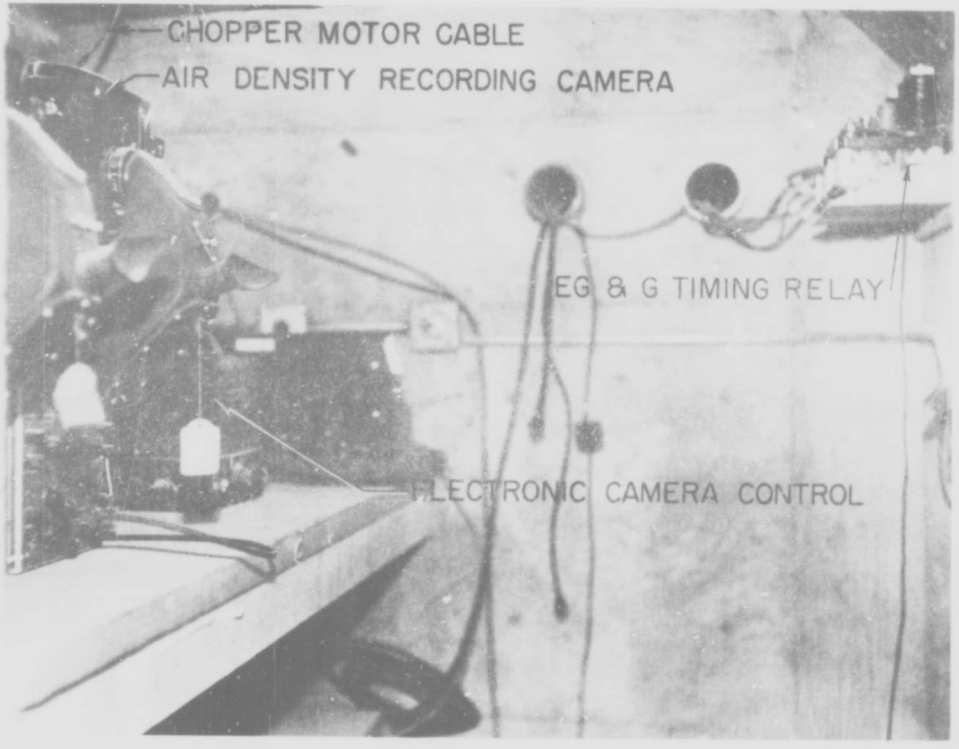

Fig. 4.7—Underground instrument shelter for the beta densitometer, Station 620.

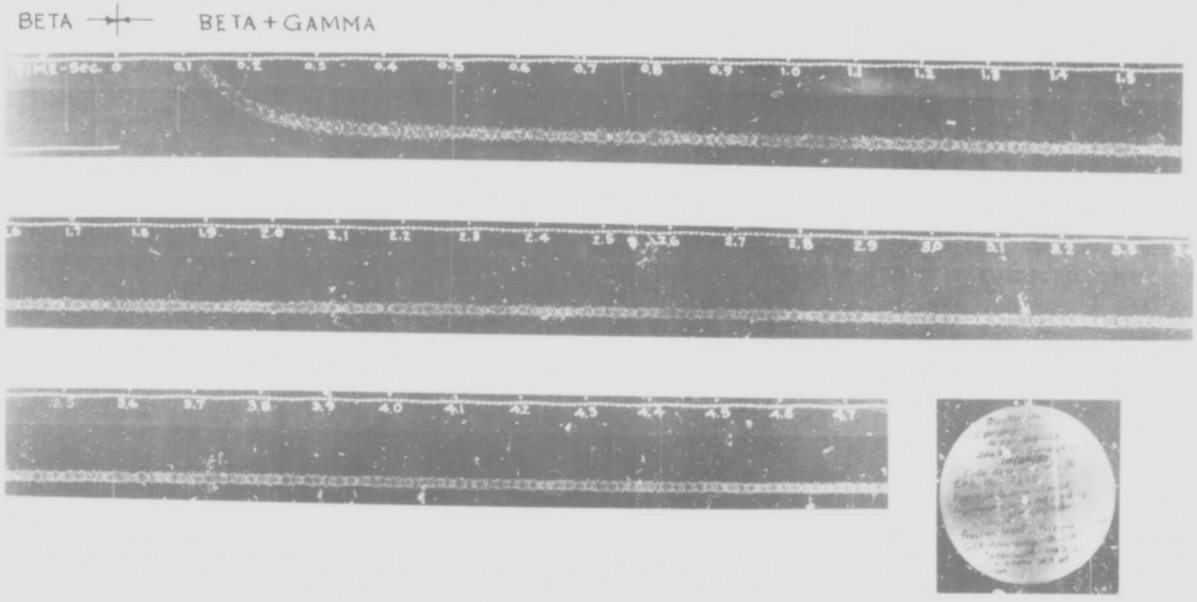

Fig. 4.8—Beta and gamma record, Buster-Charlie.

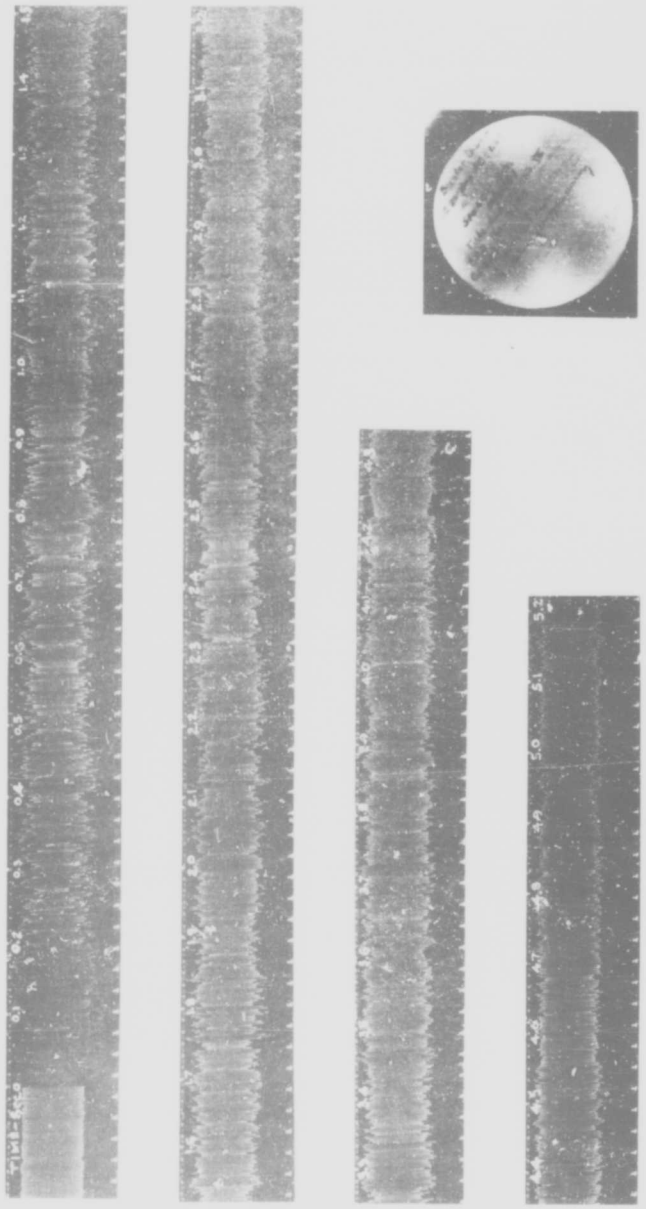

Fig. 4.9—Beta record, Buster-Charlie.

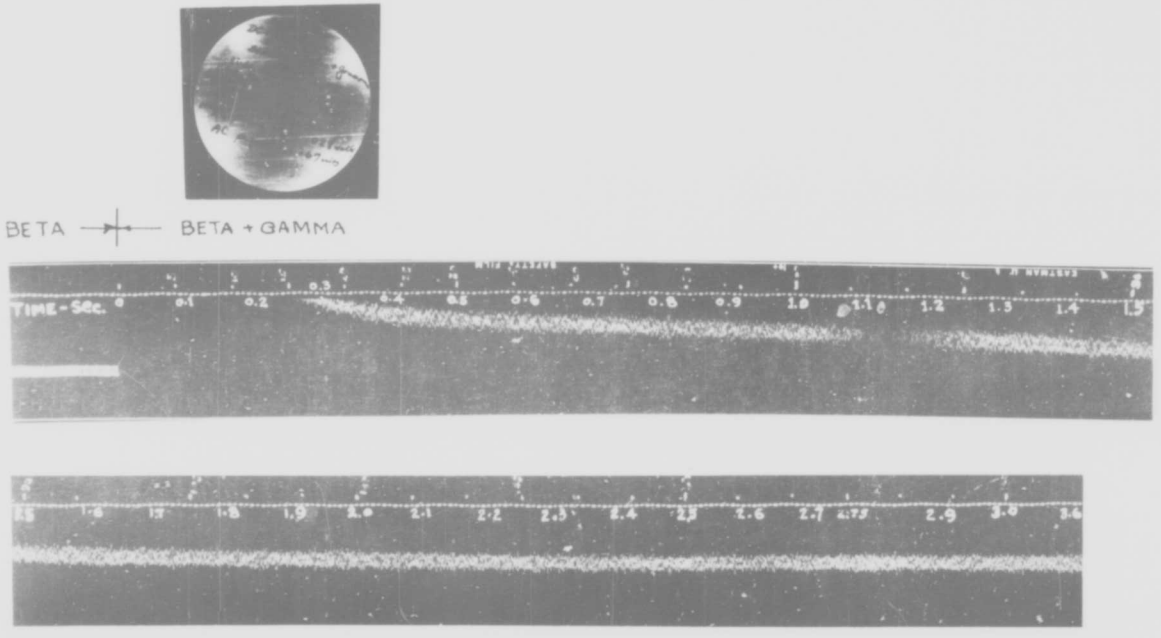

Fig. 4.10—Beta and gamma record, Buster-Dog.

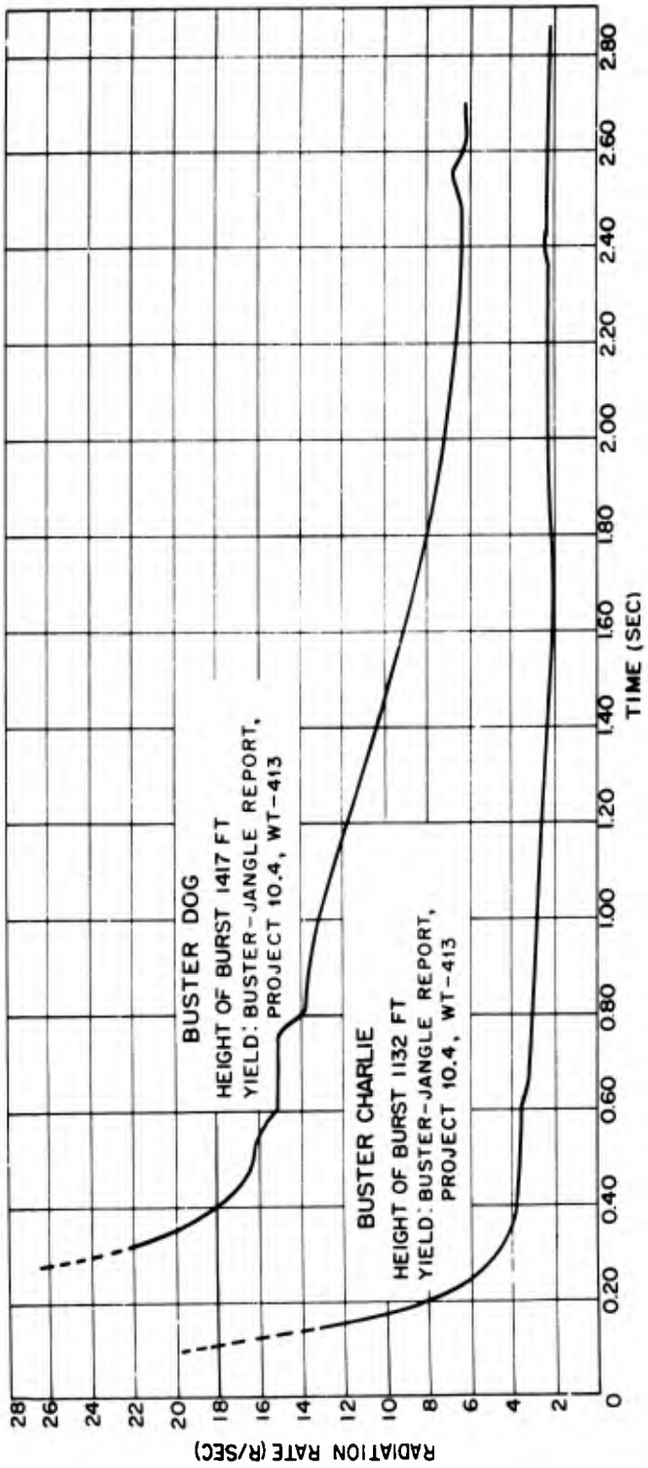

Fig. 4.11—Gamma-radiation rate as a function of time, Buster-Dog and Buster-Charlie.

SECRET

components were installed before shot day, it was decided to use Buster-Able for whatever information it might yield. Neither air shock nor bomb radiation was measurable with the beta densitometer at Station 620.

4.3.2 Buster-Baker (Oct. 28, 1951)

The H−5 min timing signal failed. Consequently the oscilloscope, amplifier, and electronic camera control did not have time to warm up. The chopper motor, which was wired to interact with the H−5 min signal, was not turned on. No film record was obtained.

4.3.3 Buster-Charlie (Oct. 30, 1951)

The camera record of gamma-radiation rate as a function of time is shown in Fig. 4.8. The camera record of air density as a function of time, Fig. 4.9, had too much erratic variation of amplitude to be intelligible.

4.3.4 Buster-Dog (Nov. 1, 1951)

The camera record of gamma-radiation rate as a function of time is shown in Fig. 4.10. The camera-to-photograph density trace was turned on at H−5 min instead of H−5 sec. As a result, the film had all been used up by the time the shock arrived, and no density record was obtained.

The gamma records converted to approximate roentgens per second as a function of time are shown in Fig. 4.11. The approximation rests on uncertainties from the following:

1 The assumption that the gamma rays in a nuclear explosion are isotropic at the receiver.

2. The comparison of the Co^{60} source, with which the device was calibrated, to the spectrum vs time of a nuclear explosion.

It is believed that the relative radiation rate in Fig. 4.11 is valid. If the results are to be interpreted further, it is suggested that Fig. 4.11 be normalized to the total radiation rate at this distance as measured from other experiments, such as those using film badges.

CHAPTER 5

DISCUSSION

5.1 MECHANICAL COMPONENTS

The mechanical components of the beta densitometer were very satisfactory. The system of loading and unloading the beta sources, which could be done quickly and safely with the use of the loading cartridge, was particularly satisfactory. The use of a brass case for each beta source also proved valuable in protecting the source against weather and against mechanical breakage due to repeated blasts.

The ground mount for the football shield and the chopper appeared satisfactory. It was rigid and stable, easy to assemble, and physically small yet sufficiently strong to withstand the blast encountered, and it permitted variation in beta-path length.

Some relatively minor refinements could be made to improve the mechanical components. First, a more powerful motor should be used to run the chopper. The $\frac{1}{20}$-hp motor which was used overheated because it was too small. It was used because it was the only motor with the desired speed characteristics that was available at the time of the test. Another possible improvement would be the use of interrupted threads in the couplings between the chopper and the football and their respective pipe mounts. The use of interrupted threads would make installation much easier.

5.2 PHOTOGRAPHIC COMPONENTS

For the purpose of discussion the 5-in. 304H Du Mont oscilloscopes, the 35-mm Fairchild oscillorecord cameras, and the camera electronic controls are considered together since they were closely linked functionally. They were all satisfactory, or at least nothing was observed to indicate that they were not adequate. Exception might be made of the electronic camera control. One had to be discarded owing to malfunctioning. However, these camera controls were a hand-down from Operation Greenhouse and may have had unduly rough handling.

5.3 ELECTRONIC COMPONENTS

The phototube, phototube (battery) power supply, amplifier, and connecting cables are grouped together for the purpose of discussion since they are closely related in function, namely, to receive and process an external signal. The results both of the small-charge tests and of the Operation Buster tests showed clearly that the electronic components used have serious inadequacies yet to be eliminated before the densitometer becomes a practical instrument. The results further indicate that among the electronic components the tuned amplifier needs the most improvement. A great deal of improvement certainly needs to be accomplished in the microphonic and electromagnetic shielding of the amplifier. This is quite evident by comparing the beta signal (Fig. 4.9) before and after zero time. Immediately

after zero time the film record appears as if the amplifier were picking up and passing a great burst of electromagnetic signal apart from that which could be attributed to the commonly known gamma radiation.

5.4 RECORDS OF GAMMA-RADIATION RATE VS TIME

The film records of gamma-radiation rate as a function of time had the form that was expected: a beta signal riding on a unidirectional gamma signal that decays monotonically. Undoubtedly, gamma-radiation statistics and stray electromagnetic pickup are superimposed on the beta signal.

The apparently greater sensitivity of the tube at Buster-Charlie than at Buster-Dog is due to the fact that a Vaseline phosphor was used at Buster-Charlie and none at Buster-Dog. The Vaseline was found to have retained its shape during the shot so that the aluminum foil over the collimating hole was effective in shielding the tube not only against blast but against thermal radiation as well. The Vaseline was spread over the cathode area through the Mu-metal-can window, and a 1-mil aluminum foil was taped over the window.

To measure radiation rate greater than 22 r/sec either a logarithmic scale should be used or the oscilloscope gain should be reduced.

The film records were projected in a Recordak where the amplitude of the trace could be measured within an error of ±0.1 in. (see Appendixes A and B). Hence, at $t = 0.15$ sec the record is accurate to ±1 per cent, and at $t = 3$ sec to ±5 per cent, for Buster-Charlie. For Buster-Dog the accuracy drops from ±0.5 per cent to ±2 per cent within the same time range.

The gamma records show slight rises. One occurs at about $t = 0.60$ sec, and another at $2.0 < t < 2.5$ sec. The cause of the first rise is not definitely known. The later rise is believed to be due to the air shock so that, from the gamma record, it is possible to determine roughly the time of shock arrival.

5.5 RECORD OF AIR DENSITY VS TIME

Owing to difficulties with timing signals, only one camera record of air density was obtained. The one density record available, taken during Buster-Charlie, has so much hash that identification of the shock wave is extremely difficult and inaccurate. The hash is so bad that no attempt is made here to obtain quantitative information concerning the variation of air density behind the shock. It is interesting, however, to note the pronounced decrease in beta signal at H+2.33 sec (Fig. 4.9). The beta signal from H+2.33 to H+3.00 sec is noticeably less than the signal increases. The gamma record showed a rise in radiation rate at H+2.33 sec. From this information it would be suspected that the shock arrived at H+2.3 sec.

The precise cause of the hash is not yet known. Doubtless the gamma radiation from the bomb is instrumental in some way. It is also recognized now that the bomb explosion sets up a powerful electromagnetic disturbance apart from the commonly known gamma radiation. This disturbance could conceivably have had a greater influence on the electronic instruments than the gamma radiation.

CHAPTER 6

CONCLUSIONS

6.1 FEASIBILITY OF THE BETA DENSITOMETER

The key to the development of the beta densitometer lies in the design of a detector-recording apparatus combination that can separate the beta signal from that of the background radiation. The idea behind the scheme of signal separation, modulation, and selective amplification of modulated signal appears simple enough and feasible. However, the electronic components, especially the tuned amplifier, used to perform signal separation were not adequate for their intended functions. The inadequacy is at least partly due to the presence of a powerful electromagnetic disturbance not recognized before and as yet not well understood. This is an effect on the densitometer distinct and apart from gamma radiation.

The inability of the a-c densitometer to produce a recognizable film record of air density behind a shock wave during Operation Buster does not prove that the idea behind modulation is infeasible. Less than 2 weeks was available for pretesting the complete densitometer. During Operation Buster there was only one opportunity to use the beta densitometer to measure air density behind a shock wave produced by a nuclear explosion. However, the feasibility test during Operation Buster did prove that the electronic components were not adequate to perform their intended functions in the presence of the electromagnetic disturbances that accompany a nuclear explosion.

6.2 DEVELOPMENTAL WORK

A great deal of theoretical work, basic experimentation, and instrument design has been done relative to the beta densitometer.[1,2] In its present state of development (i.e., Operation Buster model) the beta densitometer can be used to measure gamma-radiation rate as a function of time. The general pattern of instrumentation is now developed. In particular, the principal mechanical problems in modulation have been solved, and the handling of beta sources which was a hazardous procedure is now safe and easy.

REFERENCES

1. F. B. Porzel and J. E. Whitener, Feasibility Report on Measurement of Density, Temperature, and Material Velocity in an Air Shock Produced by a Nuclear Explosion, Los Alamos Scientific Laboratory Report LAB-J-719, Nov. 25, 1949 (not available).
2. F. B. Porzel and Group J-7, Measurement of Air Density in a Shock Wave, Preoperation Report for Operation Greenhouse, Los Alamos Scientific Laboratory Report LAB-J-2160, January 1951 (not available).

CHAPTER 7

RECOMMENDATIONS

In order to make the a-c beta densitometer suitable for measuring the air density behind the blast wave as a function of time, research work should be directed principally toward the development of suitable electronic equipment that will detect the beta signal and discriminate between it and the powerful background radiation from a nuclear explosion. Retaining the pattern of instrumentation used at Operation Buster, experimental work should be continued along these general lines:

1. Development of the electronic components until they can repeatedly and reliably discriminate between the beta signal and the background radiation, e.g., intense gamma radiation from a betatron or from radioactive gamma sources.

2. Performance of extensive small-charge experiments with the complete densitometer assembly until the a-c densitometer is capable of producing blast-wave traces on camera film without distorting the record by pickup.

3. Calibration of the densitometer in a pressure tank, after items 1 and 2 are accomplished, and comparison of the measurements from small-charge tests with other independent data.

A reasonable procedure would be to delay further tests on nuclear explosions until after the a-c densitometer has been intensively pretested in the laboratory along the lines suggested. If this pretesting were done a great over-all saving in time and effort would result.

APPENDIX A

COMPUTATION OF GAMMA-RADIATION RATE VS TIME, BUSTER-CHARLIE

Station 620, 4000 ft from ground zero
Height of burst: 1132 ft
Yield: see Buster-Jangle Report, Project 10.4, WT-413

A.1 GAMMA RECORD

The d-c output with 5 curies of radioactivity, using $\frac{1}{16}$ in. of Vaseline phosphor, is 20.0 μa. The beam deflections with 20.0 ι, as viewed in the Recordak, are as follows:

y, in. (±0.05)	y, in. (±0.05)
1.55	1.50
1.55	1.45
1.55	1.45
1.50	1.50
1.50	1.55
1.50	1.55
1.50	1.55
1.50	1.55
1.50	1.50
1.45	1.45
1.45	1.50
1.50	1.55
1.50	1.50
1.55	1.50
1.50	1.50

$\Sigma y = 45.20$

$$\text{Average deflection} = \frac{45.20}{30} = 1.51 \text{ in. for } 20.0\ \mu a$$

or

$$\frac{20.0}{1.51} = 13.2\ \mu a/\text{in.}$$

Phototube RCA 1P21 IX is 10.6/10.2, or 1.04, times more sensitive than RCA 1P21 I. From the Co^{60} experiment, assuming isotropic scattering and neglecting the difference in

spectrum, the integrated response for 1 r/sec is 0.546 μa with bare RCA 1P21 I phototube. An addition of $\frac{1}{16}$ in. of Vaseline phosphor multiplies the sensitivity of RCA 1P21 IX by

$$\frac{220 \times 10^{-3}}{10.34 \times 10^{-3}} = 21.5 \text{ times}$$

$$\text{Conversion factor} = \frac{1}{1.04} \times \frac{1}{21.5} \times \frac{13.2}{0.55} = 1.08 \text{ r/sec/in. deflection}$$

Table A.1—GAMMA-RADIATION RATE VS TIME, BUSTER-CHARLIE

Time, sec	Beam deflection, in. (±0.1)	Radiation rate, r/sec	Time, sec	Beam deflection, in. (±0.1)	Radiation rate, r/sec
0 – 0.10	>14.0	>15.1	1.60	1.9	2.1
0.15	11.8	12.8	1.65	1.9	2.1
0.20	7.7	8.3	1.70	1.9	2.1
0.25	5.5	5.9	1.75	1.9	2.1
0.30	4.5	4.9	1.80	2.1	2.3
0.35	4.0	4.3	1.85	2.1	2.3
0.40	3.5	3.8	1.90	2.0	2.2
0.45	3.4	3.7	1.95	2.0	2.2
0.50	3.3	3.6	2.00	2.0	2.2
0.55	3.3	3.6	2.05	2.0	2.2
0.60	3.3	3.6	2.10	2.1	2.3
0.65	3.0	3.2	2.15	2.1	2.3
0.70	2.9	3.1	2.20	2.1	2.3
0.75	2.9	3.1	2.25	2.1	2.3
0.80	2.8	3.0	2.30	2.1	2.3
0.85	2.8	3.0	2.35	2.1	2.3
0.90	2.7	2.9	2.40	2.3	2.5
0.95	2.7	2.9	2.45	2.1	2.3
1.00	2.6	2.8	2.50	2.2	2.4
1.05	2.6	2.8	2.55	2.1	2.3
1.10	2.5	2.7	2.60	2.1	2.3
1.15	2.4	2.6	2.65	2.1	2.3
1.20	2.3	2.5	2.70	2.1	2.3
1.25	2.4	2.6	2.75	2.1	2.3
1.30	2.3	2.5	2.80	2.0	2.2
1.35	2.2	2.4	2.85	2.0	2.2
1.40	2.1	2.3	2.90	2.0	2.2
1.45	2.1	2.3	2.95	2.0	2.2
1.50	2.0	2.2	3.00	2.0	2.2
1.55	2.0	2.2			

APPENDIX B

COMPUTATION OF GAMMA-RADIATION RATE VS TIME, BUSTER-DOG

Station 620, 4000 ft from ground zero
Height of burst: 11,417 ft
Yield: see Buster-Jangle Report, Project 10.4, WT-413

B.1 GAMMA RECORD

The d-c output with 5 curies of radioactivity is 1.85 μa. The beam deflections with 1.85 μa, as viewed in the Recordak, are as follows:

Deflection, in. (±0.05)	Deflection, in. (±0.05)
1.65	1.65
1.60	1.65
1.65	1.70
1.60	1.60
1.55	1.65
1.60	1.65
1.60	1.70
1.60	1.70
1.60	1.60
1.70	1.50
1.55	1.60
1.55	1.65
1.60	1.65
1.60	

$\Sigma y = 43.75$

$$\text{Average deflection} = \frac{43.75}{27} = 1.62 \text{ in.}$$

Therefore a 1.62-in. deflection of electron beam corresponds to a 1.85-μa phototube output.

APPENDIX B

COMPUTATION OF GAMMA-RADIATION RATE VS TIME, BUSTER-DOG

Station 620, 4000 ft from ground zero
Height of burst: 11,417 ft
Yield: see Buster-Jangle Report, Project 10.4, WT-413

B.1 GAMMA RECORD

The d-c output with 5 curies of radioactivity is 1.85 μa. The beam deflections with 1.85 μa, as viewed in the Recordak, are as follows:

Deflection, in. (±0.05)	Deflection, in. (±0.05)
1.65	1.65
1.60	1.65
1.65	1.70
1.60	1.60
1.55	1.65
1.60	1.65
1.60	1.70
1.60	1.70
1.60	1.60
1.70	1.50
1.55	1.60
1.55	1.65
1.60	1.65
1.60	

$\Sigma y = 43.75$

$$\text{Average deflection} = \frac{43.75}{27} = 1.62 \text{ in.}$$

Therefore a 1.62-in. deflection of electron beam corresponds to a 1.85-μa phototube output.

B.2 GAMMA-RADIATION RATE VS TIME

$$1.62 \text{ in.} \triangleq 1.85\ \mu a$$

$$1 \text{ in.} \triangleq \frac{1.85}{1.62} = 1.14\ \mu a$$

Phototube RCA 1P21 IX is 10.6/10.2, or 1.04, times more sensitive than RCA 1P21 I. Radioactivity of 1 r/sec produces 0.546 μa with RCA 1P21 I. Therefore

$$\text{1-in. deflection from RCA 1P21 IX} \triangleq \frac{1.14}{1.04} \times \frac{1}{0.55} = 2.01 \text{ r/sec}$$

Table B.1—GAMMA-RADIATION RATE VS TIME, BUSTER-DOG

Time, sec	Beam deflection, in. (±0.1)	Radiation rate, r/sec	Time, sec	Beam deflection, in. (±0.1)	Radiation rate, r/sec
0–0.30	>11.0	>22.1	1.45	5.0	10.0
0.32	11.0	22.1	1.50	4.9	9.8
0.33	10.4	20.9	1.55	4.6	9.2
0.35	9.9	19.9	1.60	4.4	8.8
0.40	9.0	18.1	1.65	4.4	8.8
0.45	8.4	16.9	1.70	4.4	8.8
0.50	8.1	16.3	1.75	4.1	8.2
0.55	8.0	16.1	1.80	4.0	8.0
0.60	7.5	15.1	1.85	3.8	7.6
0.65	7.5	15.1	1.90	3.8	7.6
0.70	7.5	15.1	1.95	3.6	7.2
0.75	7.5	15.1	2.00	3.5	7.0
0.80	6.9	13.9	2.10	3.6	7.2
0.85	6.8	13.7	2.15	3.4	6.8
0.90	6.7	13.5	2.20	3.3	6.6
0.95	6.7	13.5	2.30	3.2	6.4
1.00	6.5	13.1	2.35	3.2	6.4
1.05	6.4	12.9	2.40	3.2	6.4
1.10	6.1	12.3	2.45	3.1	6.2
1.15	5.9	11.9	2.50	3.2	6.4
1.20	5.9	11.9	2.55	3.4	6.8
1.25	5.7	11.5	2.60	3.1	6.2
1.30	5.4	10.9	2.65	3.1	6.2
1.35	5.2	10.5	2.70	3.1	6.2
1.40	5.1	10.2			

SECRET

Part II

INTERFEROMETER-GAUGE PRESSURE-TIME MEASUREMENTS

by

Daniel F. Seacord, Jr.

63-64

SECRET

CHAPTER 1

INTRODUCTION

Blast waves observed by pressure-time gauges near the surface of the ground exhibited very slow rise times on Operation Greenhouse. The purpose of the experiment on Operation Buster was to determine, if possible, the effects of different surfaces on this slow-rise phenomenon. More specifically, one pair of interferometer gauges was placed in a very dusty area (50- by 100-yd ploughed area in front of the gauges) and another pair was placed in an asphalt-surfaced area. Unfortunately, the result of this experiment is inconclusive owing to the paucity of data obtained.

CHAPTER 2

EXPERIMENTAL PROGRAM

2.1 INSTRUMENTATION

Shots B, C, and D, Operation Buster, were instrumented. Two gauges were placed in the asphalt area (Station 641) and two in the dusty area (Station 642) outside the 1500-ft-radius asphalt area. All four gauges were at a range of 2500 ft from ground zero. Figure 2.1 shows the instrumentation plan. Boxes for the gauge and battery power supply were placed in the ground so that the tops (in the case of the gauge box, the top of the lead shielding) were flush with the surface. The gauge boxes were shielded with lead brick as follows: top, 8 in.; side toward zero, 8 in.; other sides, 4 in.; and bottom, 4 in.

Figures 2.2 and 2.3 show the completed installation in the asphalt and dust areas, respectively. Figure 2.4 shows a gauge installed in the box top prior to sealing the box and placing the lead brick on top. An abbreviated circuit diagram for the operation of the gauge is shown in Fig. 2.5. Two EG&G timing signals were provided: a −5 min signal to start the gauge lamp and a −1.5 sec signal to start the camera. It may be seen from Fig. 2.5 that the camera will not operate solely on receipt of the −1.5 sec signal; the −5 min signal must first have been received. A discussion of the gauge may be found in "Handbook of Operation and Maintenance of the Interferometer Gauge," Los Alamos Scientific Laboratory, Group GMX-9 publication.

2.2 RESULTS

On Shot B the −5 min signal was not received owing to EG&G transmission-line difficulties; therefore the gauges did not operate, and no records were obtained.

Shot C produced one record from a gauge in the dusty area. The result is shown in Fig. 2.6. Of the remaining three gauges, gauge 1 ran, but the mercury light went out before a record was obtained; gauge 2 failed to run at all; and gauge 3 (in the asphalt) ran, but the pressures obtained were absurdly low. The failure of gauges 1 and 2 may be ascribed to the fact that dust probably clogged the relay contacts of the motor and/or lamp circuit. The poor record of gauge 3 may be due to dust clogging the pressure inlet hole extending through the lead brick shielding.

On Shot D all four gauges ran, and partial records were obtained; the −1.5 sec signal was 3 sec late, and therefore the shock wave had passed before the cameras were running. Only the extreme end of the pressure decay was recorded on the film.

On the one record obtained (Shot C), the slow rise to the maximum overpressure is clearly evident; this was expected from a gauge located in a very dusty area.

In addition to gauges in the target area one gauge was operated at the C.P. to measure peak pressure at that point. The following pressures were recorded: for Shot B, less than 0.1 psi and for Shot C, 0.18 psi.

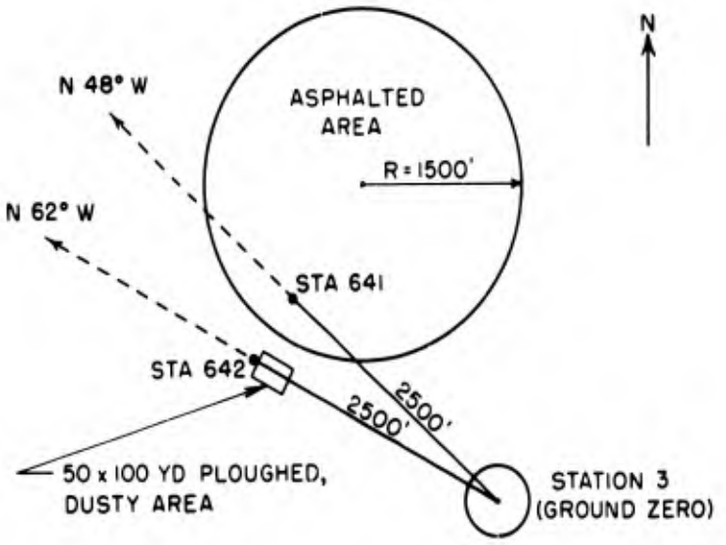

Fig. 2.1 — Interferometer-gauge stations.

SECRET

Fig. 2.2—Completed interferometer-gauge installation in the asphalt area.

Fig. 2.3—Completed interferometer-gauge installation in the dust area.

Fig. 2.4—Interferometer gauge prior to the placement of shielding.

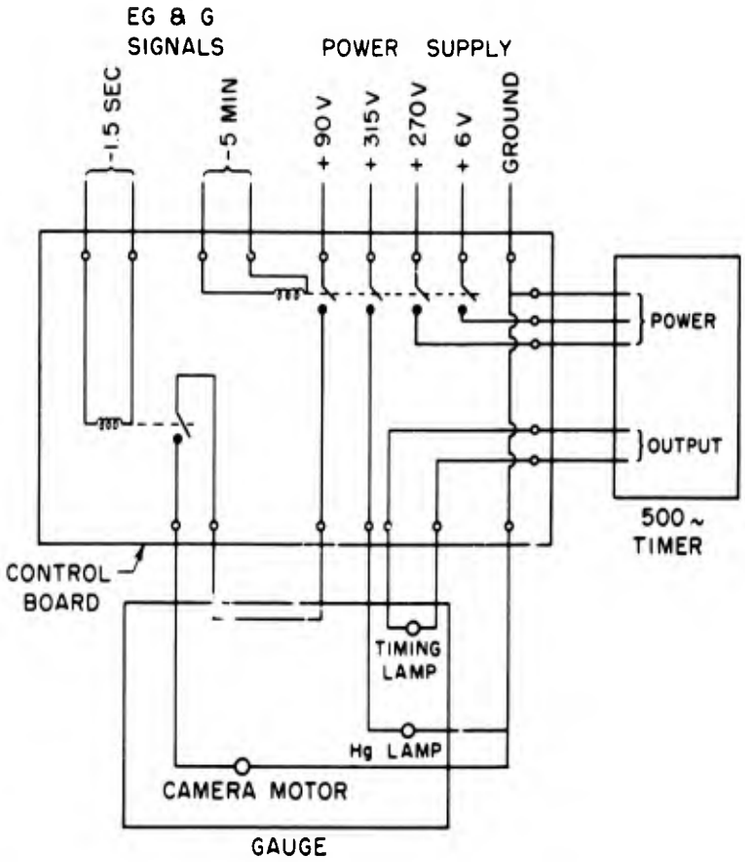

Fig. 2.5—Operational circuit design.

SECRET

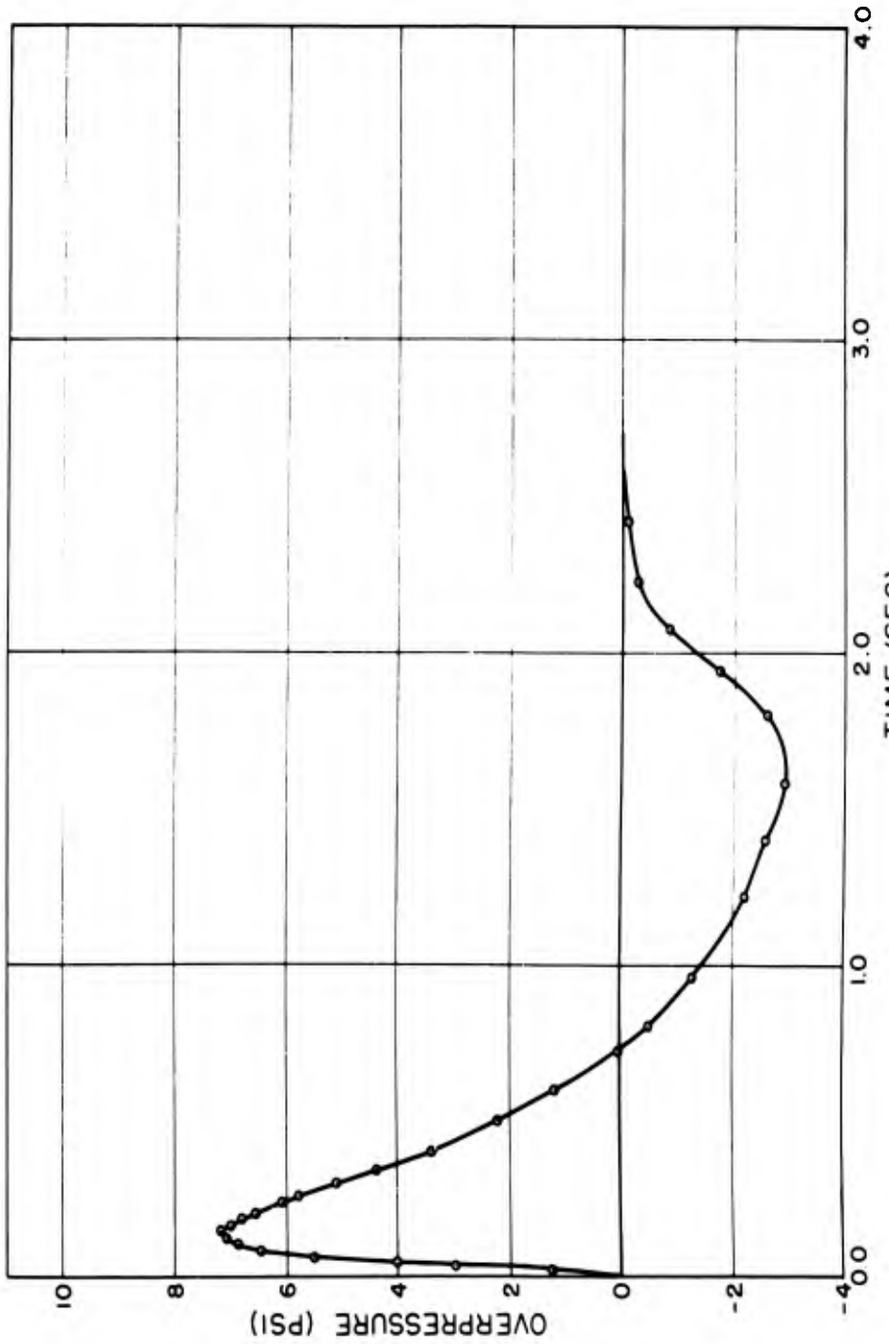

Fig. 2.6—Pressure-time record, Shot C.

CHAPTER 3

CONCLUSIONS

On Shot B the gauges recorded no data owing to the failure of the −5 min signal. One readable record was obtained from Shot C. All gauges operated on Shot D, but no significant data were obtained owing to the delay in the receipt of the −1.5 sec signal.

The single record obtained does give significant information regarding the effect of the ground surface on the shock wave from an atomic bomb. Figure 3.1 shows two curves for comparison with Fig. 2.6. One curve is the predicted theoretical shape obtained by scaling from IBM Problem M and is essentially a free-air waveform, with a theoretical peak of 12.4 psi. The other curve is an interferometer-gauge record from Greenhouse-Easy, again at the same scaled distance and with a peak pressure of 9.4 psi and a rise time of 8 msec. In comparison with the theoretical curve, the Operation Buster record shows almost complete disagreement. The peak pressure on Operation Buster is half as great, the positive phase is twice as long, and the negative phase is twice as deep. The only point of agreement is the total length of the wave, and this is a rather insensitive measure. The Wiancko gauges, installed by Sandia on a different blast line, show the same general feature to a somewhat similar degree. The Operation Greenhouse record shows the same tendencies but to a much lesser degree. The significant point is that despite the reduction in peak pressure there is no evidence of an over-all energy loss in any of these records; in fact, both the positive and negative impulses are markedly increased.

These features are expected from the theory of surface loss which this experiment was designed to test. On the other hand the incompleteness of the record precludes further quantitative comparison at present. A record over a dust-free area such as asphalt is needed to determine whether the distortion to the waveform is caused by mechanical effects, such as dust and turbulence, or by thermal effect alone. A duplicate measurement under the same condition of dust is necessary to eliminate positively the possibility of the single record being a freak. Finally, the Operation Buster record is that of a reflected wave over an ideal surface at this pressure level and height of burst. For this comparison a theoretical curve is desirable as the ideal case, but at present no theory exists for the Mach region. If an empirical waveform is used, it should be that from a measurement over an ideal surface such as water rather than over sand surface as in the Operation Greenhouse record.

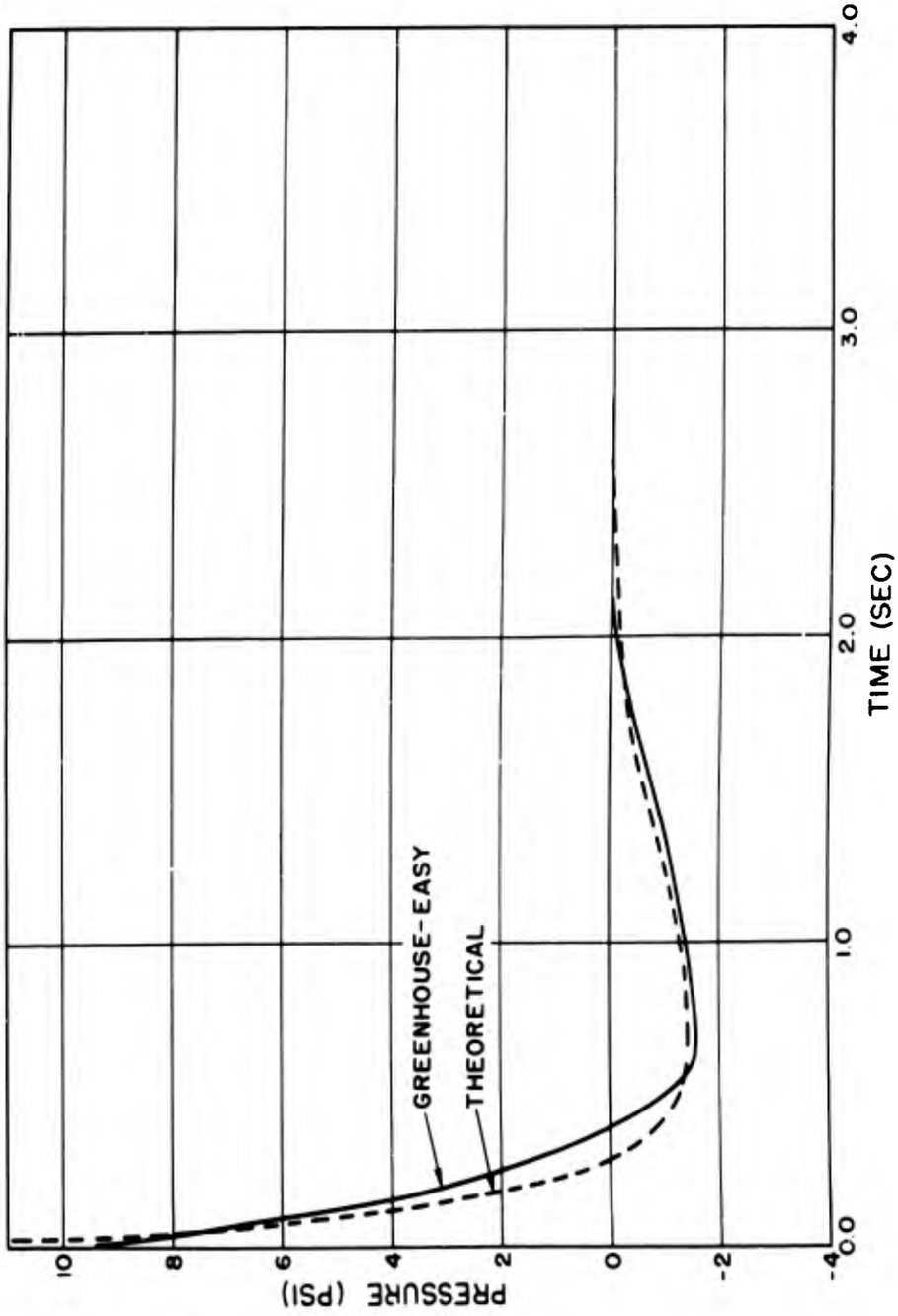

Fig. 3.1—Pressure-time record, Shot E, Operation Greenhouse, and theoretical curve from the IBM run.

SECRET

Part III

BLAST-WAVE-MATERIAL VELOCITY MEASUREMENTS

by

Daniel F. Seacord, Jr.

75-76

SECRET

ABSTRACT

This part of the Program 10.10 report presents the data obtained during Operations Buster and Jangle on material velocity in the blast waves associated with nuclear detonations.

The primary purpose of the experiment was to ascertain the feasibility of the measurement of mass motion in a nuclear explosion. The feasibility was demonstrated, and primary hydrodynamic data were obtained, from which material velocities and peak pressures were deduced. In addition, considerable information was obtained concerning the interaction of the ground surface with the blast wave generated by a nuclear explosion.

SECRET

CHAPTER 1

INTRODUCTION

1.1 PURPOSE OF EXPERIMENT

The purpose of the experiment was to ascertain the feasibility of measuring material velocity and of utilizing these measurements to provide an independent method of determining peak pressures associated with a blast wave from a nuclear explosion.

The development of the mass-motion method* has a broad underlying purpose, which is to find an ideal hydrodynamic experiment for the study of blast waves. An obvious requirement is to make measurements where the gauge itself does not disturb the flow. This is a limitation on all types of pressure-time devices by which pressure is necessarily measured at a surface, precisely where the disturbance is the greatest. In this regard a measurement "in the large" is always superior to a measurement at a point. Measurement of shock velocity is such a method, but although it has been very successful on small charges and at high pressures, it is subject to considerable inaccuracy at pressures below 10 psi. At low pressures the shock velocity approaches sonic velocity; in a measurement of this velocity the percentage error in calculated pressure increases rapidly at low pressures for a given error in shock velocity. Measurement of material velocity is not subject to this limitation. The material-velocity method is equal to the shock-velocity method at high pressures and becomes increasingly accurate at low pressures.[1]

Mass-motion study is also the means of correlating all blast information, and the idea for the mass-motion method grew directly out of attempts to find a suitable method for the integration of blast waves. Mass-motion graphs furnish blueprints of the blast wave, and the data can be correlated by means of a radius-time graph, as shown in Fig. 1.1. This graph is applicable only to a blast wave in free air or to a tower shot where the effect of the height of burst is small and the wave can be described using only a single-space variable, such as radial distance, and the time. It depicts time of shock arrival directly, and the slopes of the lines depict shock and material velocities. The theoretical form for the equations of the mass lines are known in case of strong shocks, and it is expected that these can be extended to weaker shocks. The large number of mass points permit a fit of the empirical equations over a space instead of merely a line.

The distance between any two parallel mass lines labels a particular shell of air, and density is deduced directly from the equation of continuity of mass

$$\rho r^2 \, dr = \text{constant} = \rho_0 R^2 \, dR \tag{1.1}$$

where r refers to the space variable within the wave and R refers to the position of the shock front. Having determined density as a function of space and time, pressure relations can then be derived directly using the adiabatic law

* Material contributed by F. B. Porzel.

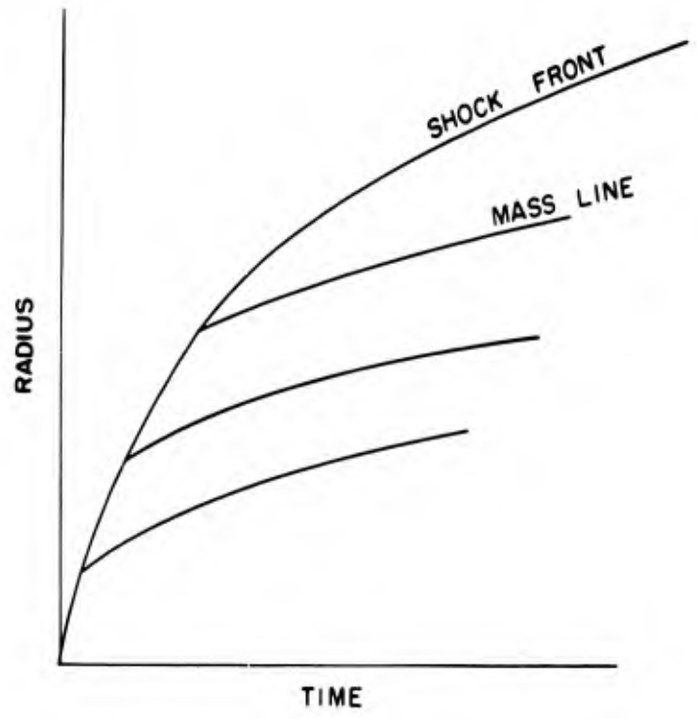

Fig. 1.1—Shock-front radius vs time.

$$\frac{P}{\rho\gamma} = \text{constant} = \frac{P_S}{\rho_S\gamma} \tag{1.2}$$

The mass lines define the paths along which the adiabatic law is applicable and give the values of P_S and ρ_S to be inserted into the equation. Sound velocity as a function of space and time can then be calculated from

$$C = \sqrt{\frac{\gamma P}{\rho}} \tag{1.3}$$

Temperature as a function of space and time can then be deduced from

$$C = \sqrt{\gamma RT} \tag{1.4}$$

or from a more refined equation of state, if the ideal gas law does not apply.

If sufficient points are available so that both the shock velocity and the material velocity are defined, then as a separate check it is possible to derive all the peak variables independently of the space and time calibration of the films. The ratio of shock velocity to material velocity is a function of density only and is given in Eq. 1.5.

$$\frac{U}{u} = \frac{V_0}{V_0 - V} = \frac{\frac{1}{\rho_0}}{\frac{1}{\rho_0} - \frac{1}{\rho}} = \frac{\rho}{\rho - \rho_0} \tag{1.5}$$

From this equation, all other peak variables can be calculated, except in strong shocks.

The method of integration described is appropriate to a waveform which depends on a single-space variable. The integration is much more difficult for reflected-pressure patterns, but here mass-motion graphs offer the additional advantage of showing the geometry of the reflection process. It is possible to measure both free-air and reflected pressures by proper choice of location of stations.

Mass motion becomes of further importance as a consequence of the theory of surface loss. As was shown at Operation Buster, the nature of the surface affects pressures by factors of 2 or 3; hence in the future tests of atomic bombs a measurement away from the surface is necessary as a control experiment which gives the "ideal" values of pressure and other variables with which the measurements at the surface can be compared.

A second advantage is the simplicity of the system. With the exception of aligning the cameras, a blast line of 10 stations to label the air with smoke may easily be installed in several hours. No electronic equipment, which needs extensive calibration, is necessary. Compared to a gauge such as the LASL interferometer gauge, no lead shielding is required. Units may be placed as close to ground zero as desired, limited only by the restriction on photography imposed by fireball illumination.

Finally, because the method is photographic, a great deal of supplementary data can often be expected. For example, it was expected that the photography used on Operation Buster to follow smoke-labeled air would at the same time yield considerable information regarding dust and turbulence behind the shock front.

Mass-motion study is subject to several limitations. It requires a measurement of preshock sound velocity, although the accuracy required is not so great as in the case of the shock-velocity method. The opacity of a smoke cloud to thermal radiation tends to raise sound velocity locally and thus raises the material velocity as well as the pressures deduced from it. The mass of the smoke particles may tend to "drag" the blast wind. Both the thermal and viscosity limitations can be reduced, if not eliminated, by making the volume of smoke-labeled air sufficiently small and tenuous.

1.2 PRIOR DEVELOPMENT

Although data on material velocity were incidentally obtained at Operation Trinity from photographs of exploding balloon cables, the first deliberate attempt at an experimental program was made in October 1950 at Los Alamos (to the best of the author's knowledge) as a direct and independent outgrowth of hydrodynamic theory by F. B. Porzel, who had shown that the method had considerable promise as an ideal blast measurement. At that time Porzel and R. A. Houghten conducted small-charge experiments using meteorological balloons as "labeling" particles to test the generic idea of mass motion. As an extension of these preliminary experiments, E. J. Zadina and B. Brixner attempted to photograph smoke motion on Shot Item in the Operation Greenhouse series; no results were obtained because of obscuration of the smoke pots used. From present blast theory of the interaction of the surface with the blast wave from an atomic bomb, it appears that the obscuration there was probably due to ground smoke or dust raised by thermal radiation prior to shock arrival and possibly to some contribution from dust raised by ground shock.

1.3 HYDRODYNAMIC RELATION

Photography of the motion of a parcel of air labeled with smoke particles enables the determination of the material velocity u associated with the blast wave. This velocity may then be substituted into the following formula, derived from the Rankine-Hugoniot equations, and the peak overpressure can be computed:

$$\frac{u}{c_0} = \frac{1}{\gamma}\frac{P_S}{P_0}\frac{1}{\sqrt{\frac{\gamma+1}{2\gamma}\frac{P_S}{P_0}+1}}$$

where c_0 = ambient sound velocity
γ = ratio of specific heats of air
P_0 = ambient pressure
P_S = peak overpressure

In the pressure regions which were investigated (less than 50 psi), γ may be considered constant. Meteorological data provided values of ambient pressure and temperature. The sound velocity was computed from the latter.

1.4 METHODS OF LABELING AIR

Two methods of labeling the air with visible particles were tried. A JATO (jet-assisted-take-off) unit, placed in the ground nozzle end up, produces a column of white smoke upon ignition. This column, extending vertically for about 150 ft in a cone of 20°, may be easily photographed. Possible disadvantages (more fully discussed in Appendix B) include effects of density, vertical velocity components, and continuous smoke production.

During the program at the Nevada Proving Grounds, a second method of producing smoke was investigated experimentally, which consists in firing vertically an aerial bomb (commercially available fireworks) and then photographing the resultant puff of smoke accompanying the bursting of the bomb in the air. Many of the disadvantages listed above for the JATO method were thereby removed.

REFERENCE

1. F. B. Porzel and J. E. Whitener, Feasibility Report on the Measurement of Density, Temperature, and Material Velocity in an Air Shock Produced by a Nuclear Explosion, Los Alamos Scientific Laboratory Report LAB-J-719, Nov. 25, 1949 (not available).

CHAPTER 2

HIGH-EXPLOSIVE SHOTS

In preparation for Operation Buster a series of exploratory high-explosive shots were fired at Los Alamos during the period Sept. 15 to Oct. 1, 1951. Answers were sought to the following questions:

1. Do the smoke particles achieve sufficient motion under the influence of a blast wave?
2. What is the most reliable ignition system for field use of the JATO unit?
3. What are the optimum photographic parameters (lens, camera distance, and aperture and shutter settings)?

These were satisfactorily answered during a series of 14 JATO firings; decisions on camera aperture and shutter settings necessarily had to await a nuclear detonation. The high-explosive charges consisted of granulated TNT ranging from 100 to 2000 lb. Film analysis revealed motion of the smoke columns about as expected. Resolution was below that expected on a nuclear explosion due to the much shorter positive phase associated with small charges.

Figures 2.1 and 2.2 are illustrative of the photographic results.

Figure 2.1 shows the smoke column after it has been moved about 3 ft by the blast wave. Initially the high column issued from the JATO nozzle; when the blast wave impinged on the column, it was moved to the left (the charge was located about 20 ft to the right). After passage of the blast wave the smoke again issued from the nozzle, producing the low column seen directly over the nozzle. Figure 2.2 shows the approximate spherical form of the blast wave as it reaches the smoke column.

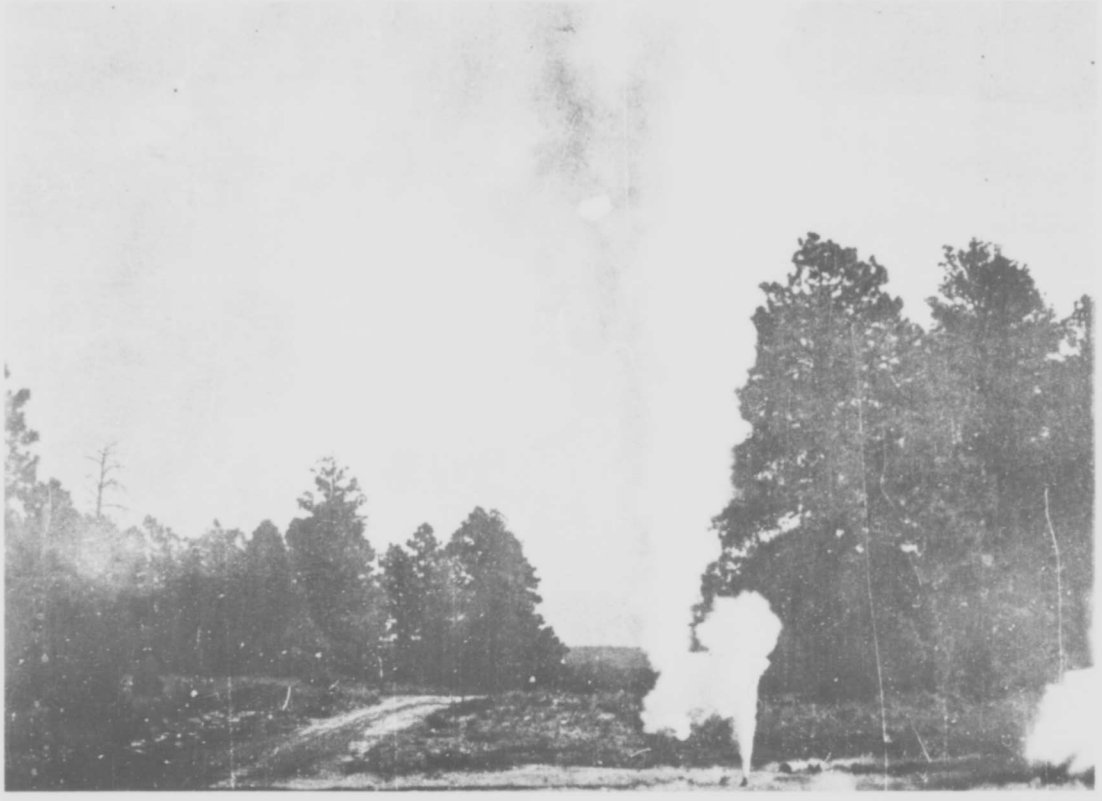

Fig. 2.1 —JATO motion on a high-explosive shot.

Fig. 2.2—Outline of the shock front on JATO high-explosive shot.

CHAPTER 3

OPERATION BUSTER SHOTS

3.1 GENERAL

As a result of the preliminary work at Los Alamos the final instrumentation was decided on for use on Operation Buster. The JATO units were procured from Kirtland Air Force Base. Two Mitchell high-speed cameras were provided by Group GMX-9, LASL. The field installation was accomplished by members of the Los Alamos Blast Measurements Group, J-10, with little difficulty. All shots were instrumented although participation was originally planned for only Shots B, C, and D.

Instrumentation for Shot A was more in the nature of a dry run since the JATO stations were located at too great a range for such low pressures as were expected. Shot E was over the target area in which the JATO units were located, and, by stopping down the camera, it was hoped that data might be obtained in spite of the intense fireball illumination. Positive results were not obtained on these two shots.

3.2 INSTRUMENTATION

Two JATO units were installed for each shot, one at a range of 2000 ft from target ground zero and one at 4000 ft; both units were on the same radial line from ground zero. A Mitchell camera was located approximately 7800 ft and another 7200 ft from the JATO units. Figure 3.1 shows the spatial relation described.

The JATO units were buried in a vertical position with the nozzle end up and at approximately ground level. The ignition circuit is shown in Fig. 3.2; each unit was ignited at H−5 sec upon completion of the circuit through an EG&G relay.

To facilitate movement and to provide weather protection the two Mitchell high-speed 35-mm cameras, with their battery power supplies and relay control board, were mounted in a plywood trailer that was placed in position at Station 633. The cameras were started at H−5 sec and allowed to run a total of 20 sec, after which time they were automatically stopped. The camera power and timing circuit is shown in Fig. 3.3. The 6-volt−110-volt inverter was necessary to provide alternating current for the timing unit.

The camera observing the 2000-ft JATO unit was equipped with a 24-in.-focal-length lens and operated at f/5.3 with a shutter-sector opening of 30°; the camera observing the 4000-ft JATO unit had a 36-in. lens and operated at f/6.3 with 120° shutter. Microfile film was used on all shots. No equipment was available at the time for producing timing marks on the film; reliance was to be placed on the expected camera film speed of 100 frames/sec. However, this speed was found to be extremely erratic, and a third method of film-speed determination, as described in Sec. 3.3, was ultimately used.

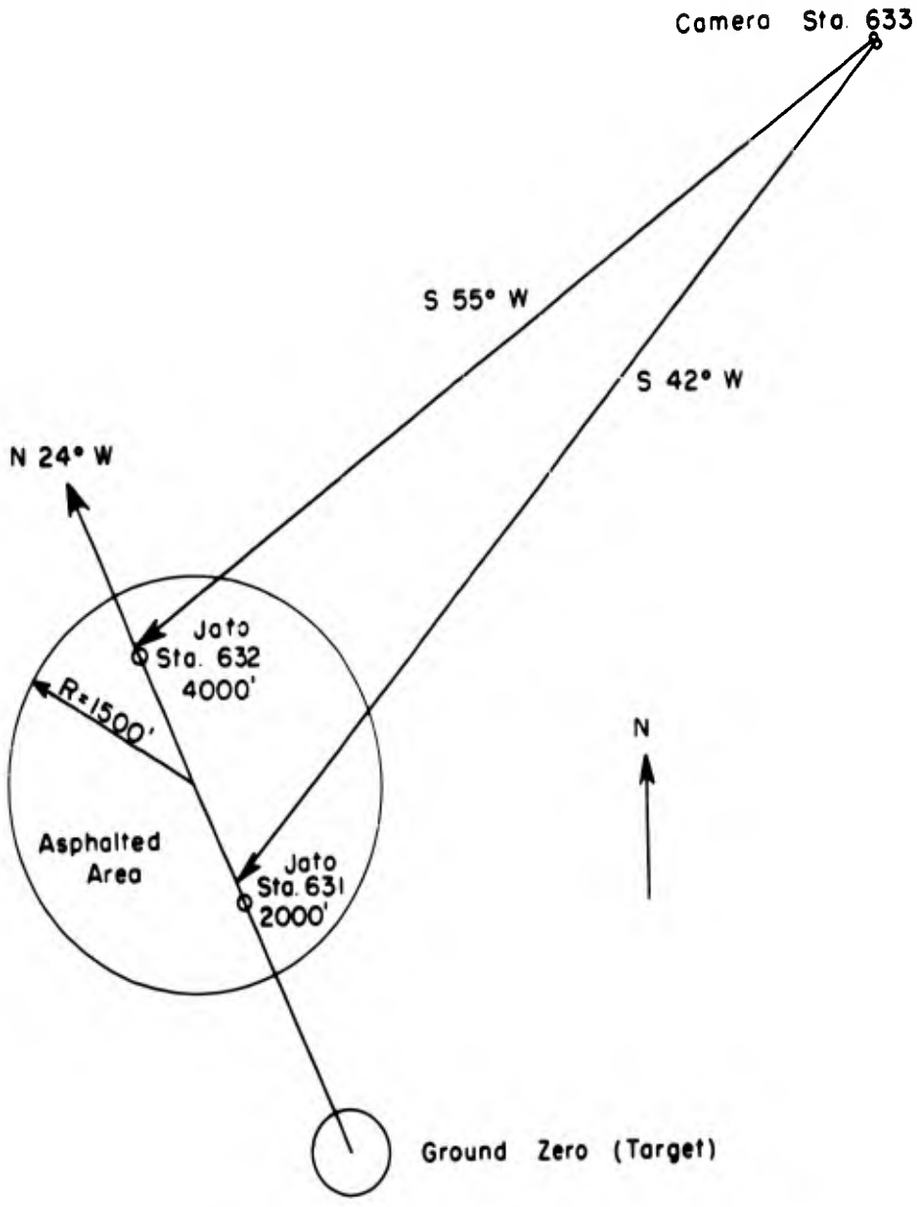

Fig. 3.1—Operation Buster JATO instrumentation plan.

SECRET

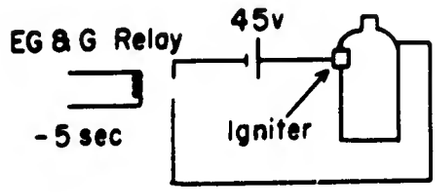

Fig. 3.2—JATO ignition circuit.

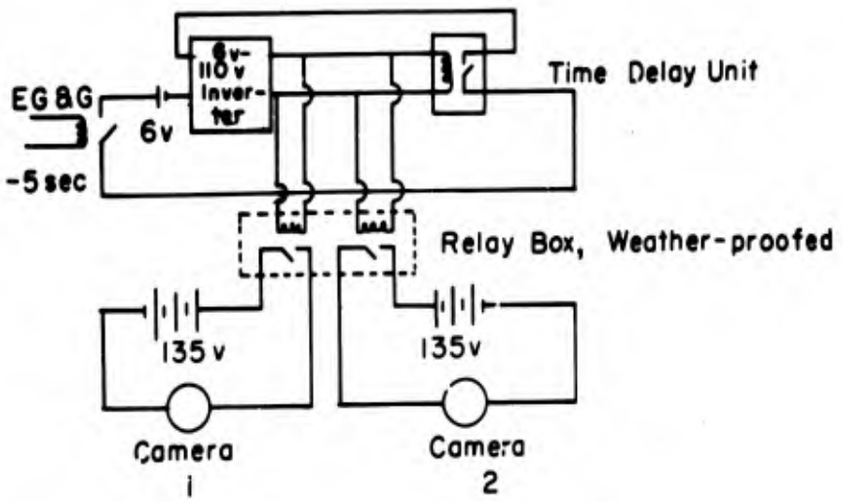

Fig. 3.3—Camera power and timing circuit.

SECRET

3.3 METHOD OF PHOTOGRAPHIC ANALYSIS

The 35-mm films were analyzed, frame by frame, by enlargement and projection on a Recordak. The original fields of view of 320 ft (24-in. camera) and 198 ft (36-in. camera) were magnified by the Recordak to give reading conversion factors of 0.66 and 0.42 ft/mm, respectively. To check these figures, calculated from object-image distance relations, markers were photographed on all shots; the measured conversion factors agreed with those above to within 1 per cent.

The outline of the JATO smoke column was traced, and, from the series of resultant "contours," displacement-time curves were drawn. Material velocity (with a time base in terms of film frames) was then determined as the maximum slope of these curves.

Whenever possible, several determinations of the material velocity were made, plotting displacement vs time at several elevations within the smoke column. Small inconsistent variations were noted as a function of altitude; the series of velocities were averaged to obtain a representative material velocity at about 100 ft above the ground. An exception to this is the case of the Shot-B 2000-ft JATO, where the triple point passed through the smoke column; both free-air and reflected pressures were obtained here. This example is shown in Fig. 3.4 to illustrate the contour plot.

The measured material velocity was then subjected to two corrections: (1) obliquity factor and (2) wind velocity. The obliquity factor is due to two causes. For reasons of operating convenience the cameras were not placed on a line perpendicular to the JATO blast line, and the point of detonation was not directly over the planned target ground zero. Therefore the motion of the smoke column, as observed on the film, was a component of the true motion. Since the appropriate geometry was known, a cosine correction was applied in order to arrive at the true velocity. Prior to shock arrival the ambient wind velocity was measured on the film, and a corresponding correction was applied to the observed material velocity to obtain the value it would have had in still air.

Up to this point in the analysis the material velocity was based on a time scale in terms of film frames. Although it was expected that the cameras would run at approximately 100 frames/sec, this was far from the case. In spite of the fact that the battery power supply was adequate and was frequently replaced by fresh batteries, it has become apparent that relatively small decreases in temperature seriously affect camera speed. For example, on Shot C, when the early morning temperature was down to 2.5°C, the cameras ran at approximately half speed. However, it has been possible to determine the camera speed with a fair degree of accuracy from the knowledge of the length of time the camera was running and the number of frames exposed during this time interval. Zero time of the detonation is well established on the film; therefore a count of frames from this point to the end of the film and the known time interval between zero and the time when the camera is automatically stopped give the frame rate. By counting from zero time, rather than the beginning of the film, the error due to film acceleration at the start is eliminated since the camera is up to speed at zero time. Similarly, deceleration error is minimized by observing the change in exposure when the camera begins its deceleration. This was true except for Shot D, when the −5 sec camera-starting signal was late. Frame rate for this shot was determined from Operation Jangle (from which accurate timing was available). This large extrapolation is believed to be justified since ambient temperatures were nearly the same on the two shots and the battery power supply was identical and freshly renewed prior to each of the two shots.

By applying the frame rate, as thus determined, to the material velocity as a function of frames, a material velocity in feet per second was then obtained.

A good value for ambient sound velocity c_0 was also difficult to determine. As can be seen from Table A.1, the temperature at shot time is not very accurately known. In general, when shots occur shortly after sunrise, local heating produces a pronounced vertical temperature gradient and rapidly changing surface temperatures. For Operation Buster Shots B, C, and D, the temperature value chosen for computing sound velocity is that value for an altitude of about 100 ft since the average material velocity measured on the JATO smoke column was taken at that level. Ambient sound velocity was corrected for temperature on the basis of

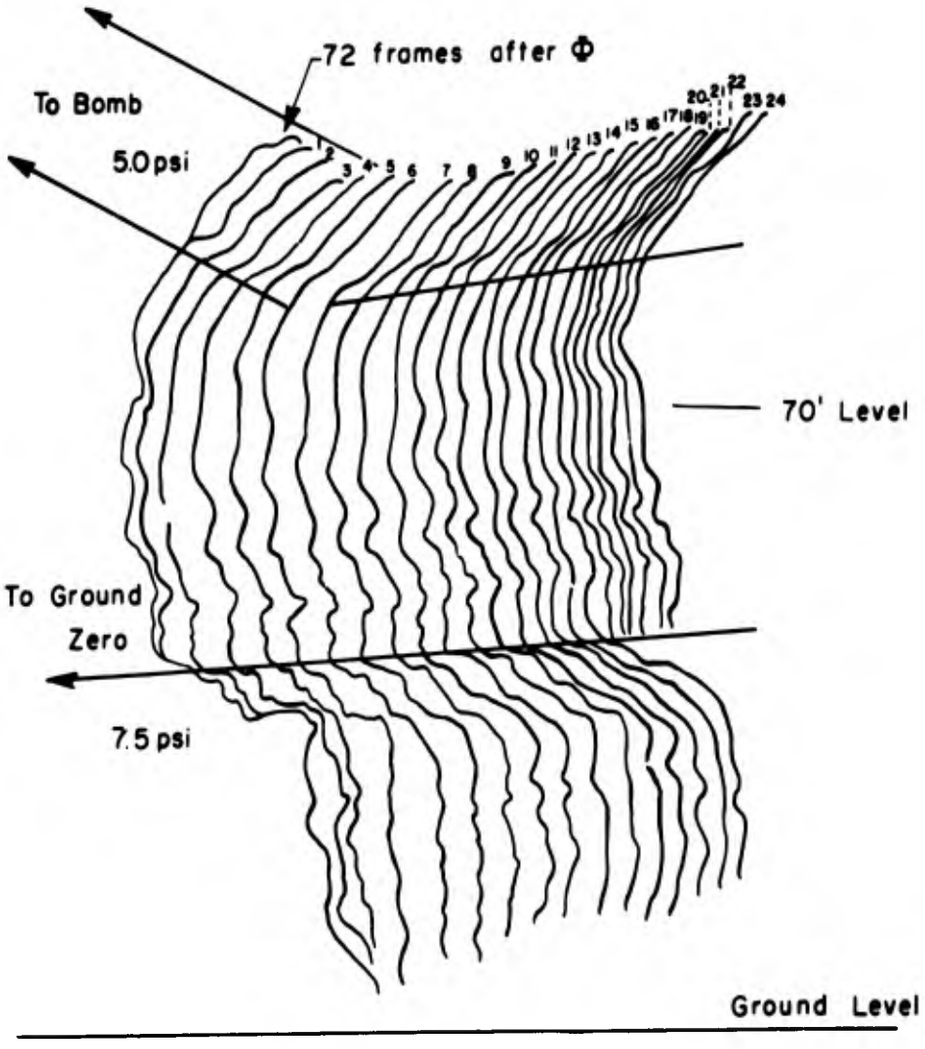

Fig. 3.4 — JATO cloud-contour plot, Shot B.

SECRET

Table 3.1—SUMMARY OF JATO MASS-MOTION DATA, OPERATION BUSTER

Shot	Height of measurement, ft	Measured material velocity u_m, ft/sec	True material velocity u, ft/sec	Temperature, °C	Sound velocity, ft/sec	u/c_0	P_s/P_0	Ambient pressure, psi	Peak overpressure, psi	Distance from ground zero, ft	Time of arrival, sec
B	~60	328	371	4.5	1094	0.339	1.585	12.7	7.5	1865	1.03
B	114	230	265	4.5	1094	0.242	1.395	12.7	5.0	1865	1.03*
C	~100	370	410	8.5	1102	0.372	1.655	12.55	8.2	3810	2.03
D	~100	1020	1113	11.2	1107	1.006	3.475	12.7	31.4	1960	0.71
D	~100	415	426	11.2	1107	0.385	1.685	12.7	8.7	3950	2.06

*Free-air measurement.

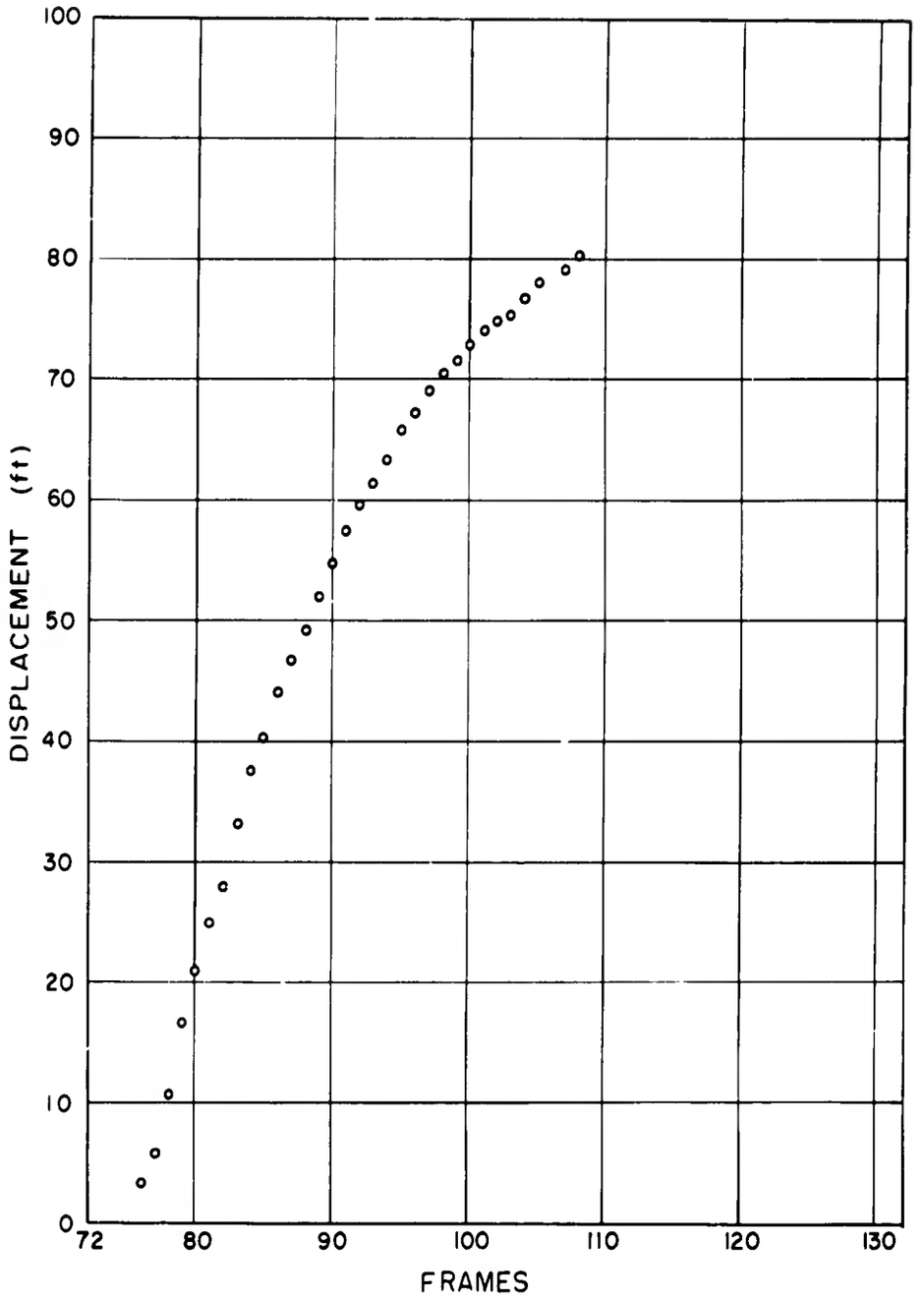

Fig. 3.5—Displacement-time data, Shot B, 1865 ft from ground zero, 24-ft elevation. Multiply frames by 14.35 to convert to milliseconds.

SECRET

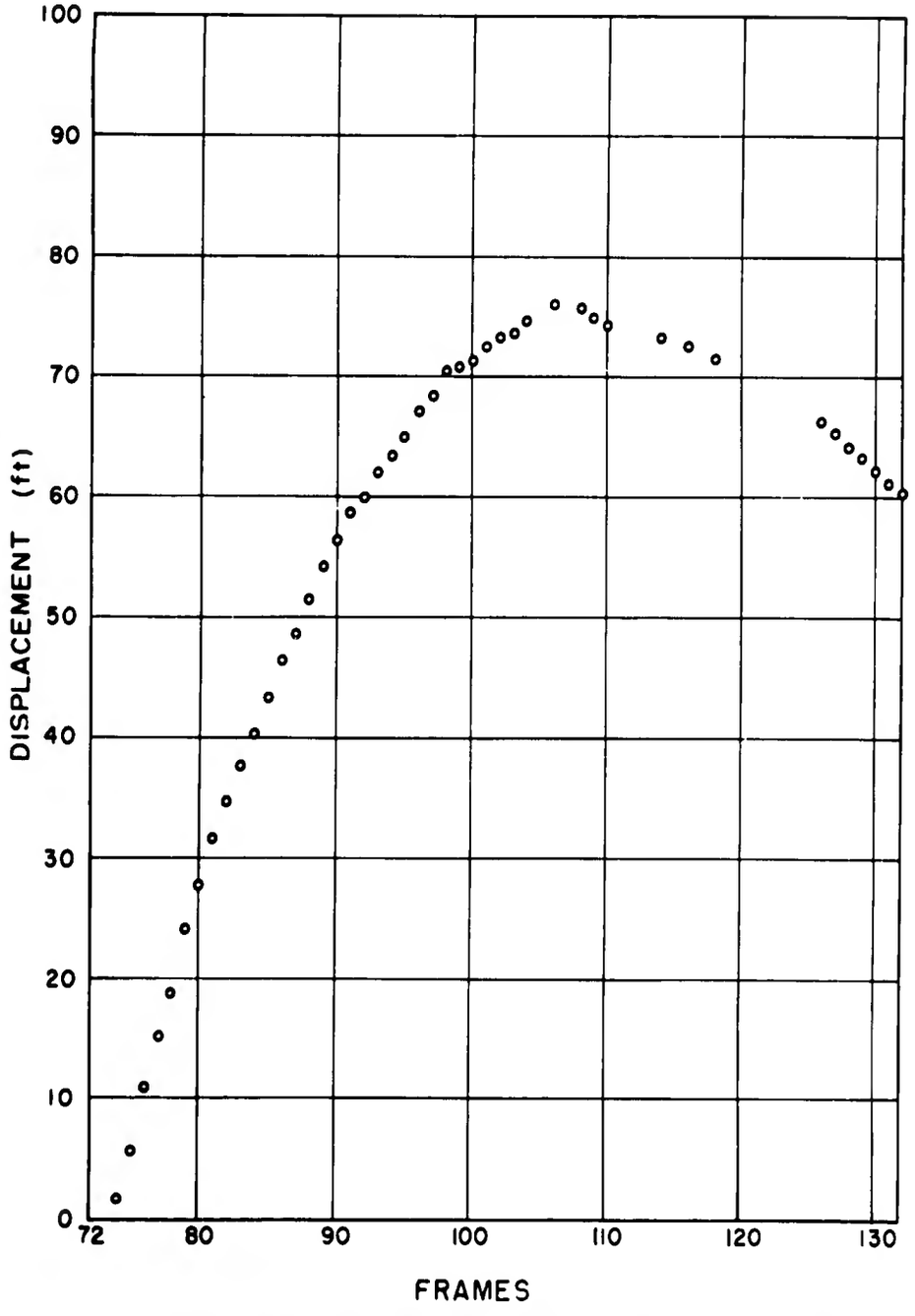

Fig. 3.6—Displacement-time data, Shot B, 1865 ft from ground zero, 57-ft elevation. Multiply frames by 14.35 to convert to milliseconds.

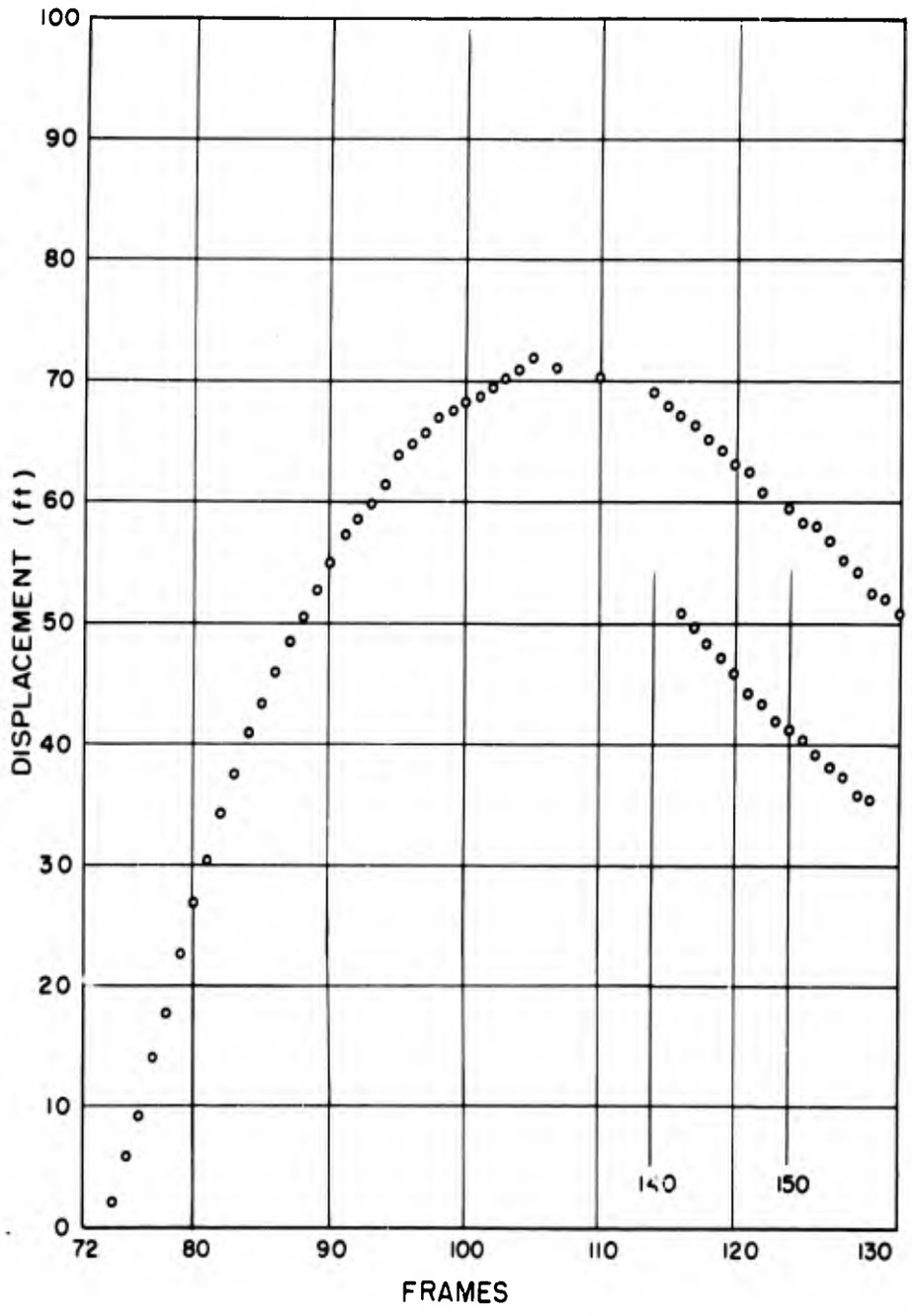

Fig. 3.7—Displacement-time data, Shot B, 1865 ft from ground zero, 70-ft elevation. Multiply frames by 14.35 to convert to milliseconds.

SECRET

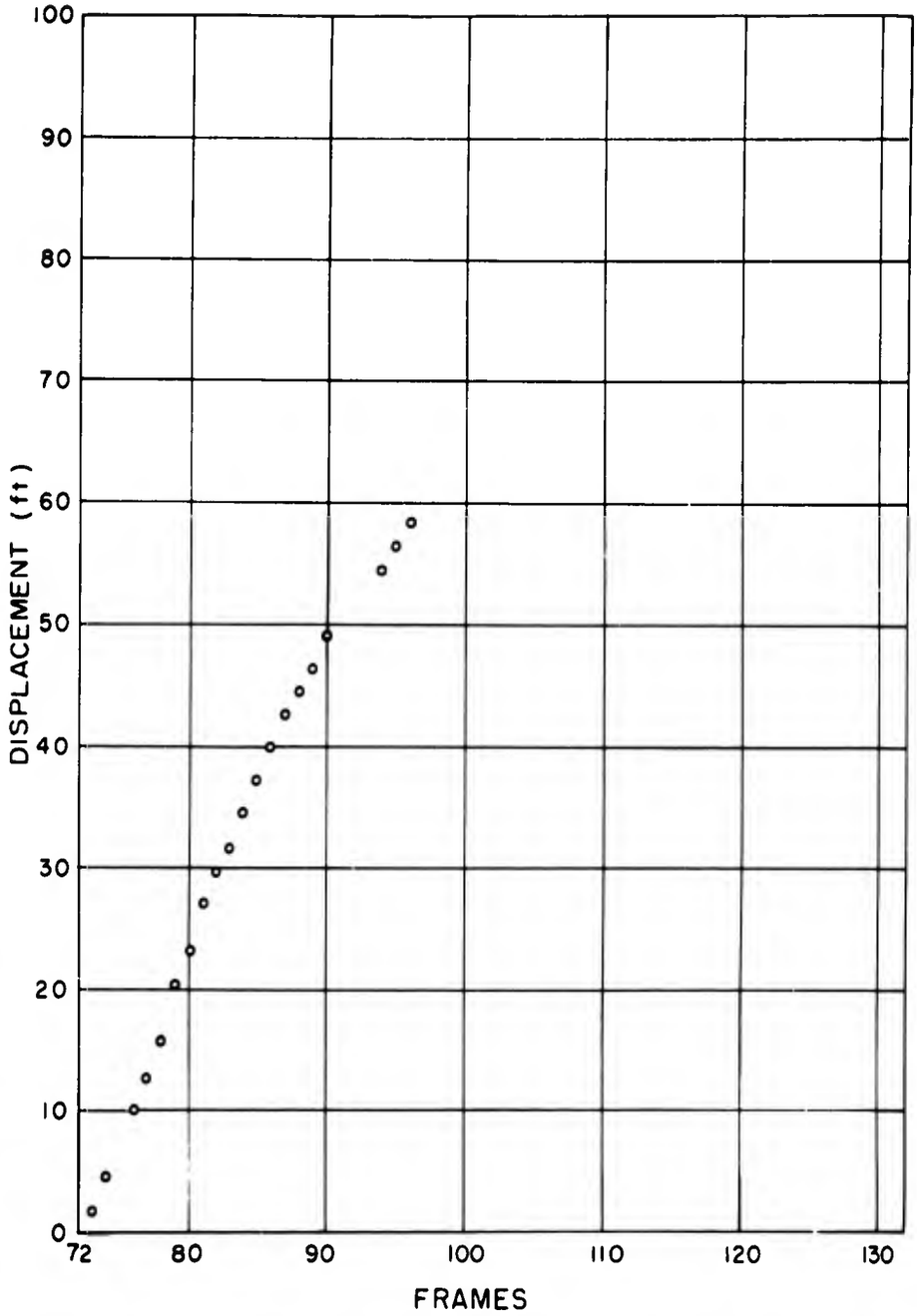

Fig. 3.8—Displacement-time data, Shot B, 1865 ft from ground zero, 114-ft elevation. Multiply frames by 14.38 to convert to milliseconds. The 114-ft elevation is in the free-air pressure region.

SECRET

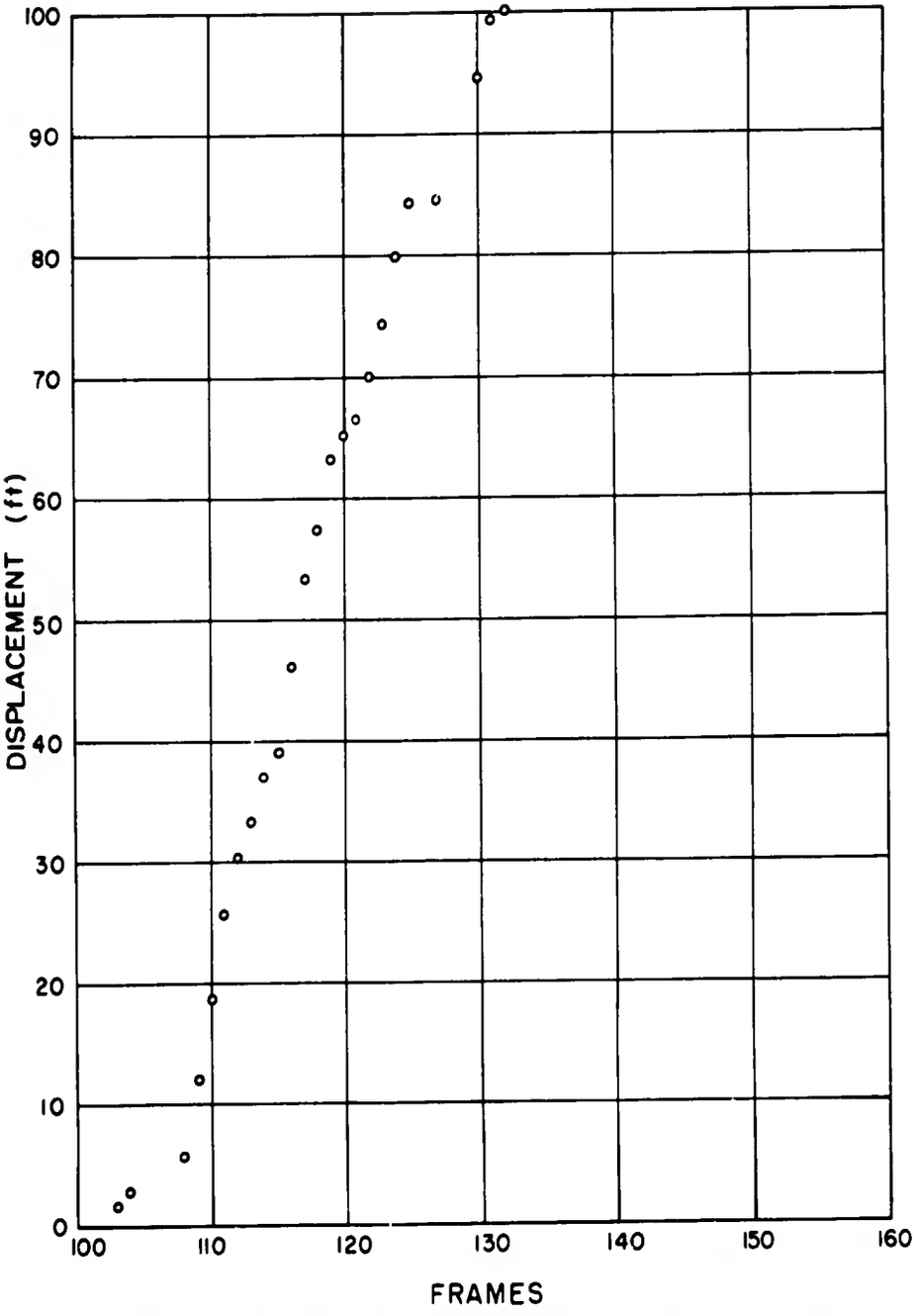

Fig. 3.9—Displacement-time data, Shot C, 3810 ft from ground zero, 48-ft elevation. Multiply frames by 19.96 to convert to milliseconds.

SECRET

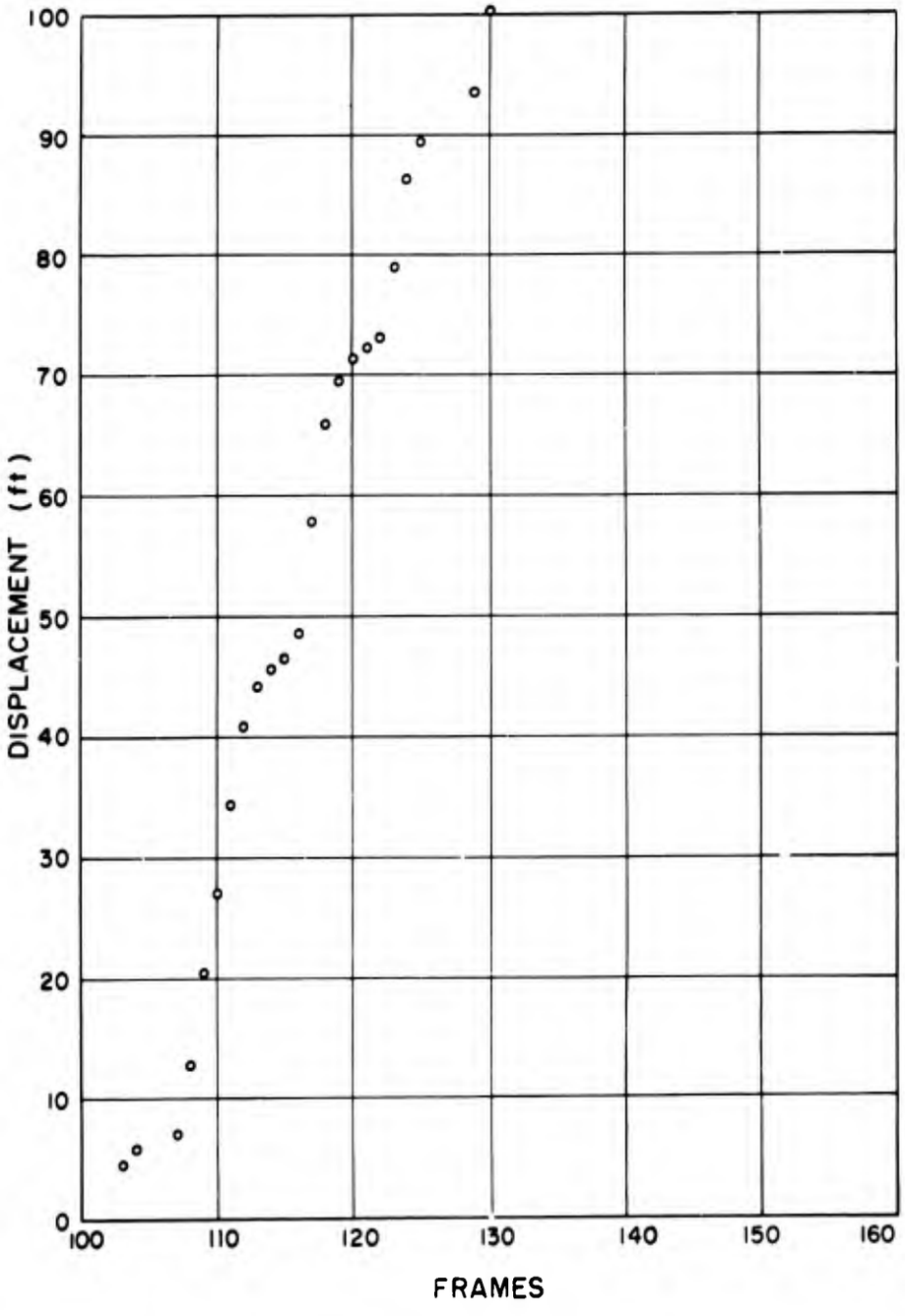

Fig. 3.10—Displacement-time data, Shot C, 3810 ft from ground zero, 74-ft elevation. Multiply frames by 19.95 to convert to milliseconds.

SECRET

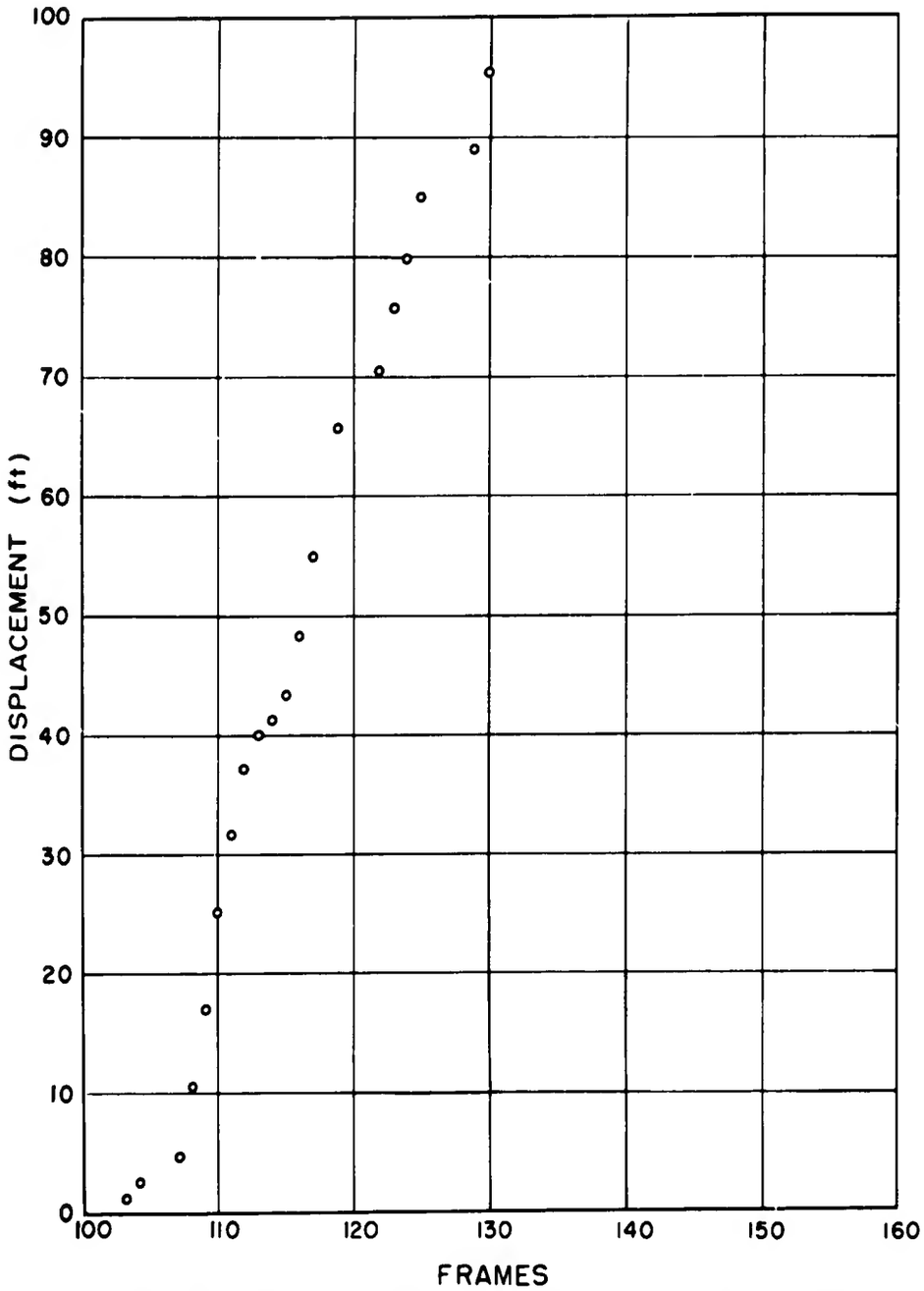

Fig. 3.11—Displacement-time data, Shot C, 3810 ft from ground zero, 115-ft elevation. Multiply frames by 19.95 to convert to milliseconds.

SECRET

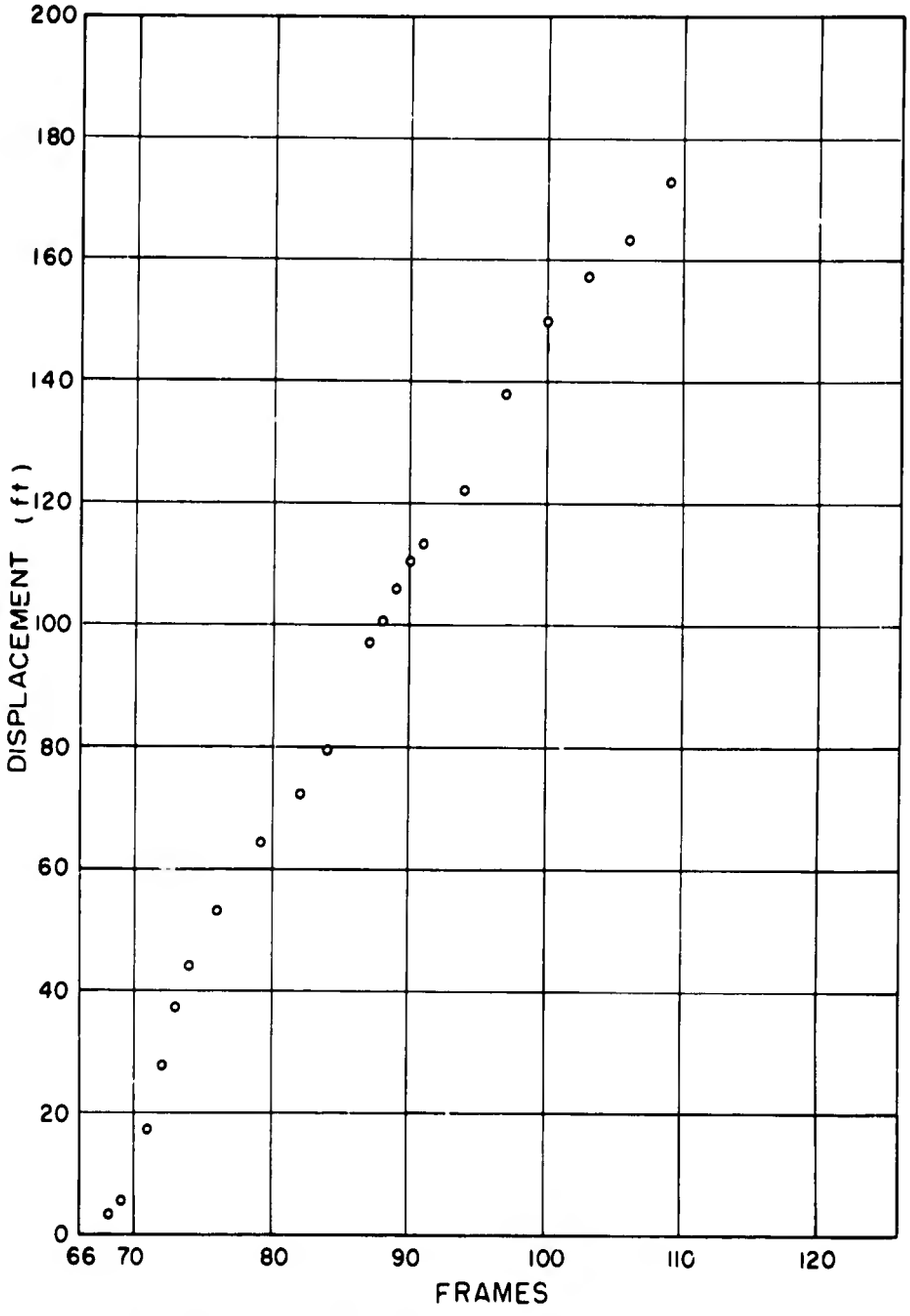

Fig. 3.12—Displacement-time data, Shot D, 1960 ft from ground zero, 100-ft elevation. Multiply frames by 10.60 to convert to milliseconds.

SECRET

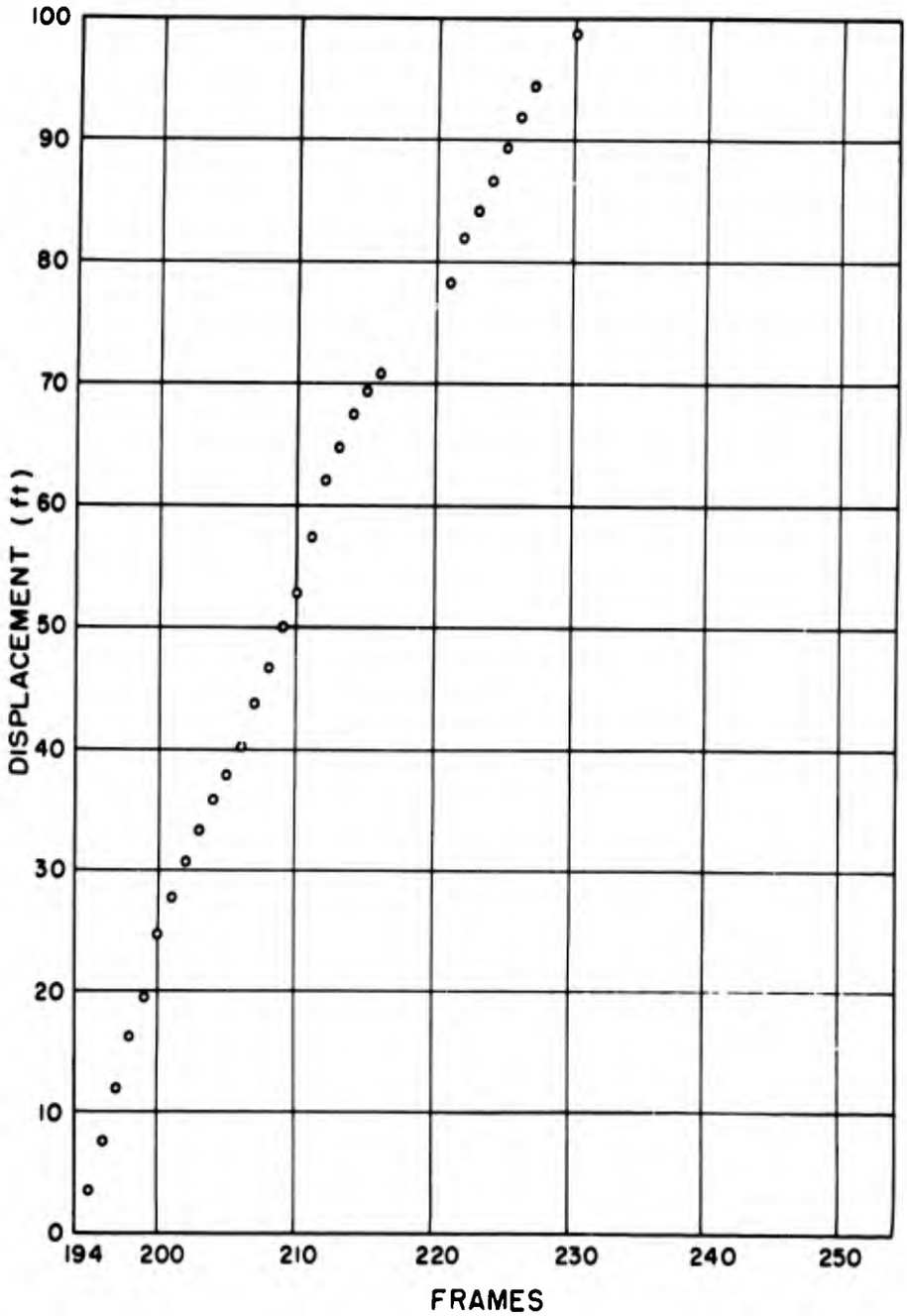

Fig. 3.13—Displacement-time data, Shot D, 3950 ft from ground zero, 100-ft elevation. Multiply frames by 10.60 to convert to milliseconds.

SECRET

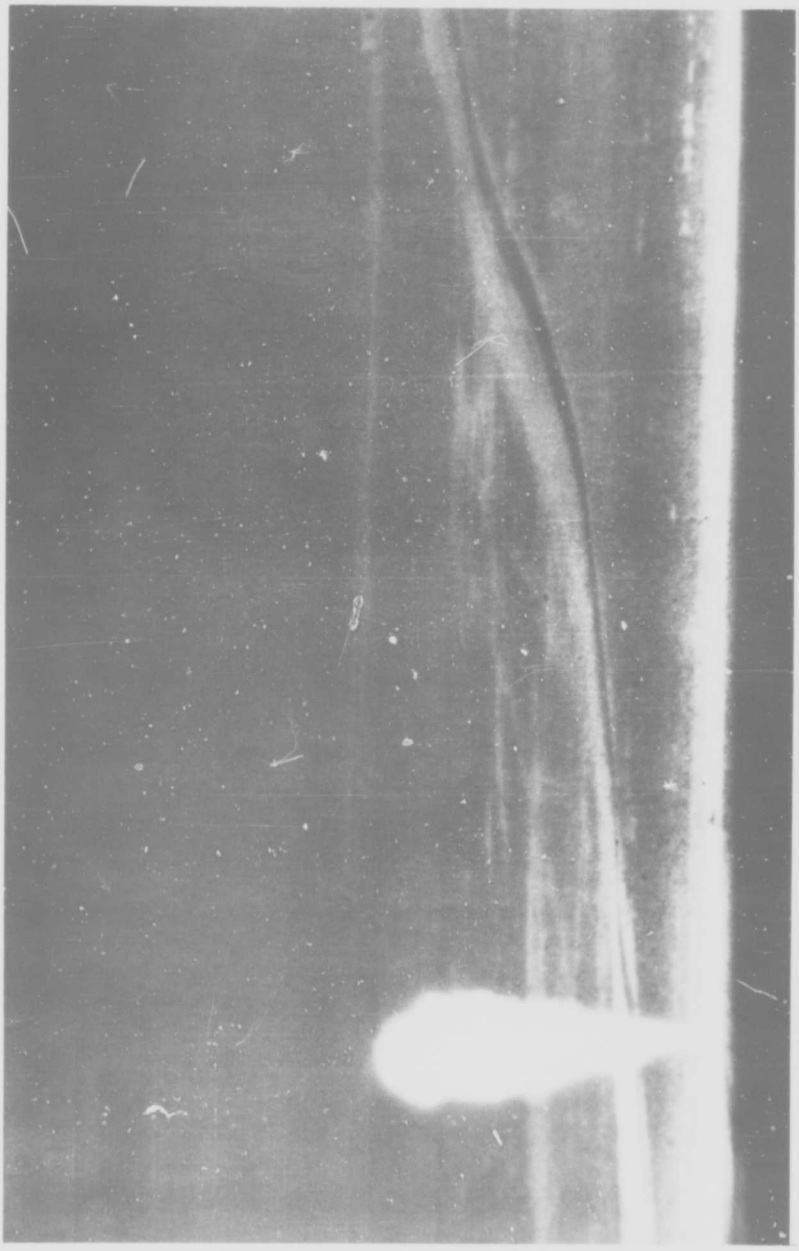

Fig. 3.14—JATO at zero time. Shot B, 1865 ft from ground zero.

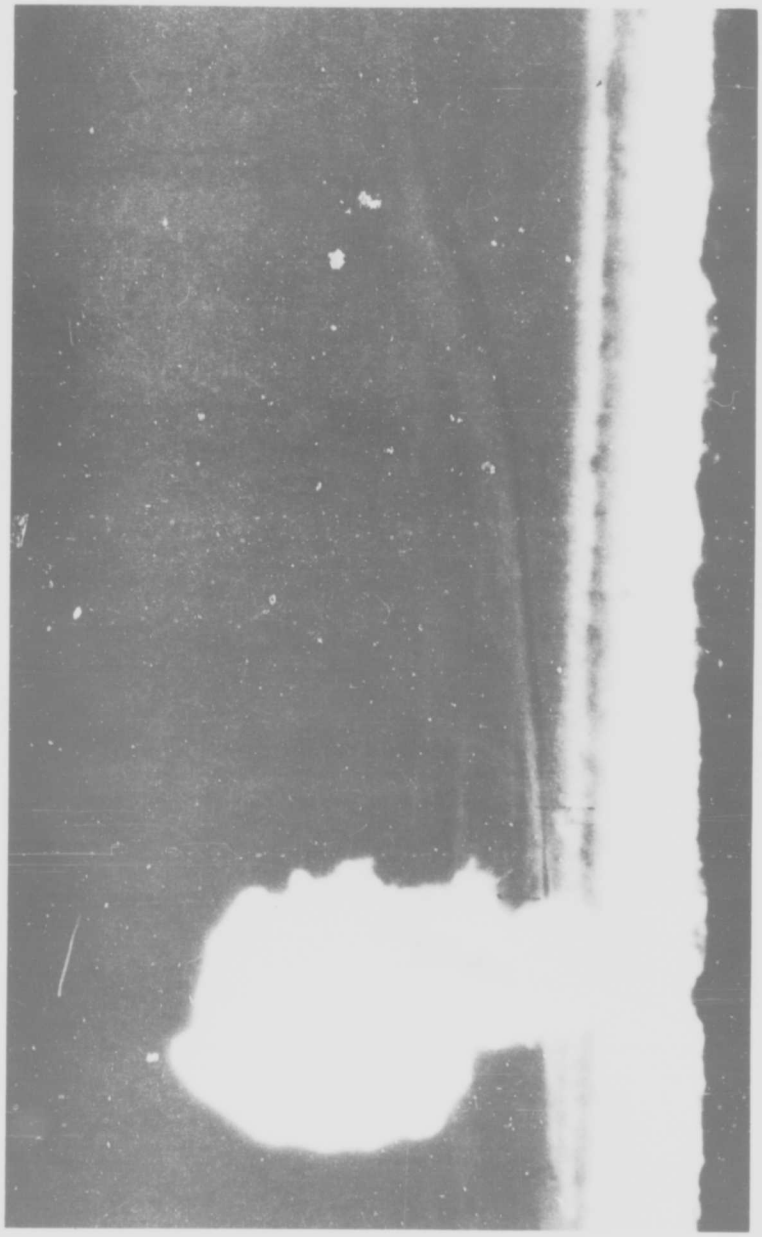

Fig. 3.15—JATO prior to shock arrival. Shot B, 1865 ft from ground zero.

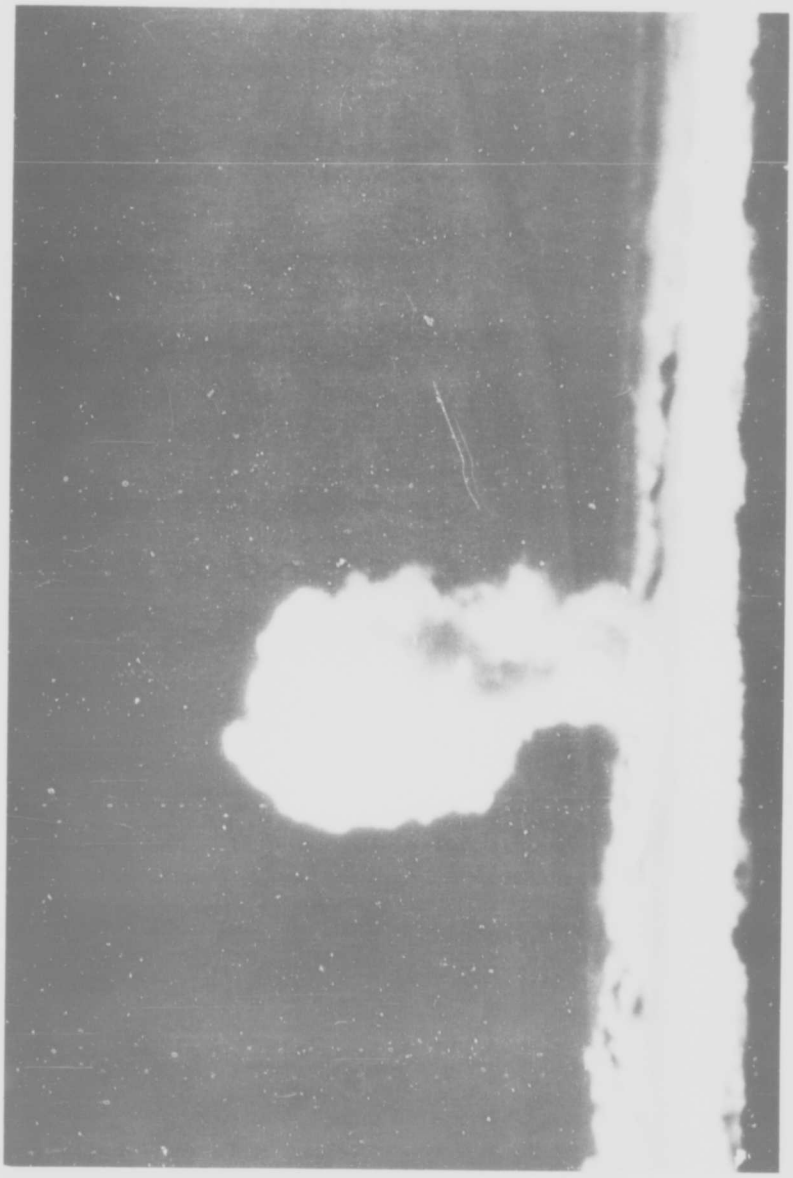

Fig. 3.16—JATO motion under influence of shock, Shot B, 1865 ft from ground zero.

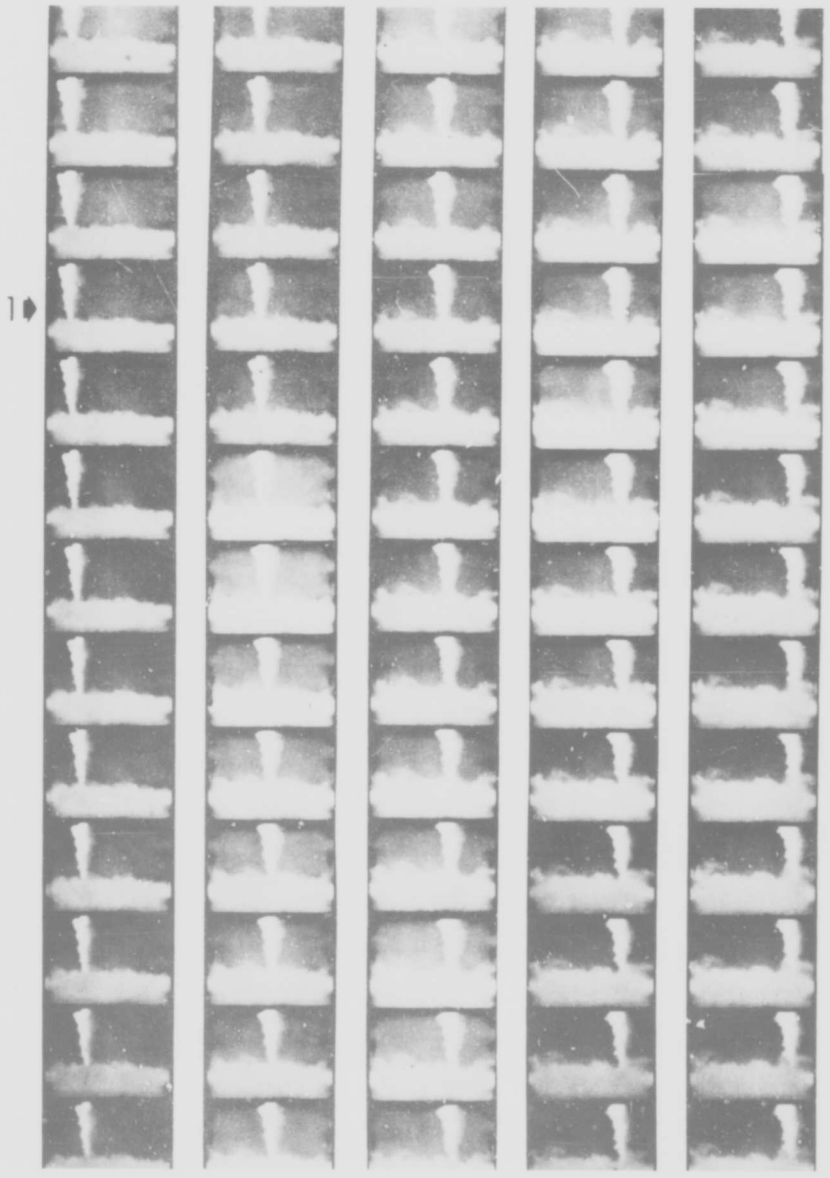

Fig. 3.17—JATO time sequence, Shot D, 3950 ft from ground zero.

sound velocity in still dry air at 0°C: 1086 ft/sec. No correction was made for wind velocity inasmuch as material velocity was corrected to still air. No correction was made for relative humidity; a sample correction showed that, during the shots under consideration, the low values of relative humidity actually recorded introduced no significant correction.

Using the best value of sound velocity obtainable from meteorological data, the ratio of material velocity to sound velocity u/c_0 was computed. Peak overpressure was then determined from the hydrodynamical relation given in Sec 1.3.

3.4 RESULTS

The results obtained using JATO units as the smoke source are summarized in Table 3.1. In this table, u_m refers to the material velocity before correction and u to the corrected value subsequently used in determining the overpressure. Distance from ground zero has been corrected for error in the point of detonation. The error in range is less than ±3 per cent; a study of the cumulative errors introduced by reading the record, timing, and sound velocity has resulted in placing a ±15 per cent limit on the pressure values. A more detailed analysis of the records and consequent better average material velocity would reduce this error somewhat, and a better knowledge of film speed would considerably reduce the limit of error. Figures 3.5 to 3.13 are original displacement-time data as measured from the contour plots. "Frames" refer to the number of frames after zero time. Conversion factors, for expressing the frame number in terms of milliseconds after zero time, are given for each curve.

The Shot-B 4000-ft record was underexposed, and dust obscured JATO motion on the Shot-C 2000-ft record.

Figures 3.14 to 3.16 are selected frames from the Operation Buster Shot-B record showing the general features of the JATO technique. Figure 3.14 shows the unit at zero time; Fig. 3.15 is the same JATO just before the shock wave arrives (the noticeable preshock dust is discussed in Chap. 5); and Fig. 3.16 shows the motion of the JATO cloud and the attendant dust raised by the shock wave.

Figure 3.17 is a time sequence showing the motion of the JATO cloud (Shot D); the frame rate is about 90 frames/sec. The numeral "1" indicates the first frame on which motion is observed.

CHAPTER 4

OPERATION JANGLE SHOTS

4.1 GENERAL

Difficulties with the JATO method became apparent over a period of time. Among these are the effects of the vertical velocity component in the smoke column, the possible drag due to the smoke mass in the lower part of the column, and the rather diffuse edges of the cloud which occasionally introduced large errors in reading the displacement of the cloud from frame to frame. In an attempt to reduce these effects a new method of smoke production was introduced for Operation Jangle.

An aerial smoke bomb was substituted for the JATO units. Fired vertically from a small mortar, placed in the ground, these bombs burst at an altitude of 250 to 350 ft, depending on the length of the mortar used. The bursting charge produced a smoke puff about 10 ft in diameter with rather sharply defined edges. In addition to the advantage of a small well-defined cloud, other advantages seem apparent when comparing the JATO and smoke-bomb methods (see Appendix B).

Blast lines of smoke bombs were installed on both the surface and underground shots. These lines are very simple to install, and, for the same expenditure of time and money, many more points may be determined by smoke bombs than by JATO units.

4.2 INSTRUMENTATION

For the surface shot a line of 11 mortars was installed as shown in Fig. 4.1. Short mortars (producing a burst at 250 ft) were placed 150 ft apart, starting at 600 ft from ground zero. These mortars were supplemented by a long mortar (350-ft height of burst) at the 900- and 1200-ft stations. The mortars were fixed at H−5 sec. Of the 11 planned bursts, only 5 had detonated prior to the shock arrival, 2 detonated after the shock had passed, and 4 failed to detonate. It is believed that the method of firing mortars in parallel was the direct cause of these failures.

Two Mitchell high-speed 35-mm cameras were located at a range of 10,450 ft from ground zero as shown in Fig. 4.2. The section of the blast line nearest ground zero was covered by a 12-in. lens, and the outer stations (farthest two mortars) were viewed with a 24-in. lens. Both cameras were operated at f/8 with a 15° shutter sector.

Instrumentation for the underground shot was enlarged over that for the surface shot. A line of 18 mortars was installed running from 450 ft from ground zero out to 1950 ft (Fig. 4.3). At each station both a long and a short mortar were installed in order to obtain pressure at two altitudes. Only 4 out of 18 planned bursts were missing on the film, and of these 4, at least 3 may have been outside the field of view of the cameras. Firing each mortar from a separate relay resulted in this improvement over the surface shot.

The two cameras were located as shown in Fig. 4.4.

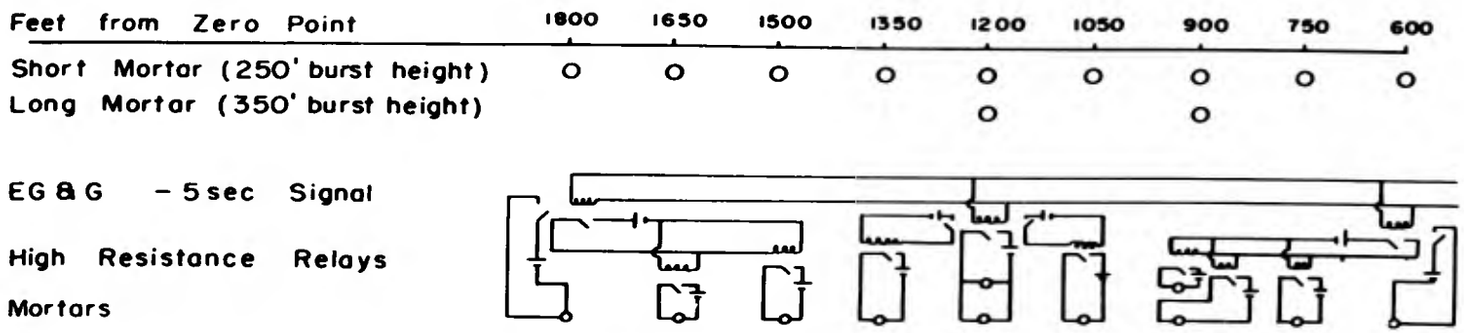

Fig. 4.1—Mortar line, Operation Jangle surface shot.

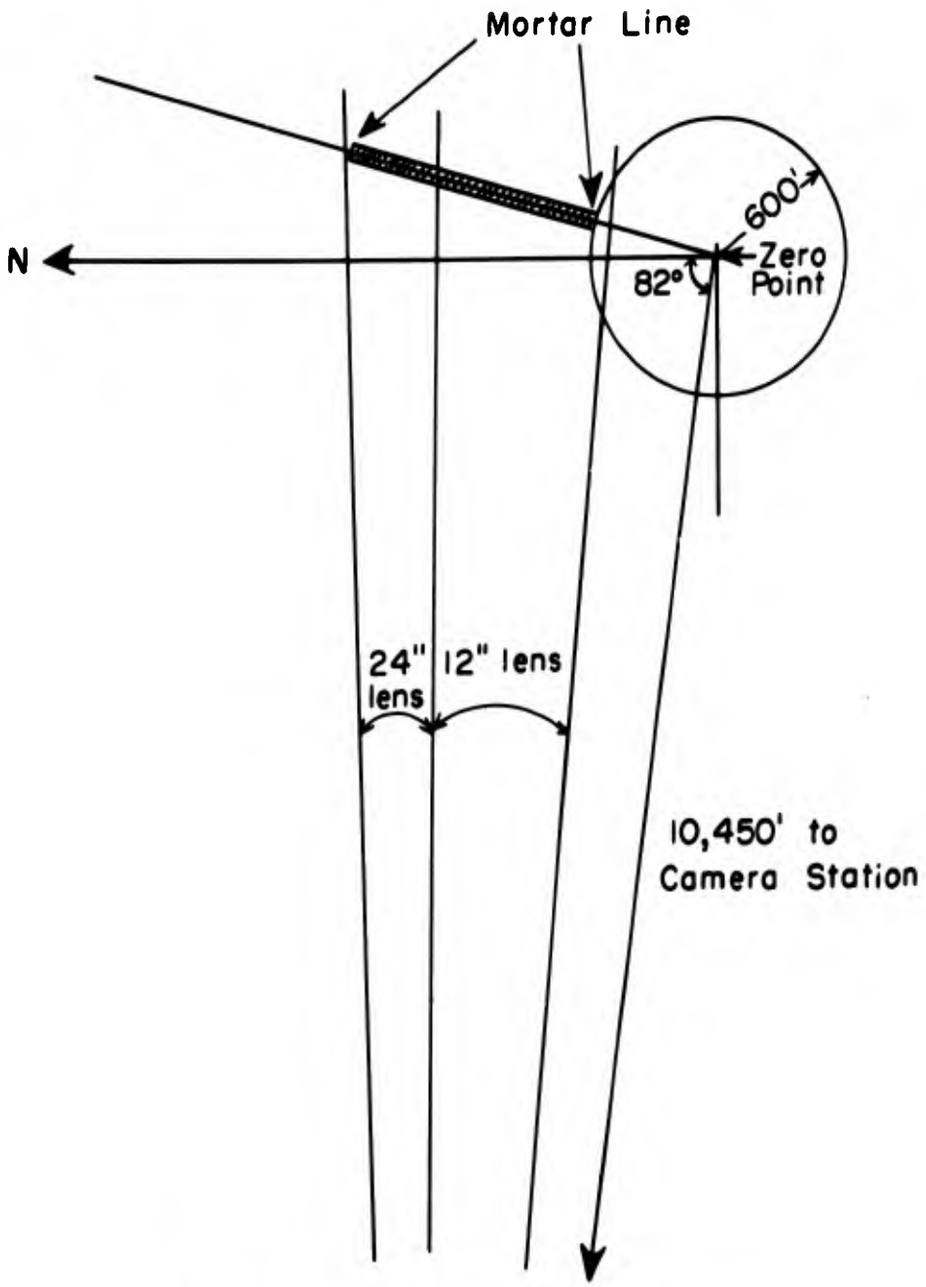

Fig. 4.2—Camera mortar-line orientation, Operation Jangle surface shot.

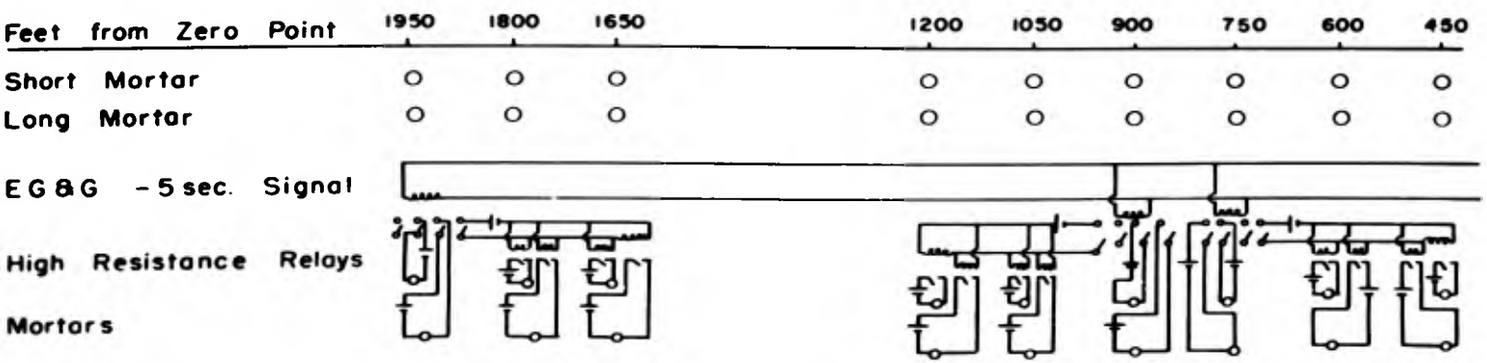

Fig. 4.3—Mortar line, Operation Jangle underground shot.

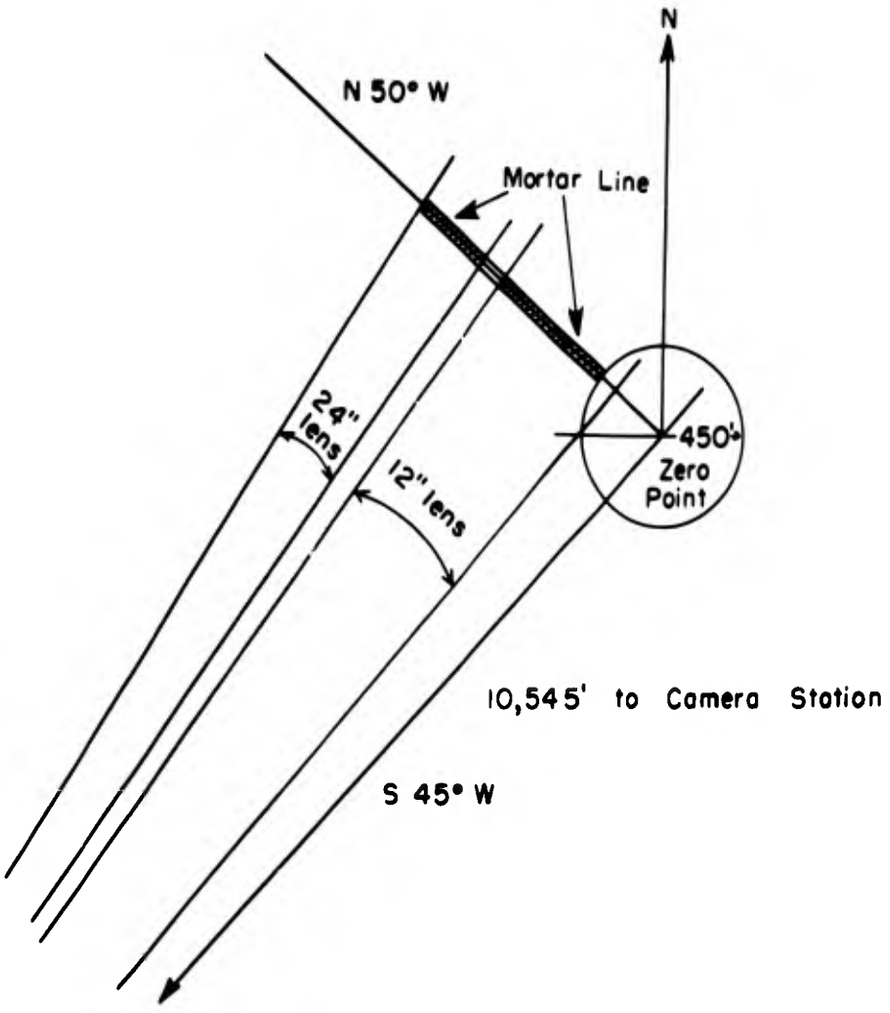

Fig. 4.4—Camera mortar-line orientation, Operation Jangle underground shot.

SECRET

Table 4.1—SUMMARY OF MASS-MOTION DATA, OPERATION JANGLE

Shot*	Unit	Height of measurement, ft	Measured material velocity u_m, ft/sec	True material velocity u, ft/sec	Temperature, °C	Sound velocity, ft/sec	u/c_0	P_s/P_0	Ambient pressure, psi	Peak overpressure, psi	Distance from ground zero, ft	Time of arrival, sec
S	Smoke bomb	218	875	892	1.0	1088	0.820	2.870	12.65	23.6	804	0.21
S	Smoke bomb	248	635	648	1.0	1088	0.596	2.200	12.65	15.2	997	0.31
S	Smoke bomb	300	543	555	1.0	1088	0.510	1.975	12.65	12.3	1304	0.51
S	Smoke bomb	234	339	348	1.0	1088	0.320	1.545	12.65	6.9	1686	0.79
S	Mortar	15	766	780	1.0	1088	0.718	2.550	12.65	19.6	750	0.20
S	Mortar	15	555	568	1.0	1088	0.523	2.010	12.65	12.8	1050	0.29
U	Smoke bomb	375	1041	1038	14.5	1115	0.931	3.220	12.65	28.1	434	0.15
U	Smoke bomb	286	904	901	14.5	1115	0.810	2.835	12.65	23.2	510	0.18
U	Smoke bomb	350	863	860	14.5	1115	0.772	2.715	12.65	21.7	524	0.19
U	Smoke bomb	261	704	701	14.5	1115	0.630	2.295	12.65	16.4	636	0.27
U	Smoke bomb	340	602	599	14.5	1115	0.537	2.045	12.65	13.2	699	0.31
U	Smoke bomb	266	590	587	14.5	1115	0.527	2.015	12.65	12.8	755	0.34
U	Smoke bomb	346	459	456	14.5	1115	0.409	1.735	12.65	9.3	926	0.47
U	Smoke bomb	340	333	330	14.5	1115	0.296	1.495	12.65	6.3	1007	0.51
U	Smoke bomb	288	358	355	14.5	1115	0.318	1.535	12.65	6.8	1124	0.63
U	Smoke bomb	348	308	305	14.5	1115	0.273	1.450	12.65	5.7	1124	0.64
U	Smoke bomb	320	252	249	14.5	1115	0.223	1.360	12.65	4.6	1185	0.68
U	Smoke bomb	190	320	317	14.5	1115	0.284	1.470	12.65	5.9	1450	
U	Smoke bomb	264	193	190	14.5	1115	0.171	1.270	12.65	3.4	1806	
U	Smoke bomb	365	184	181	14.5	1115	0.162	1.250	12.65	3.2	1832	
U	Mortar	15	1117	1114	14.5	1115	1.000	3.450	12.65	31.0	450	0.14
U	Mortar	15	700	697	14.5	1115	0.625	2.280	12.65	16.2	605	0.26
U	Mortar	15	575	572	14.5	1115	0.513	1.985	12.65	12.5	742	0.34
U	Mortar	15	465	462	14.5	1115	0.411	1.740	12.65	9.4	902	0.47
U	Mortar	15	360	357	14.5	1115	0.320	1.545	12.65	6.9	1052	0.57
U	Mortar	15	304	301	14.5	1115	0.270	1.445	12.65	5.6	1207	0.70

*S, surface shot; U, underground shot.

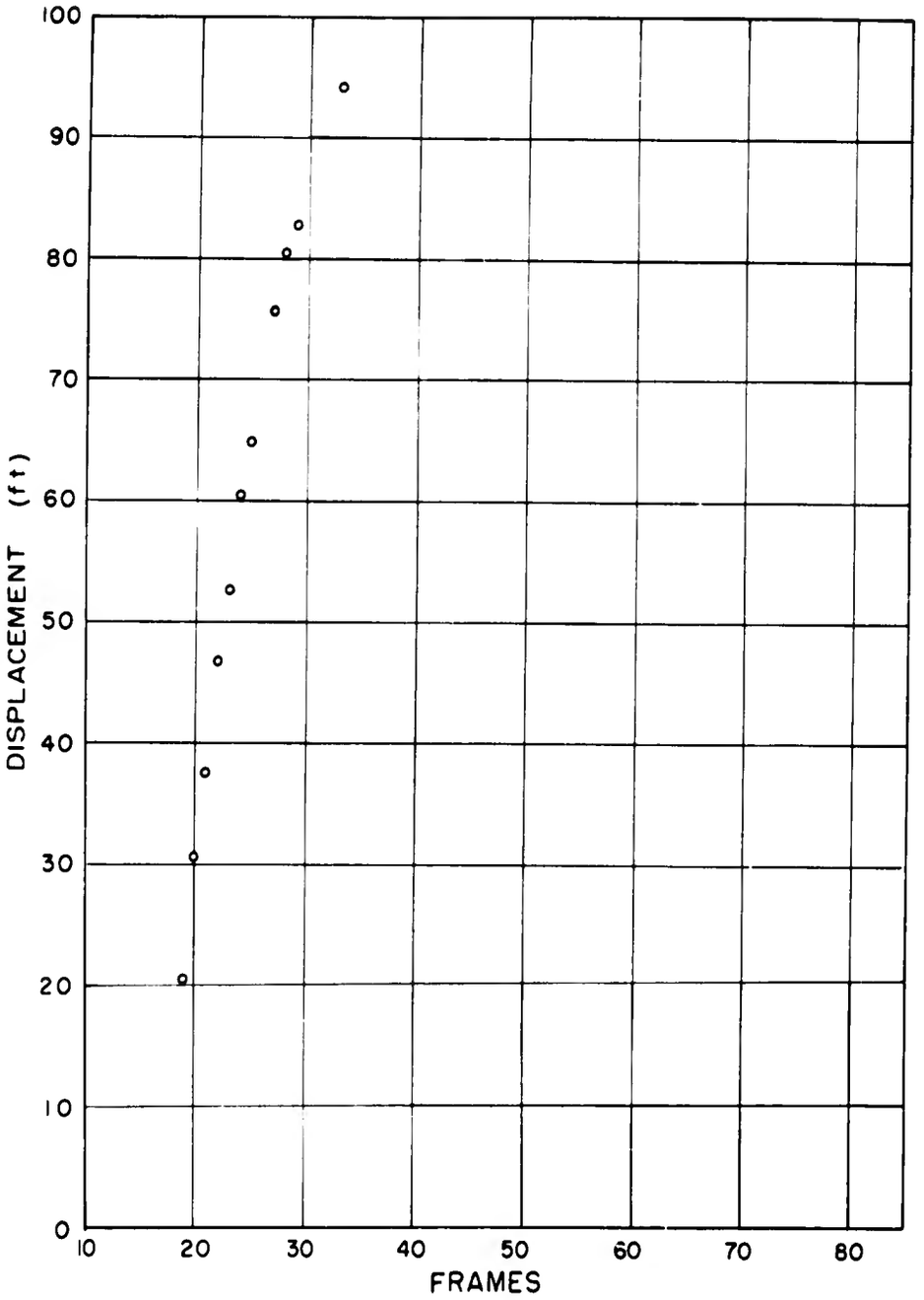

Fig. 4.5—Displacement-time data, surface shot, 750 ft from ground zero, mortar smoke. Multiply frames by 11.20 to convert to milliseconds.

SECRET

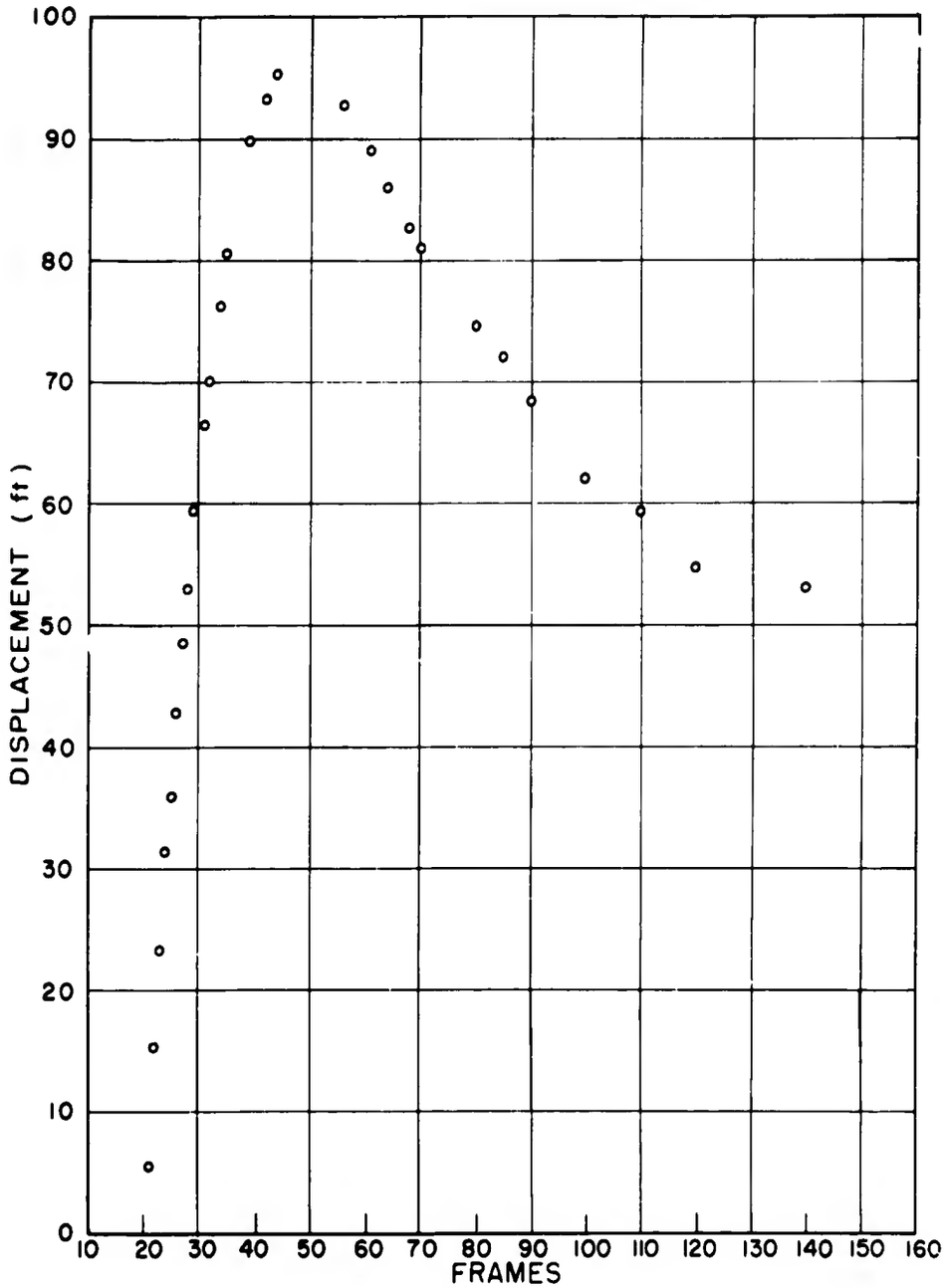

Fig. 4.6—Displacement-time data, surface shot, 804 ft from ground zero, puff. Multiply frames by 11.20 to convert to milliseconds.

SECRET

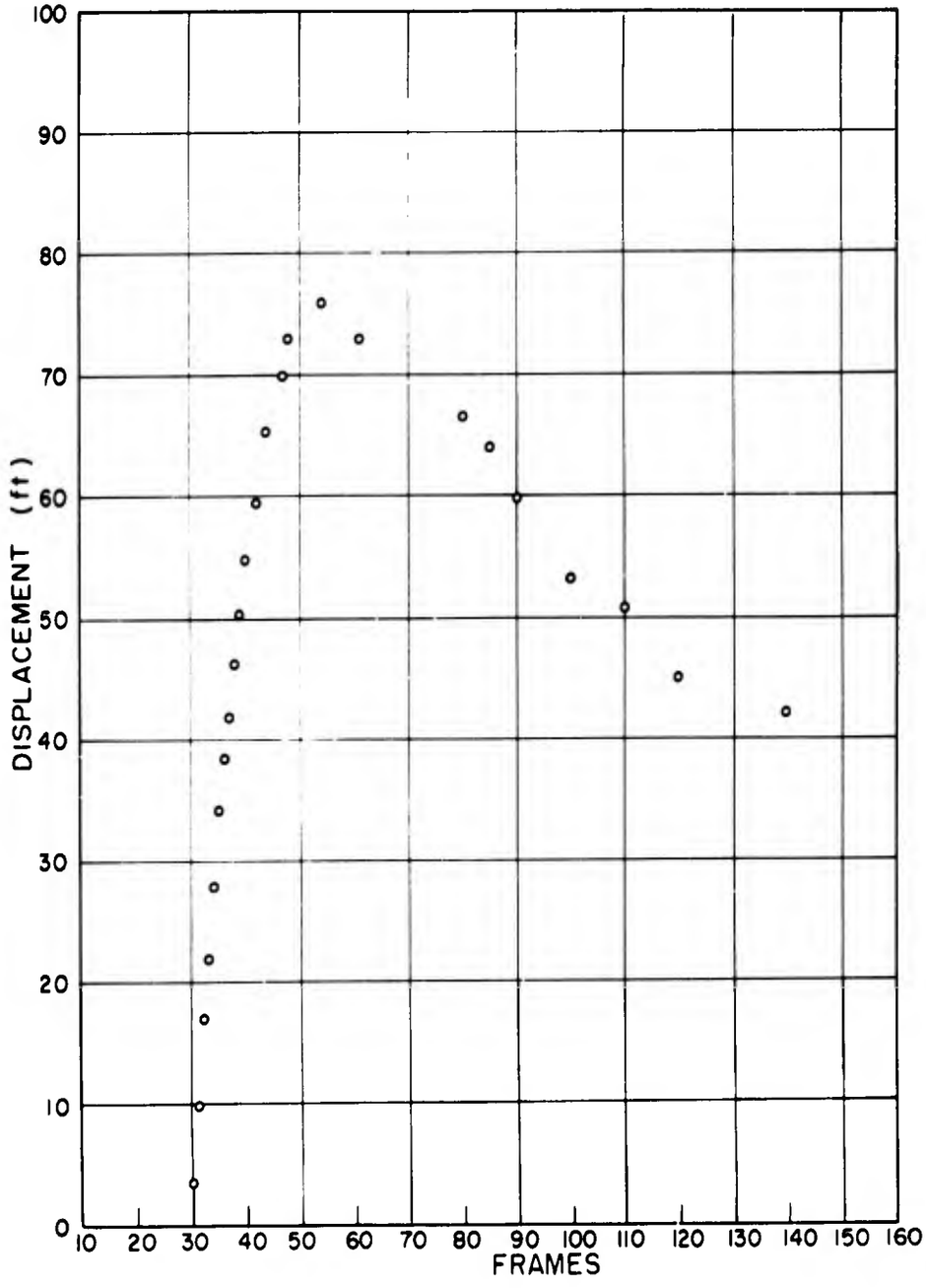

Fig. 4.7—Displacement-time data, surface shot, 997 ft from ground zero, puff. Multiply frames by 11.20 to convert to milliseconds.

SECRET

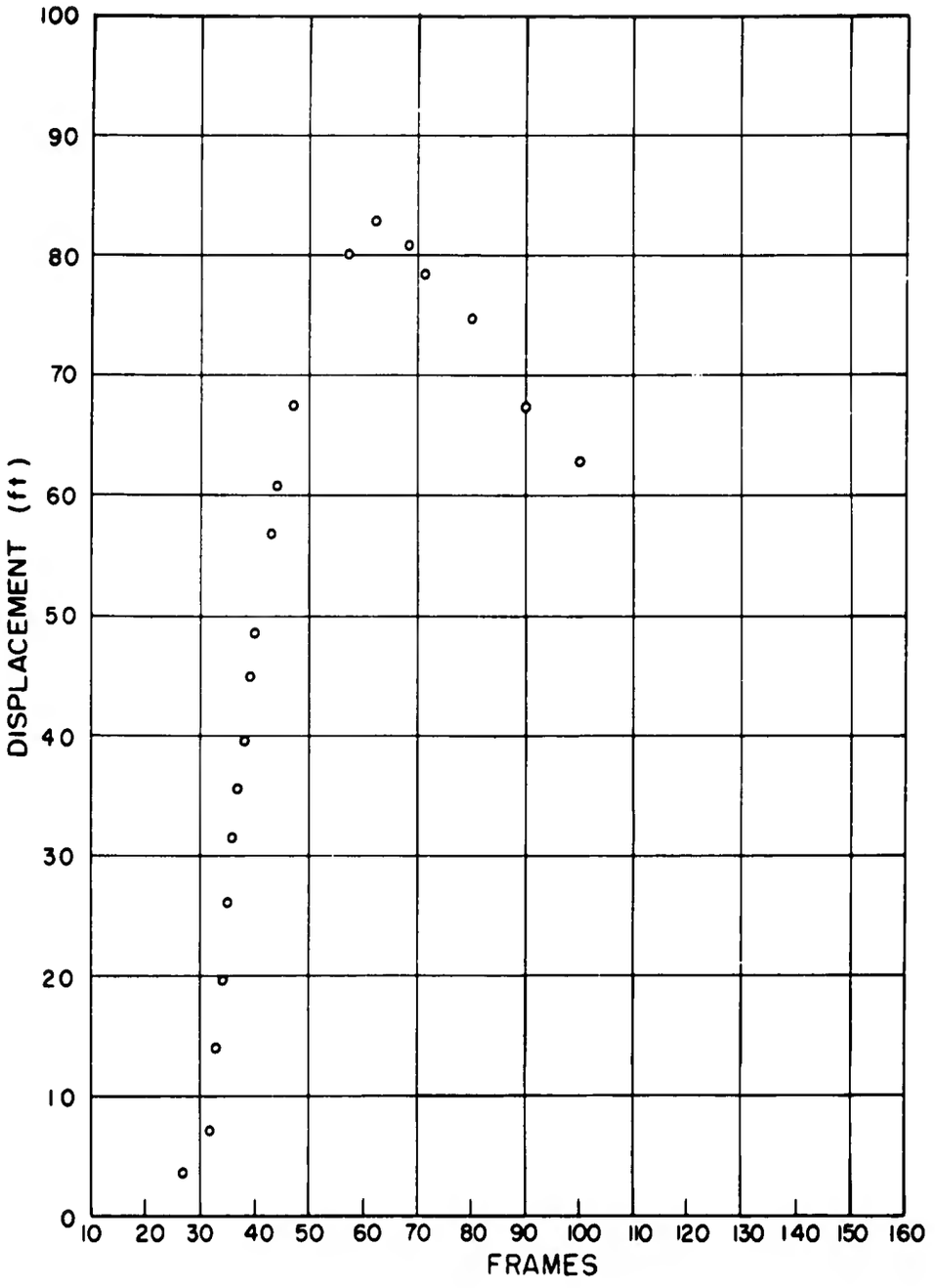

Fig. 4.8—Displacement-time data, surface shot, 1050 ft from ground zero, mortar smoke. Multiply frames by 11.20 to convert to milliseconds.

SECRET

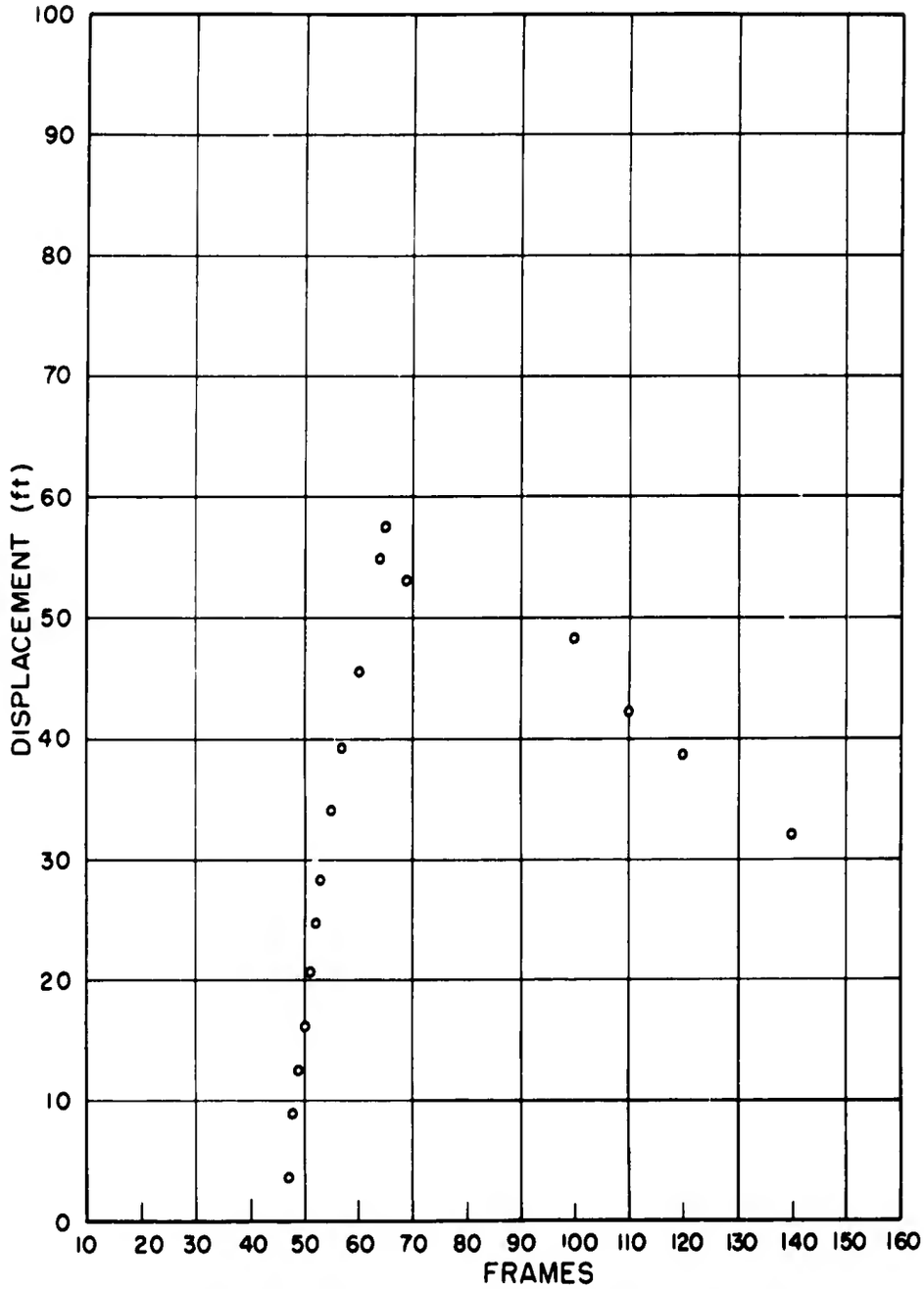

Fig. 4.9—Displacement-time data, surface shot, 1304 ft from ground zero, puff. Multiply frames by 11.20 to convert to milliseconds.

SECRET

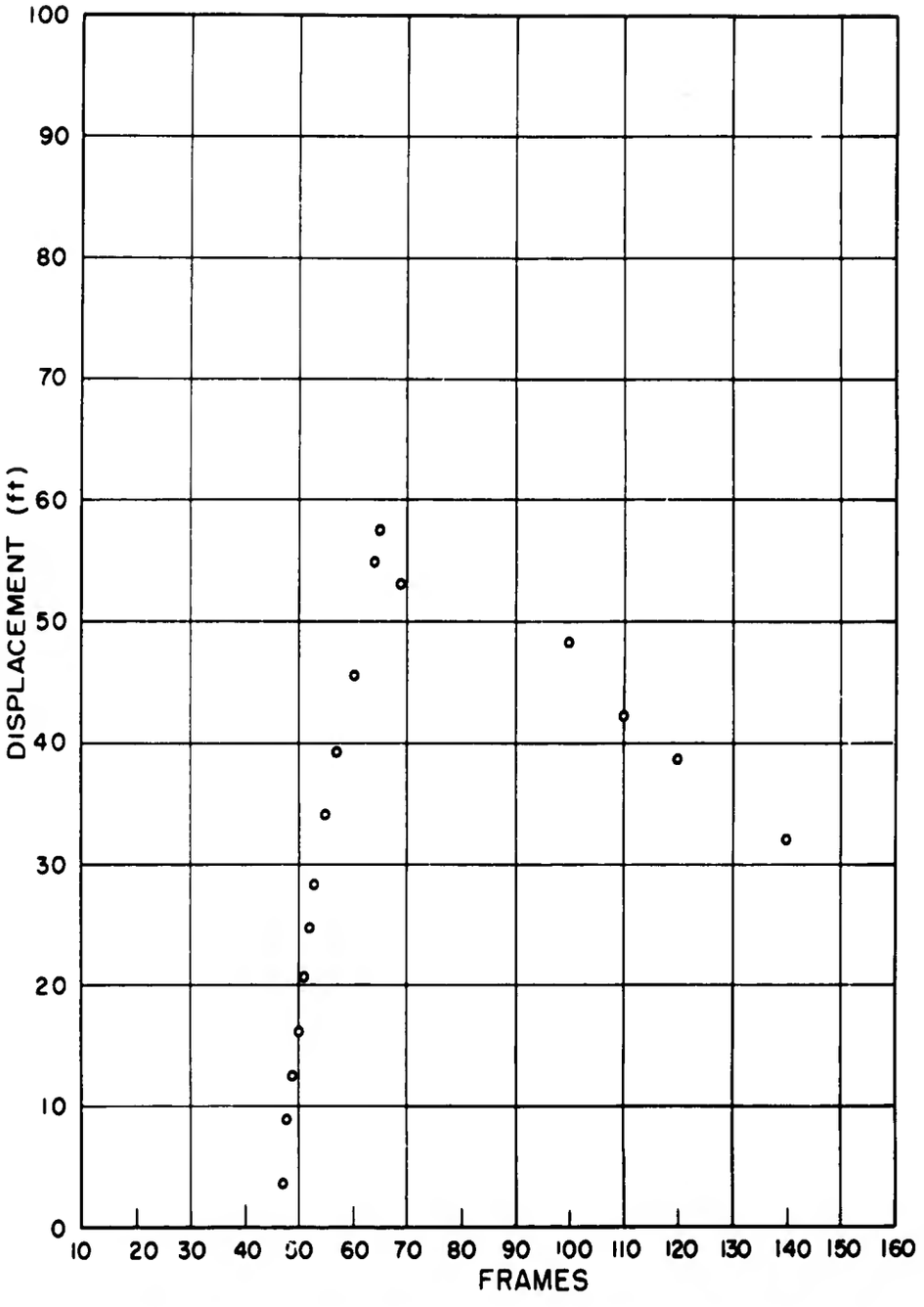

Fig. 4.9—Displacement-time data, surface shot, 1304 ft from ground zero, puff. Multiply frames by 11.20 to convert to milliseconds.

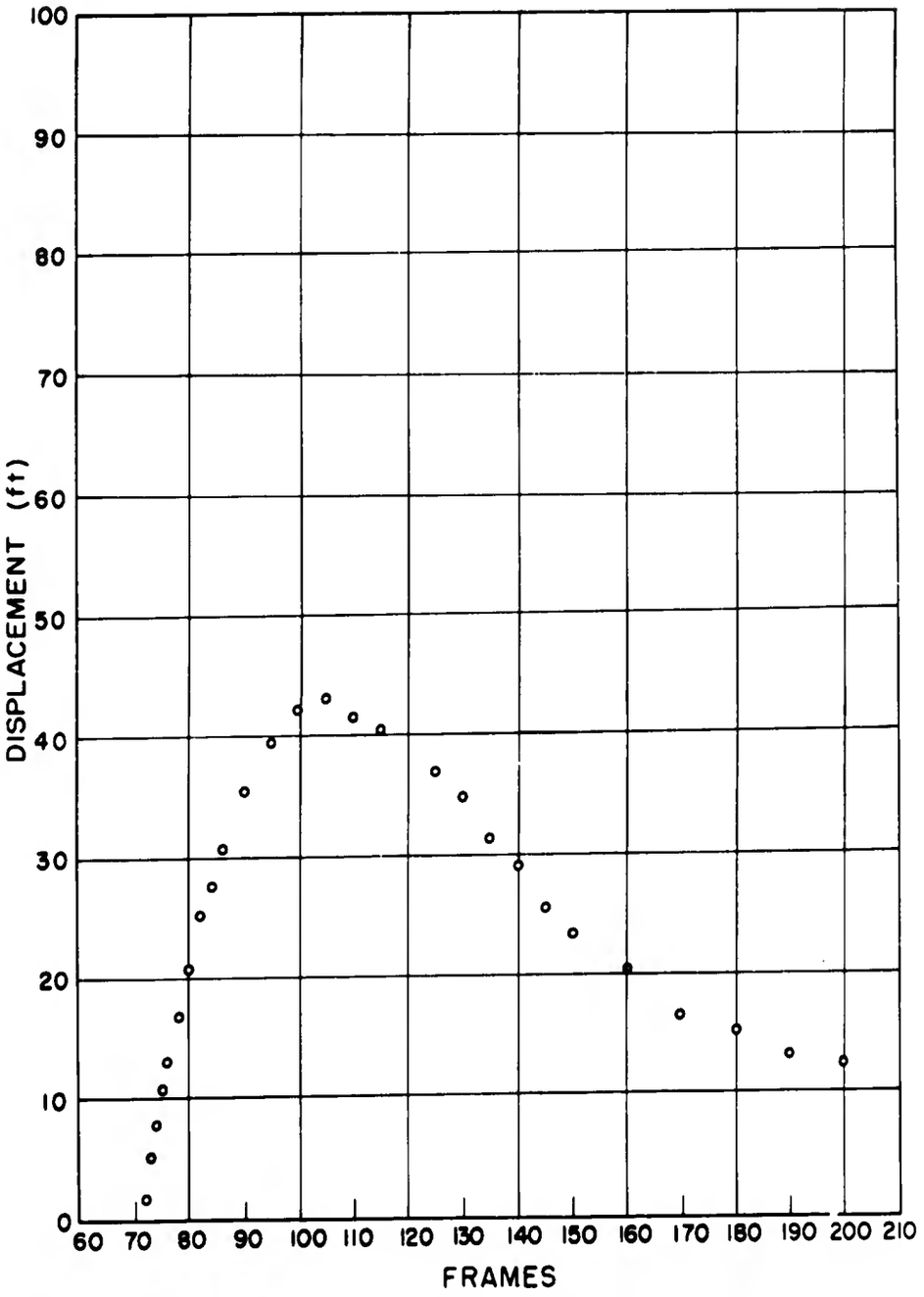

Fig. 4.10—Displacement-time data, surface shot, 1686 ft from ground zero, puff. Multiply frames by 11.20 to convert to milliseconds.

SECRET

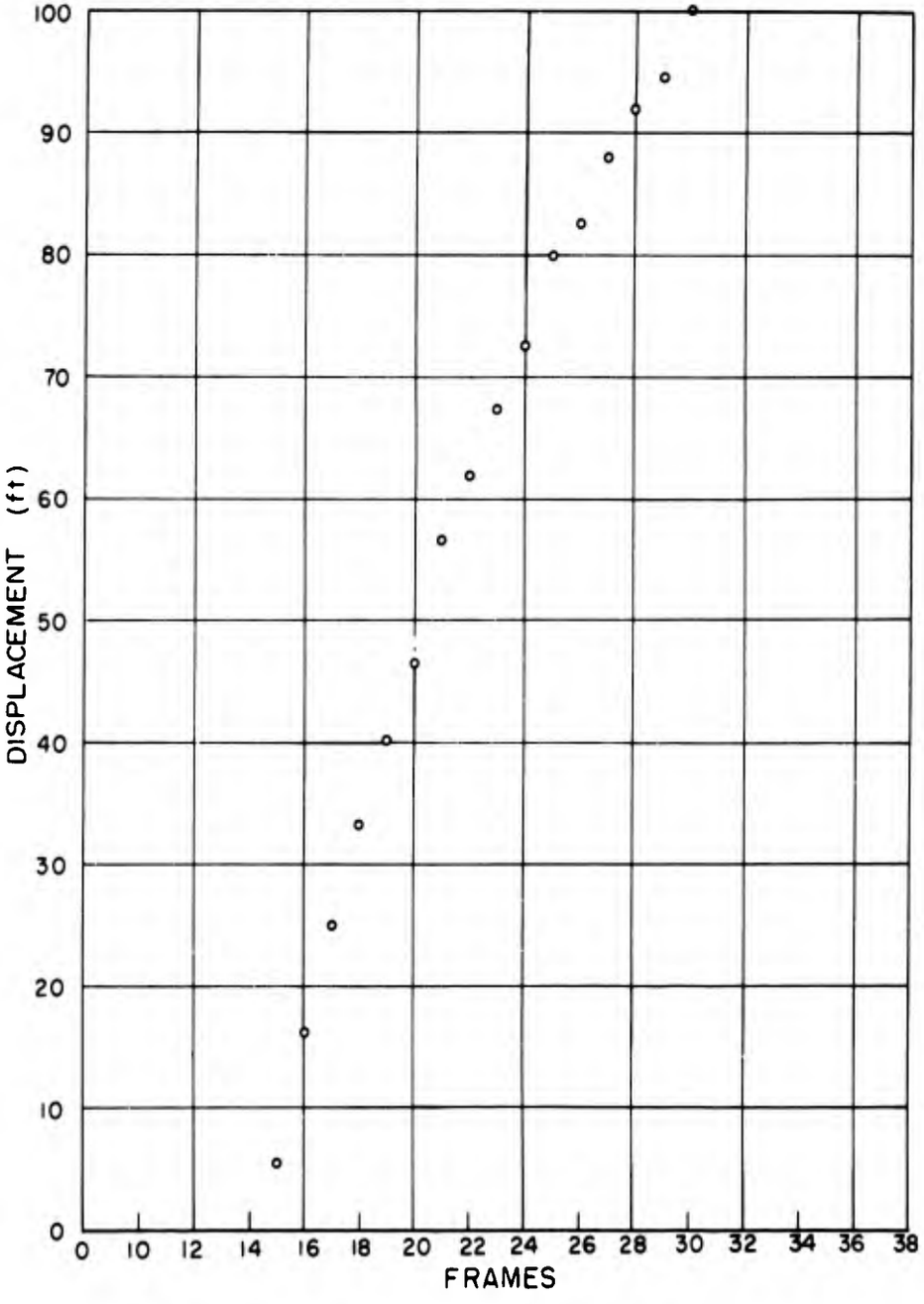

Fig. 4.11—Displacement-time data, underground shot, 434 ft from ground zero, puff. Multiply frames by 10.60 to convert to milliseconds.

SECRET

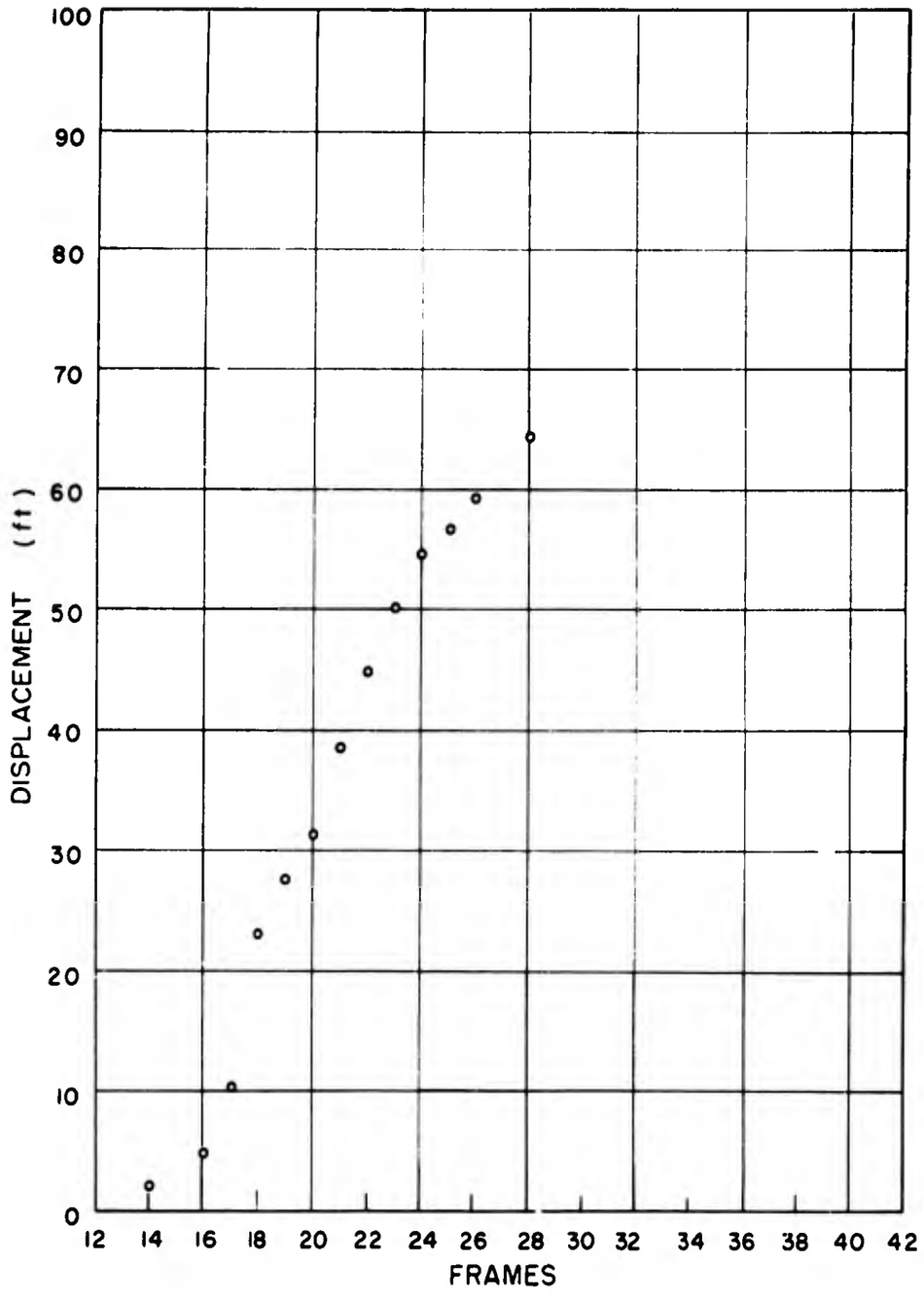

Fig. 4.12—Displacement-time data, underground shot, 450 ft from ground zero, mortar smoke. Multiply frames by 10.60 to convert to milliseconds.

SECRET

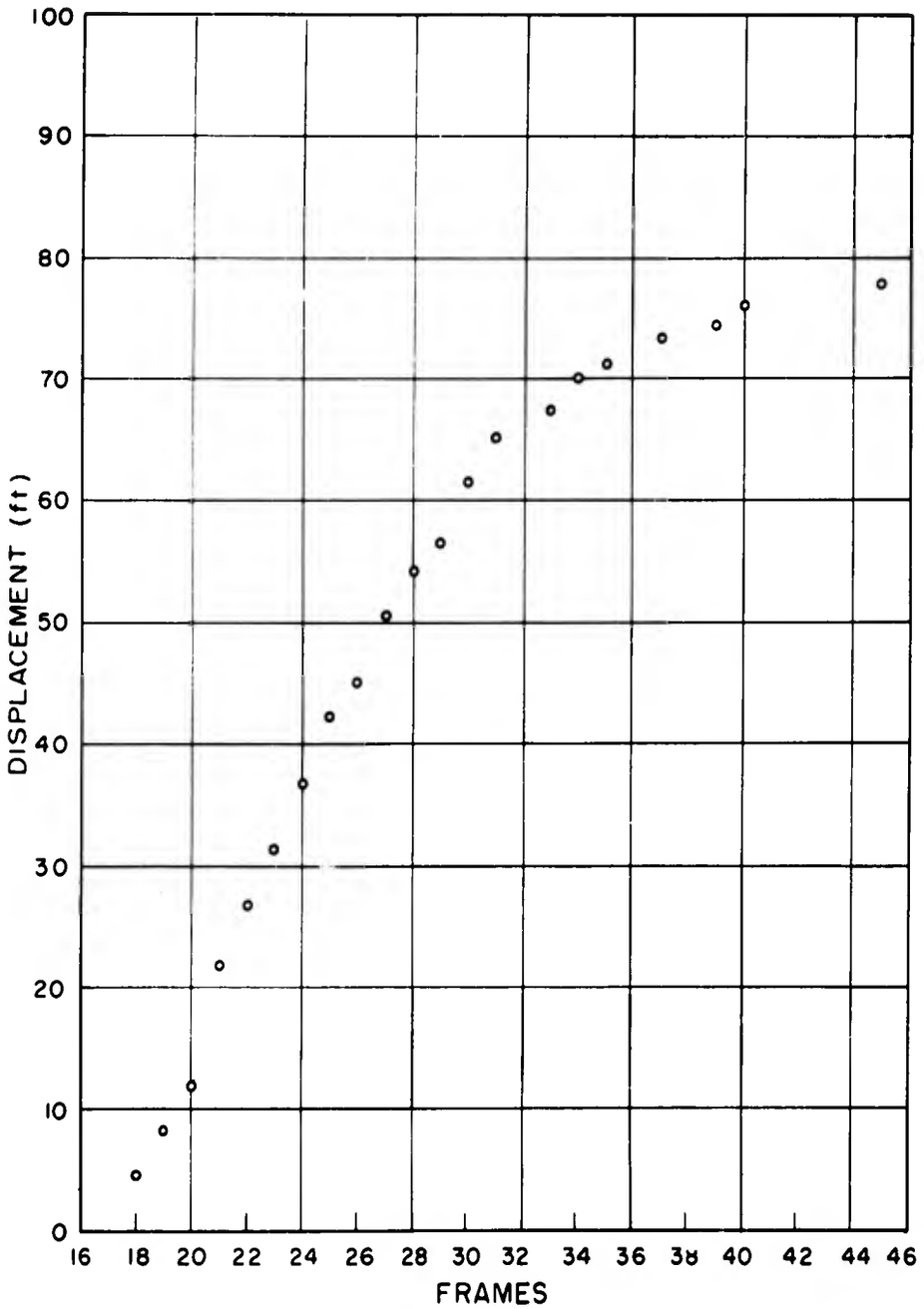

Fig. 4.13 — Displacement-time data, underground shot, 510 ft from ground zero, puff. Multiply frames by 10.60 to convert to milliseconds.

SECRET

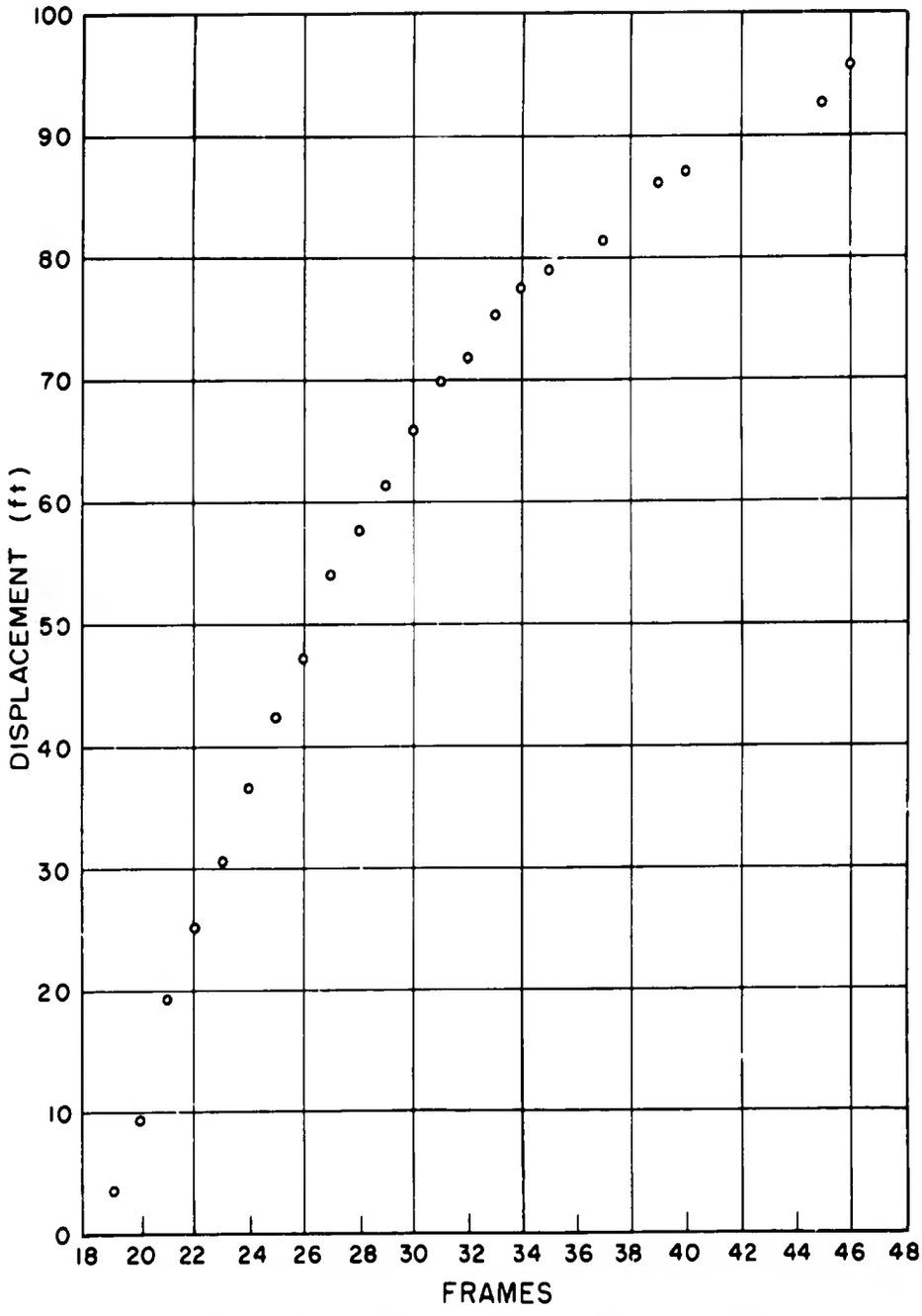

Fig. 4.14—Displacement-time data, underground shot, 524 ft from ground zero, puff. Multiply frames by 10.60 to convert to milliseconds.

SECRET

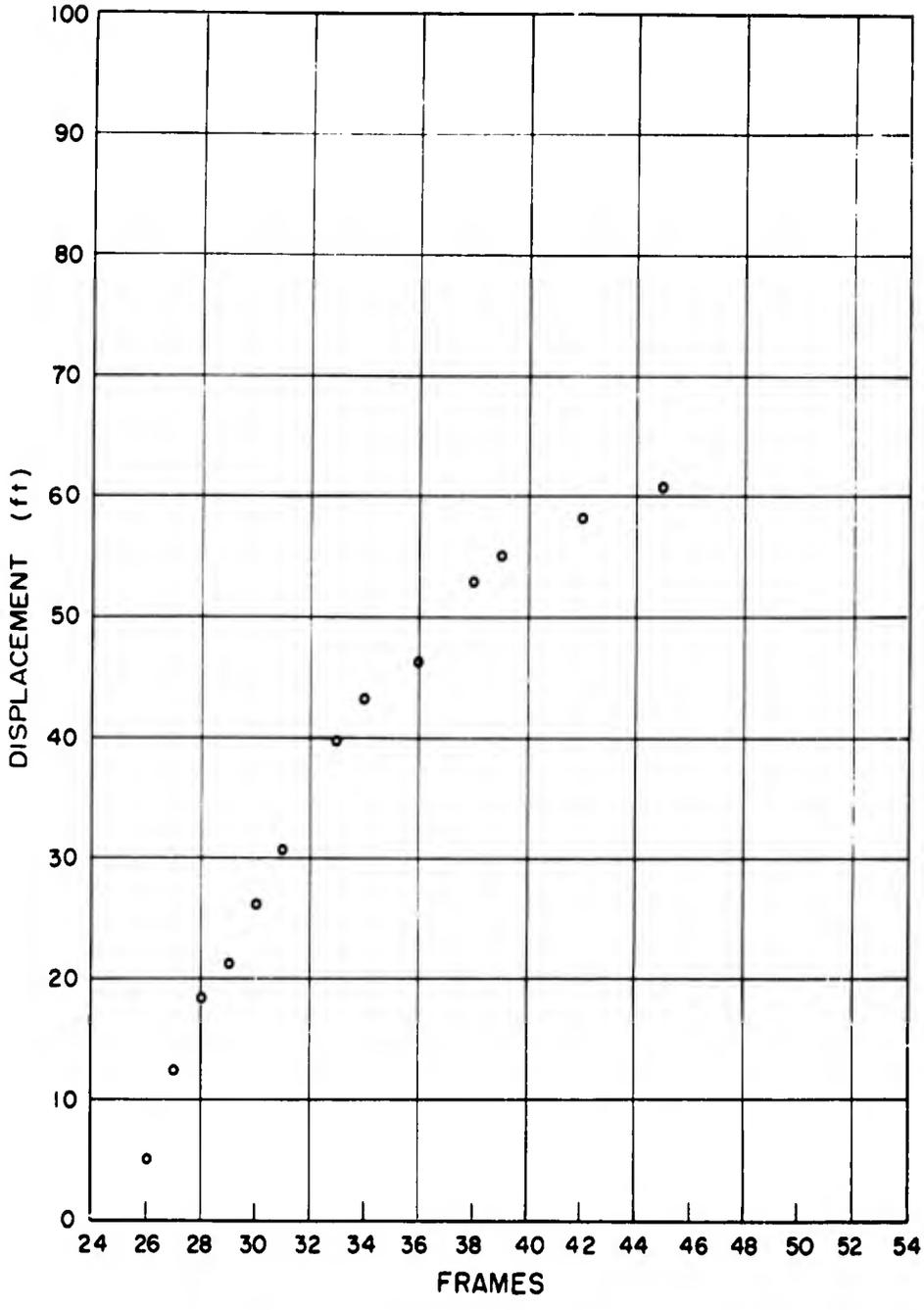

Fig. 4.15—Displacement-time data, underground shot, 605 ft from ground zero, mortar smoke. Multiply frames by 10.60 to convert to milliseconds.

SECRET

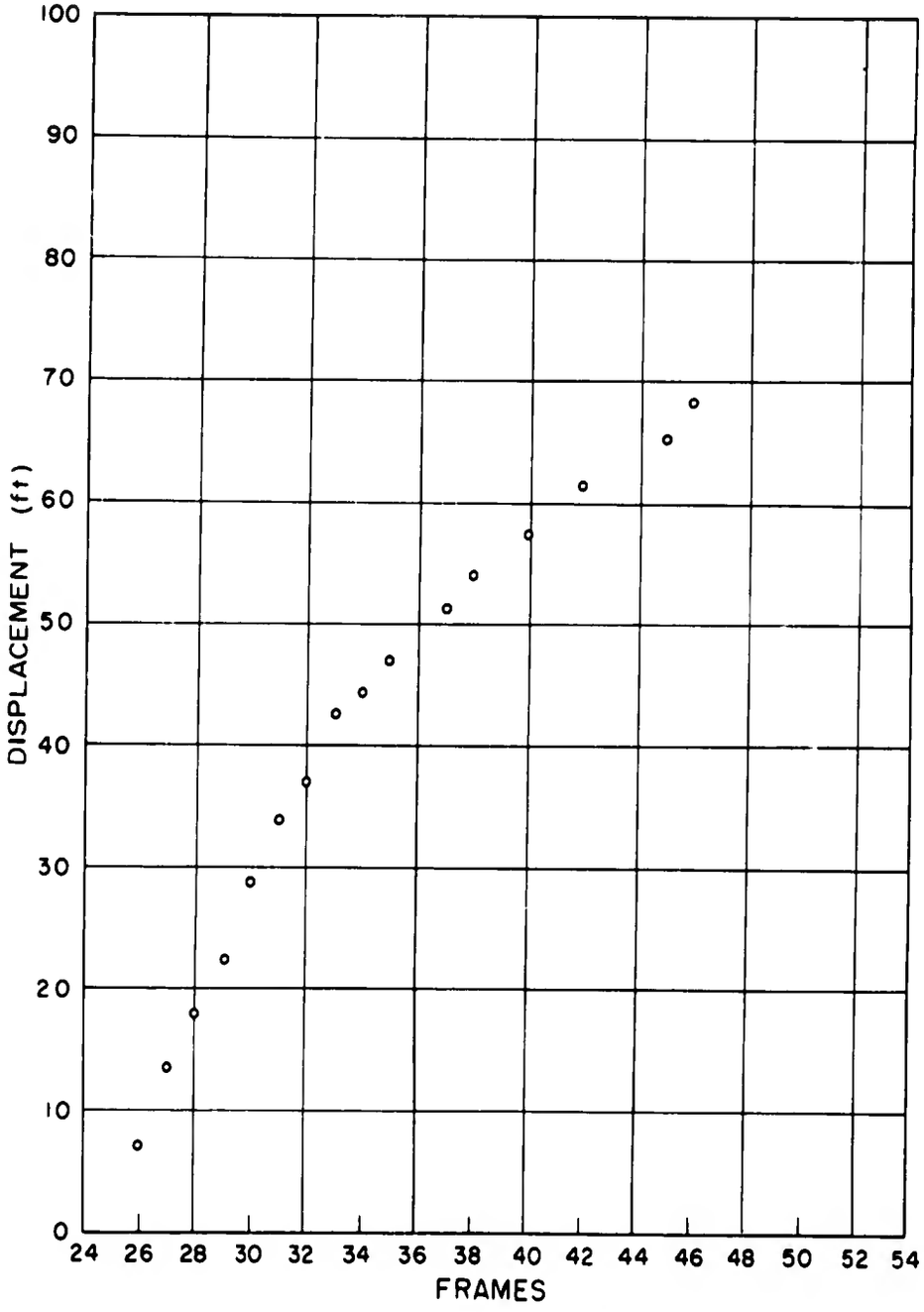

Fig. 4.16—Displacement-time data, underground shot, 636 ft from ground zero, puff. Multiply frames by 10.60 to convert to milliseconds.

SECRET

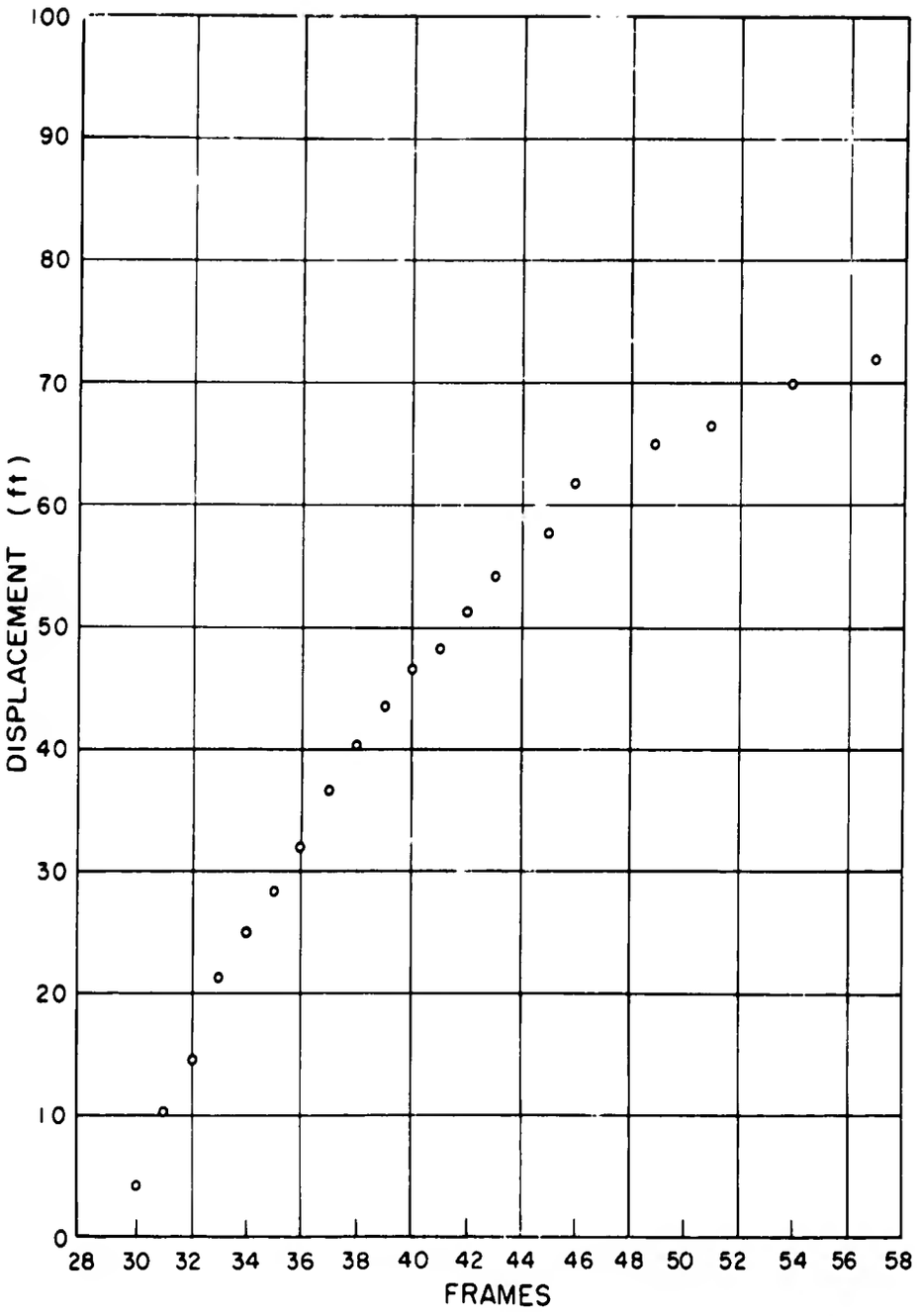

Fig. 4.17—Displacement-time data, underground shot, 699 ft from ground zero, puff. Multiply frames by 10.60 to convert to milliseconds.

SECRET

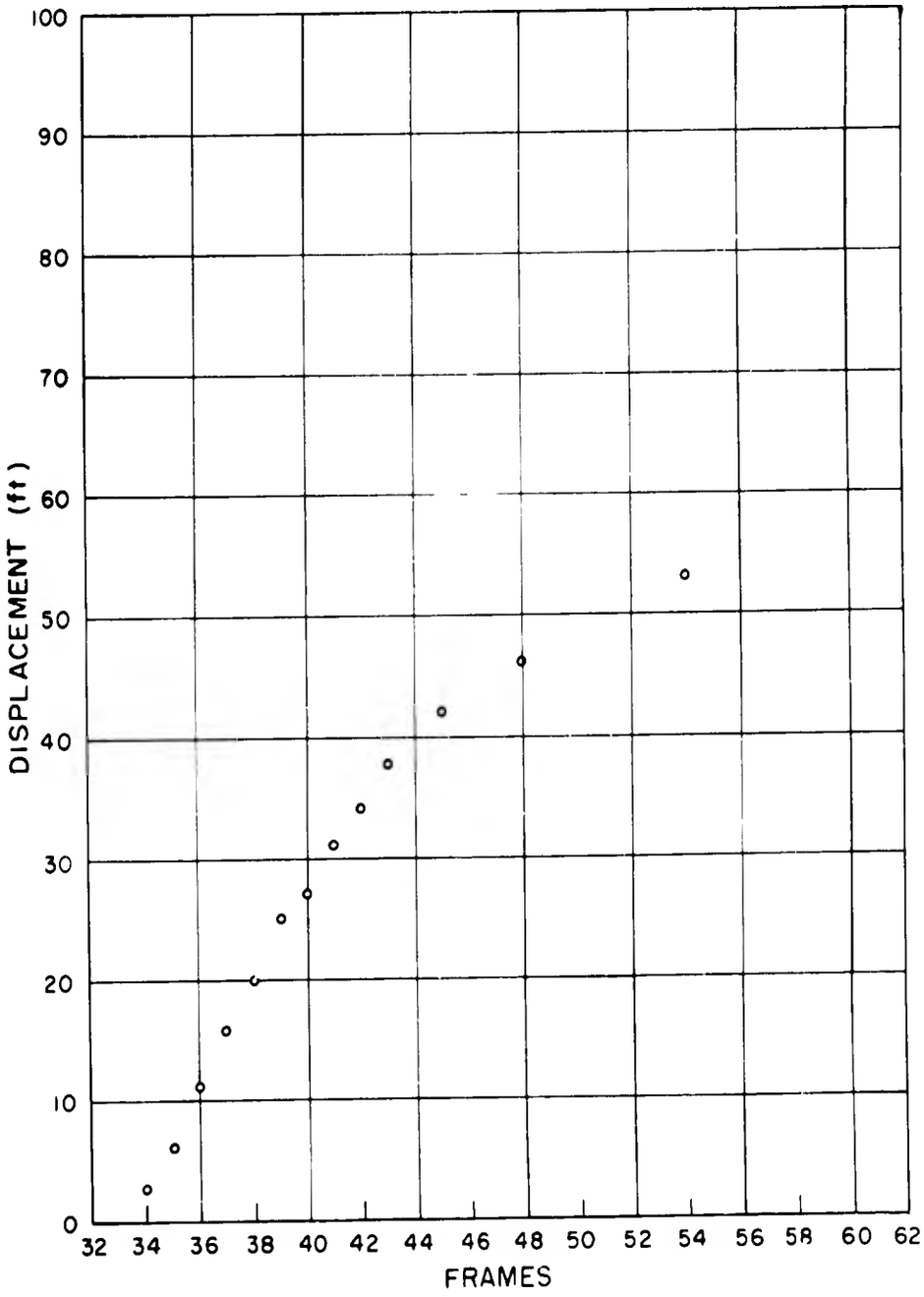

Fig. 4.18—Displacement-time data, underground shot, 742 ft from ground zero, mortar smoke. Multiply frames by 10.60 to convert to milliseconds.

SECRET

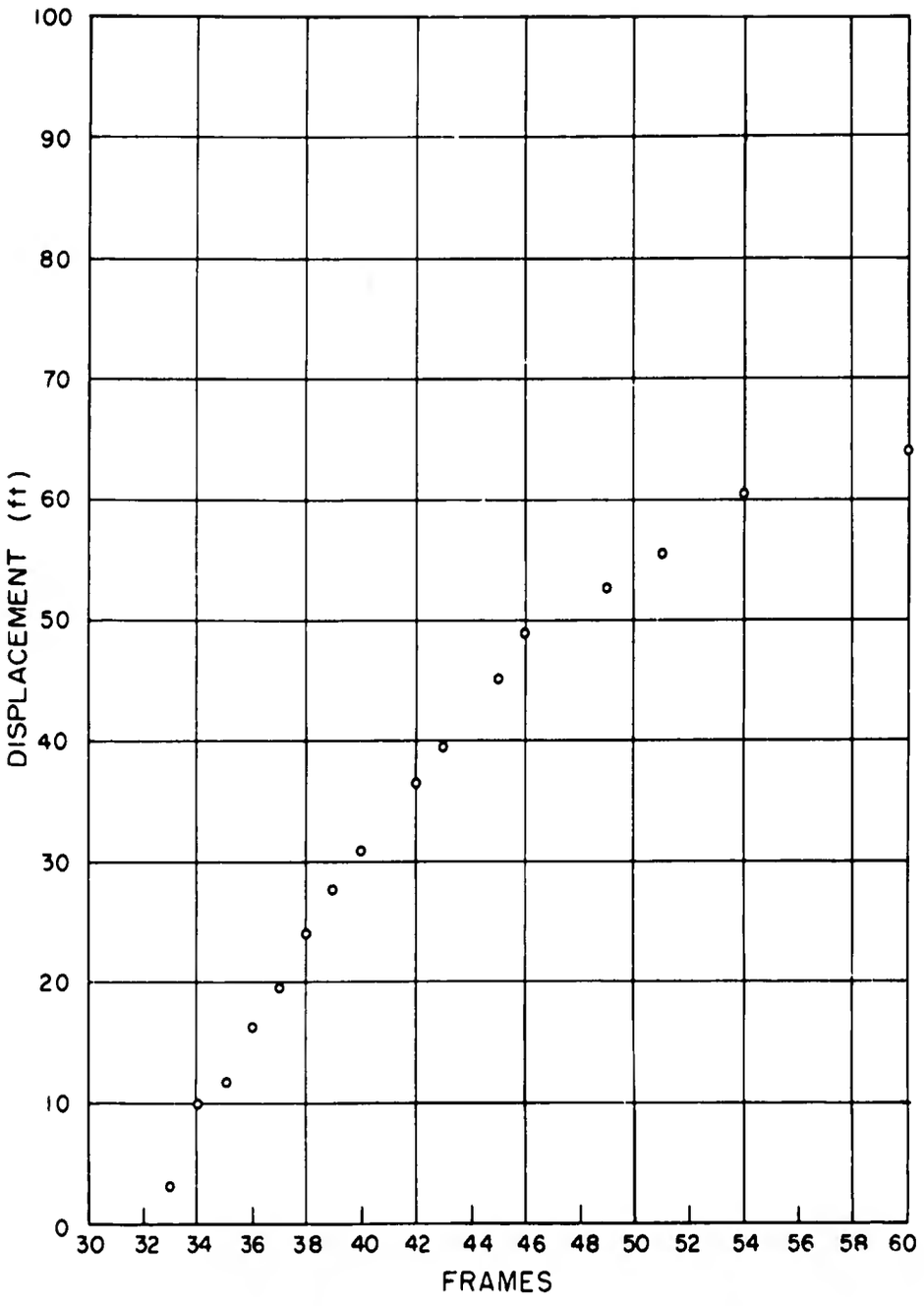

Fig. 4.19—Displacement-time data, underground shot, 755 ft from ground zero, puff. Multiply frames by 10.60 to convert to milliseconds.

SECRET

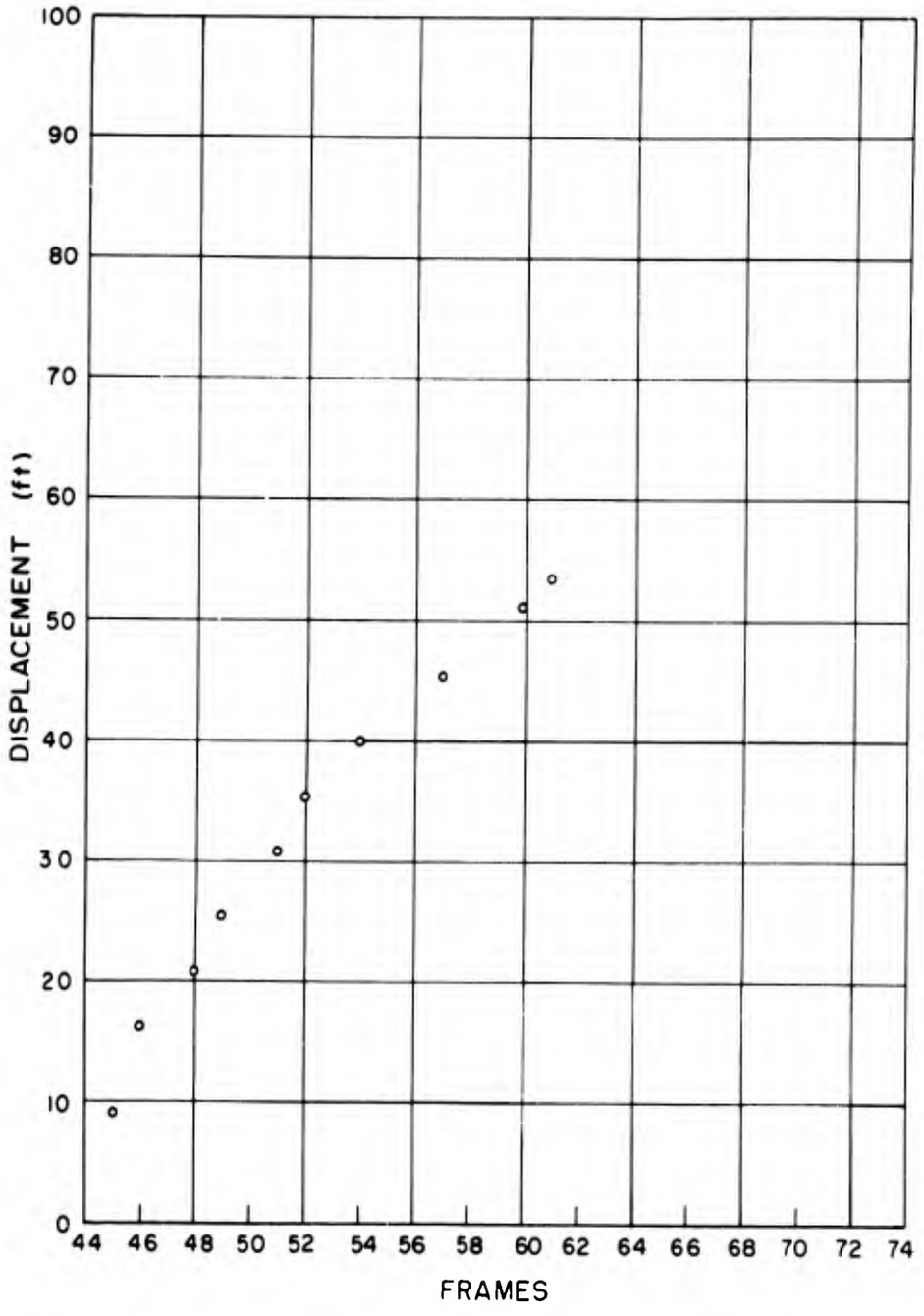

Fig. 4.20—Displacement-time data, underground shot, 902 ft from ground zero, mortar smoke. Multiply frames by 10.60 to convert to milliseconds.

SECRET

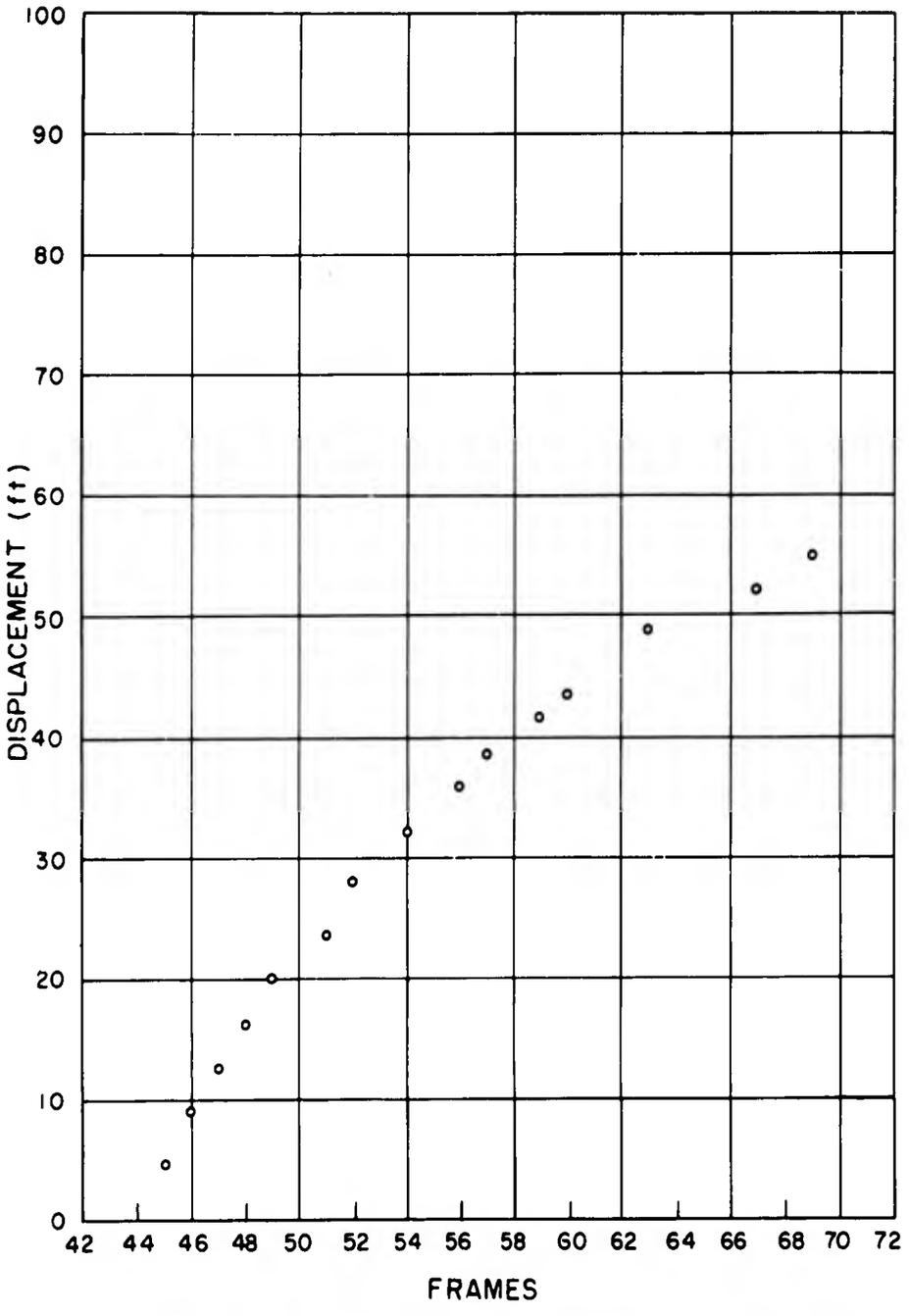

Fig. 4.21 — Displacement-time data, underground shot, 926 ft from ground zero, puff. Multiply frames by 10.60 to convert to milliseconds.

SECRET

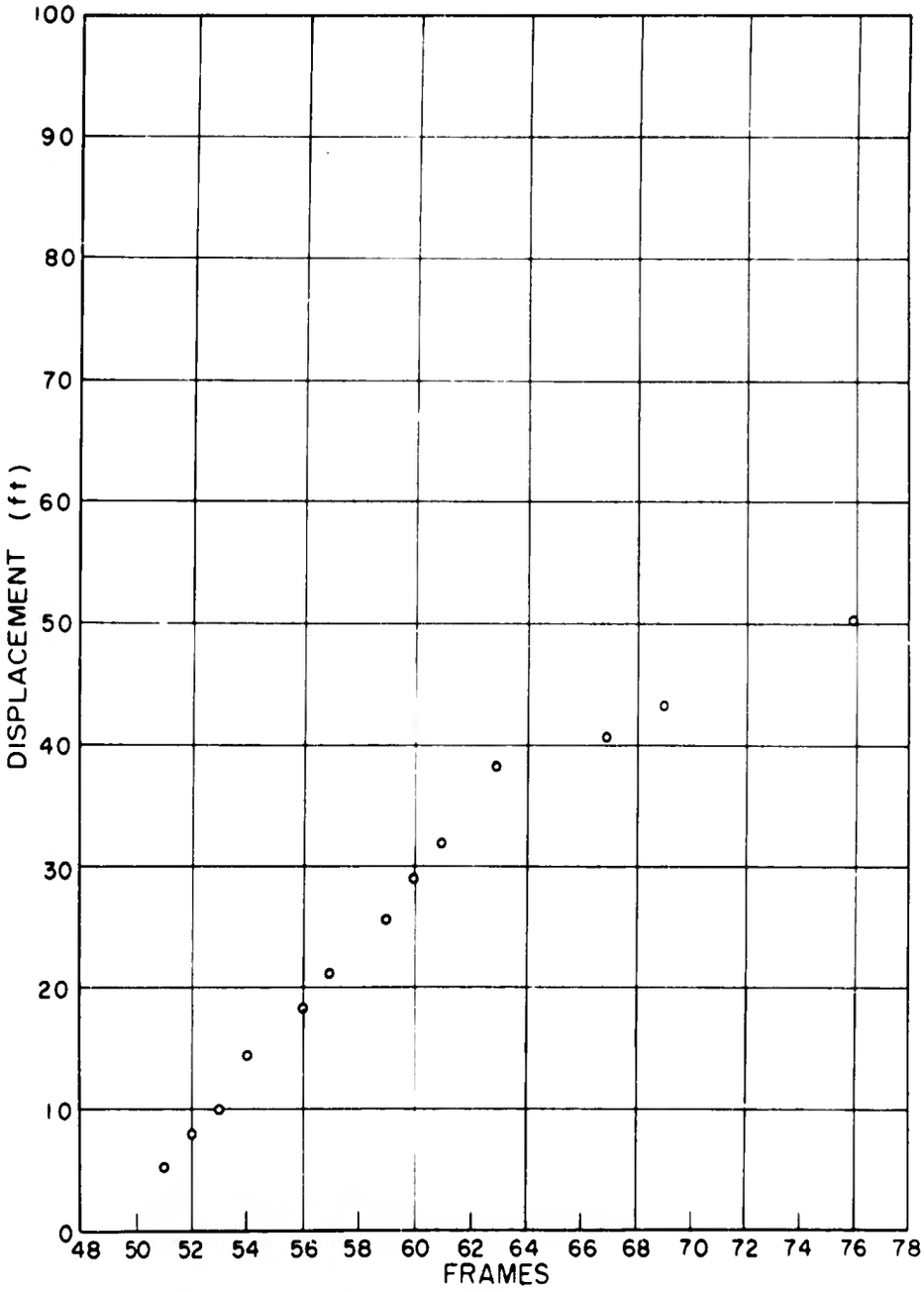

Fig. 4.22—Displacement-time data, underground shot, 1007 ft from ground zero, puff. Multiply frames by 10.60 to convert to milliseconds.

SECRET

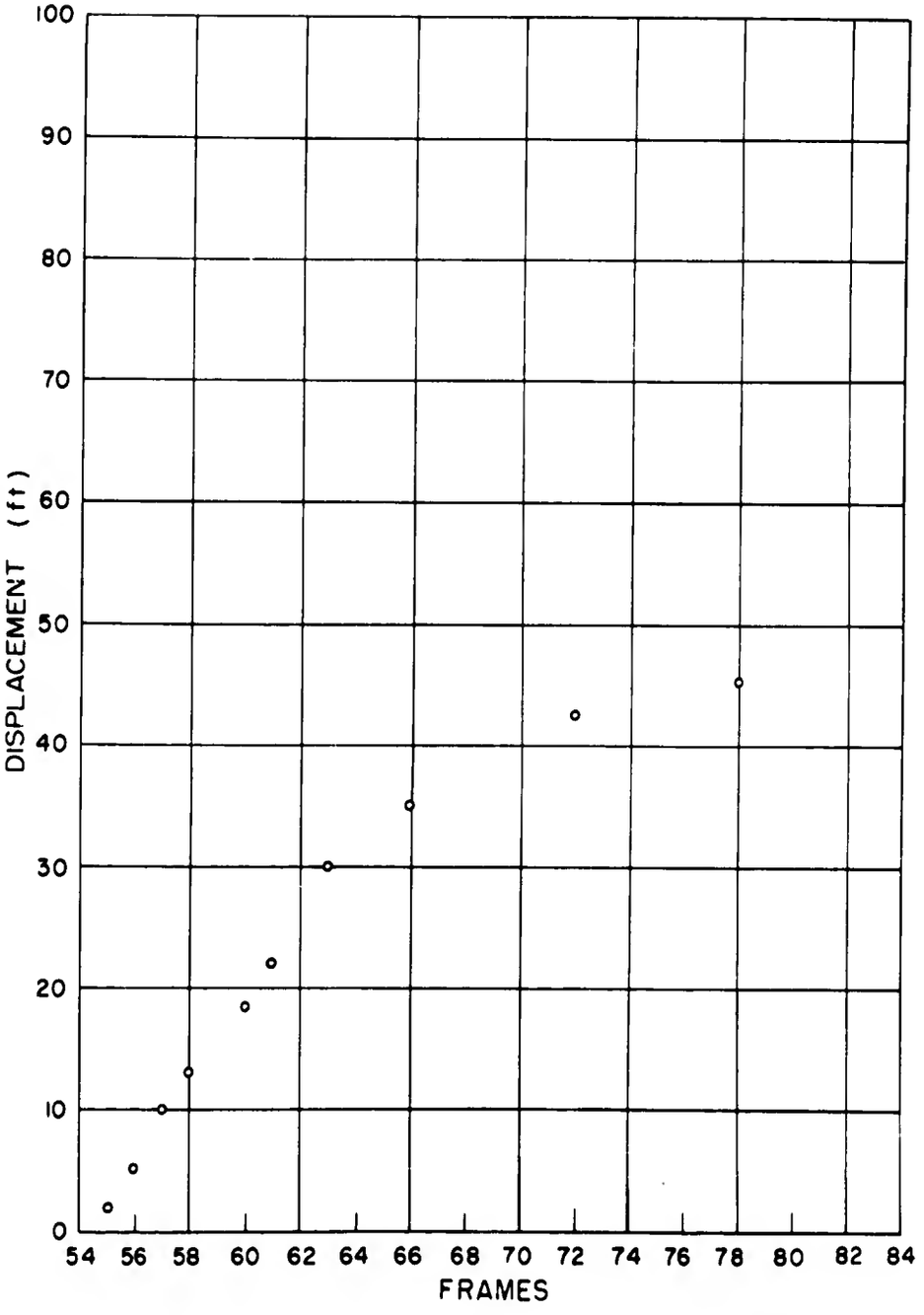

Fig. 4.23—Displacement-time data, underground shot, 1052 ft from ground zero, mortar smoke. Multiply frames by 10.60 to convert to milliseconds.

SECRET

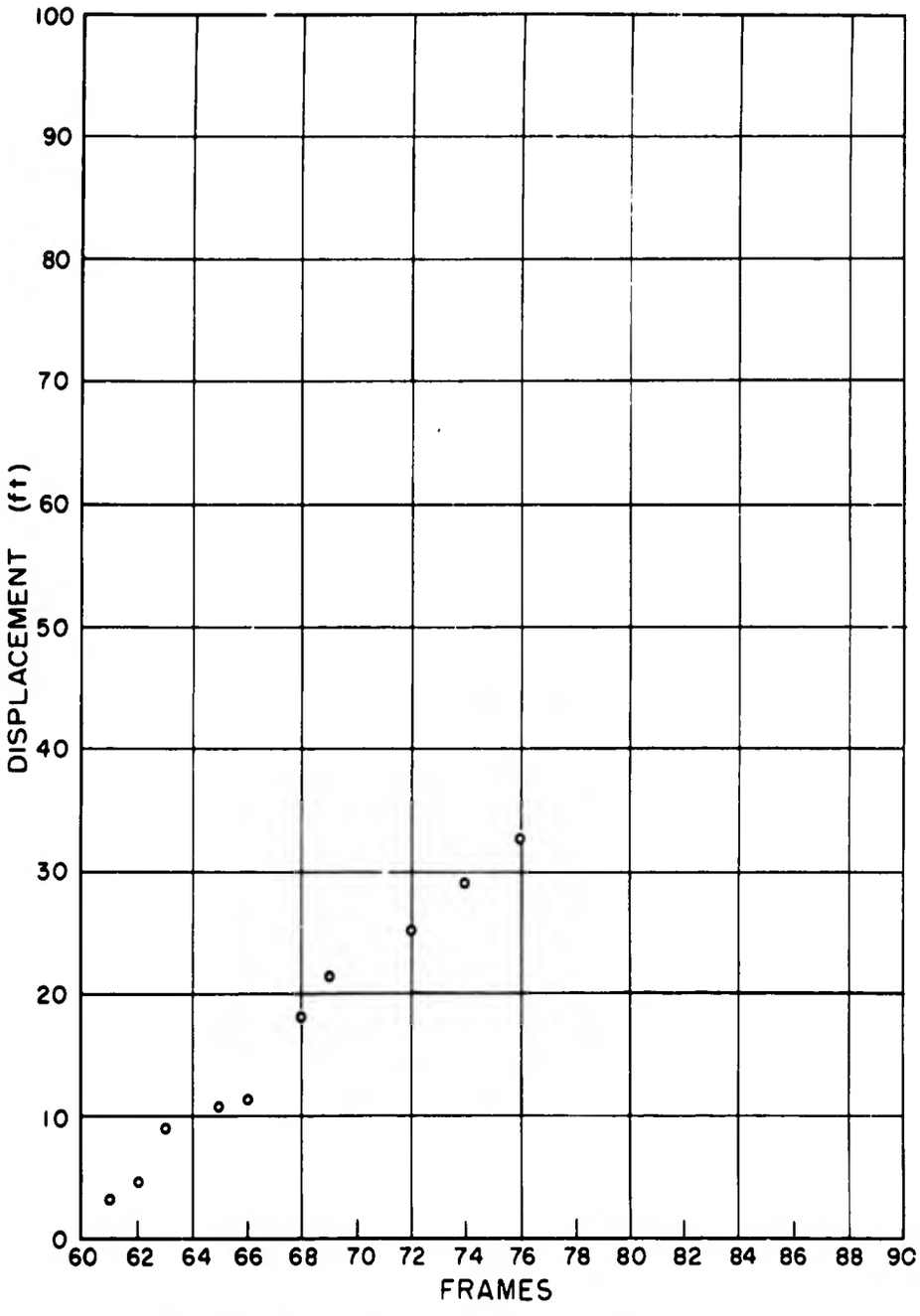

Fig. 4.24—Displacement-time data, underground shot, 1124 ft from ground zero, puff, height 288 ft. Multiply frames by 10.60 to convert to milliseconds.

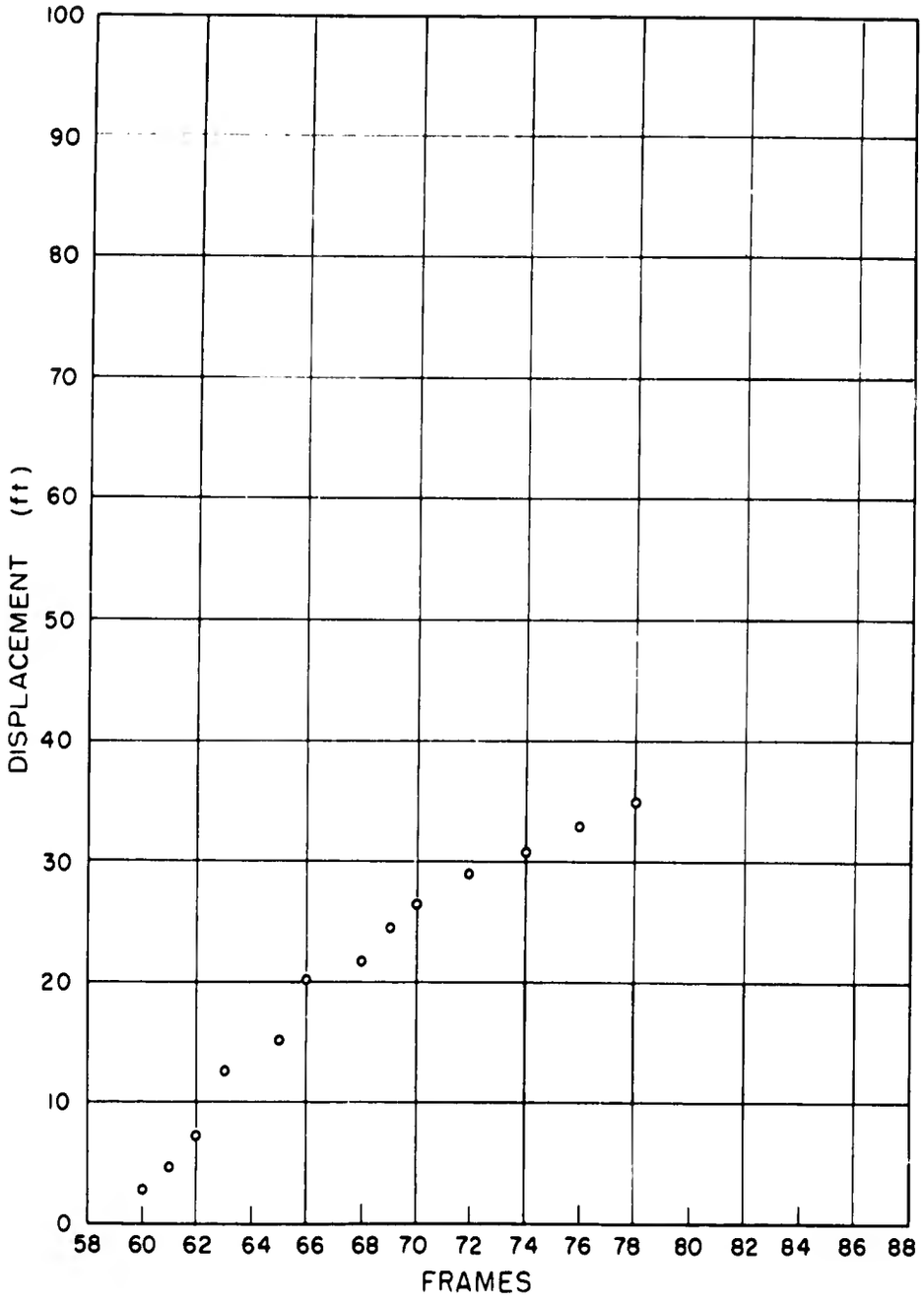

Fig. 4.25—Displacement-time data, underground shot, 1124 ft from ground zero, puff, height 348 ft. Multiply frames by 10.60 to convert to milliseconds.

SECRET

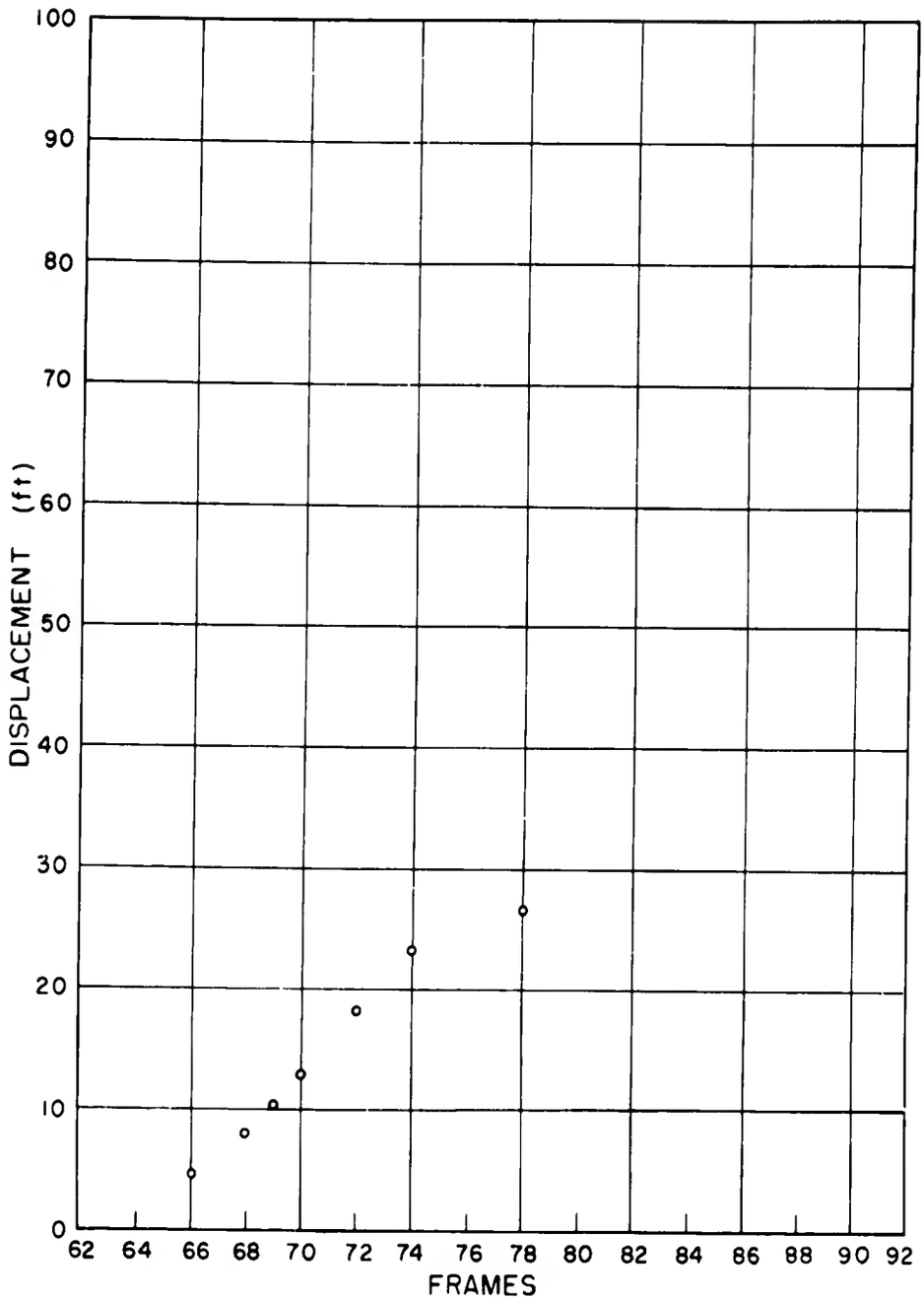

Fig. 4.26—Displacement-time data, underground shot, 1185 ft from ground zero, puff. Multiply frames by 10.60 to convert to milliseconds.

SECRET

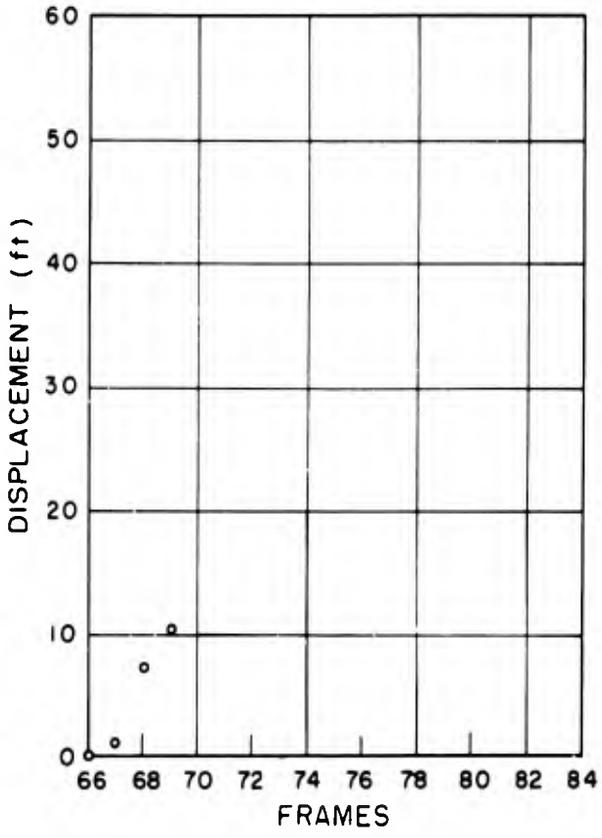

Fig. 4.27—Displacement-time data, underground shot, 1207 ft from ground zero. mortar smoke. Multiply frames by 10.60 to convert to milliseconds.

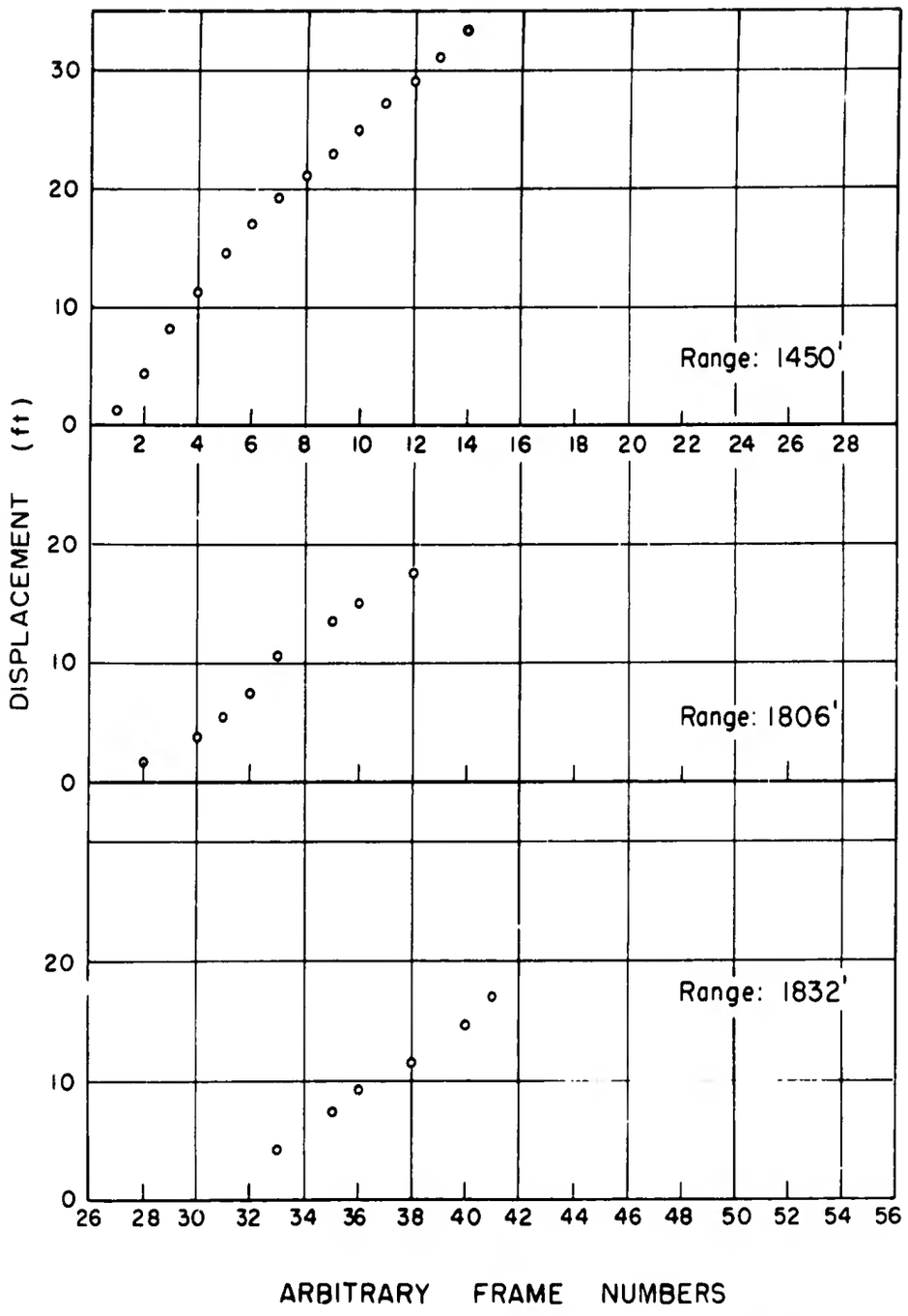

Fig. 4.28—Displacement-time data, underground shot, 1450, 1806, and 1832 ft from ground zero, puffs. Multiply frames by 10.60 to convert to milliseconds. Frame numbers are arbitrary since the zero-time frame was not distinguishable.

SECRET

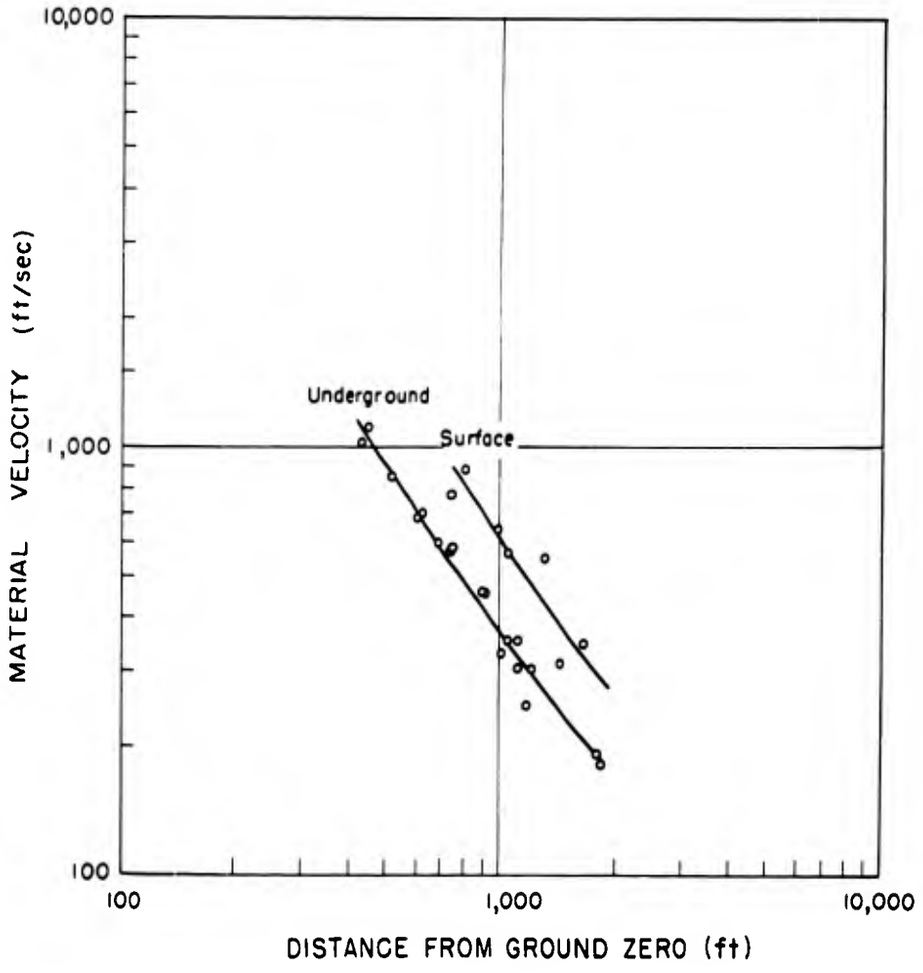

Fig. 4.29—Material velocity vs distance from ground zero, Operation Jangle shots.

SECRET

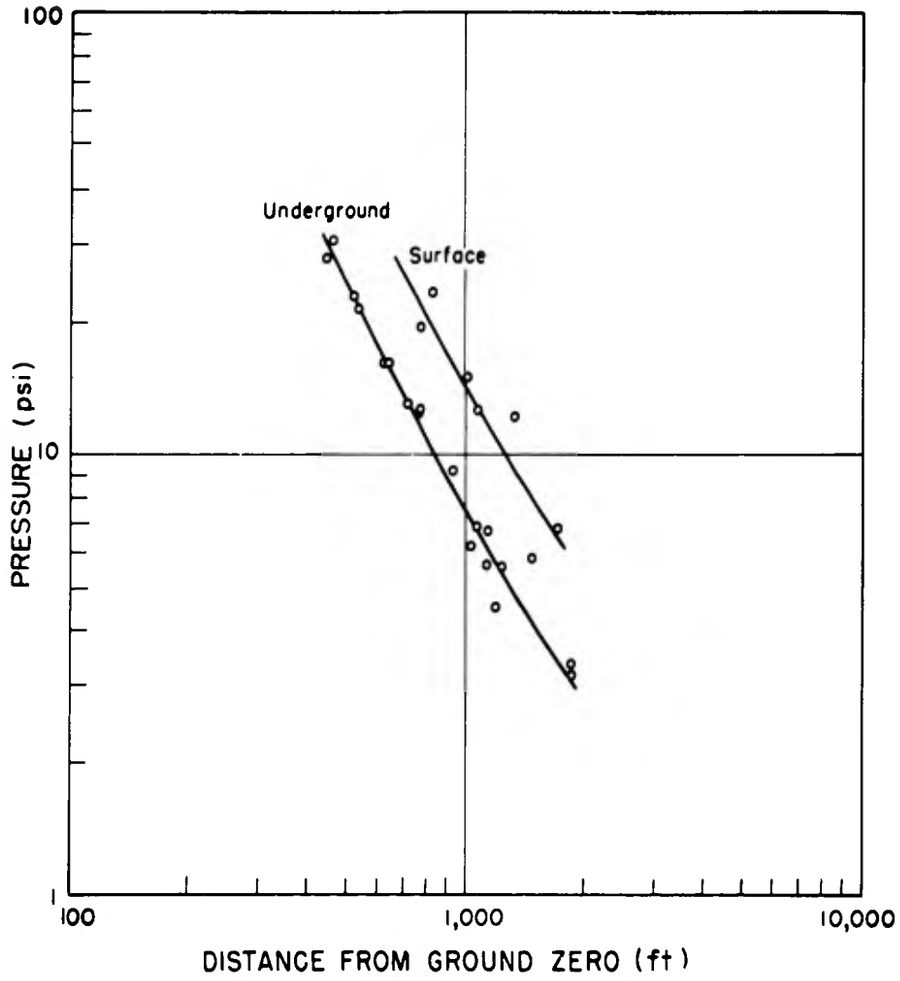

Fig. 4.30—Peak overpressure vs distance from ground zero, Operation Jangle shots.

SECRET

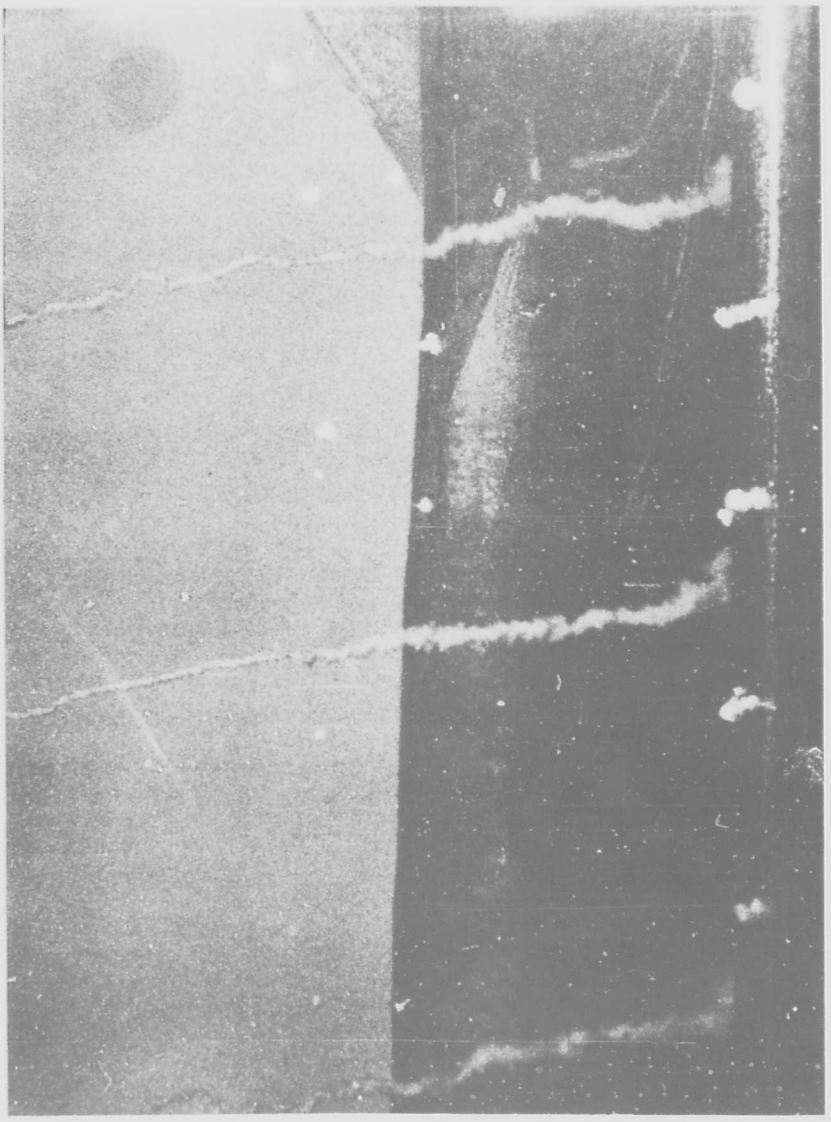

Fig. 4.31 — Smoke puffs at zero time. Operation Jangle underground shot.

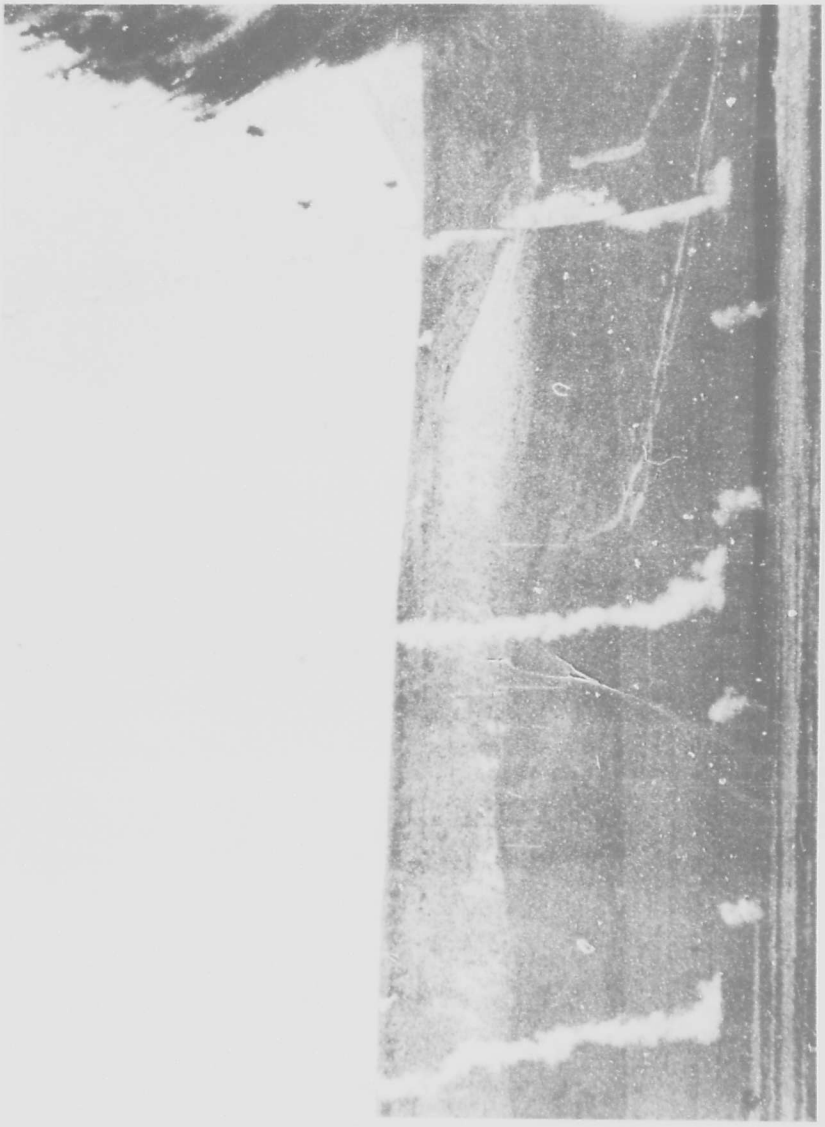

Fig. 4.32—Smoke puffs during shock-front passage, Operation Jangle underground shot.

4.3 METHOD OF PHOTOGRAPHIC ANALYSIS

As in the Operation Buster film analysis, contours of the smoke puff and, whenever it was clearly defined, of the smoke from the propelling charge in the mortar were traced from Recordak enlargements. Since the smoke puffs were much smaller than the JATO cloud, only one displacement-time curve could be drawn for each puff. The position for this measurement was taken to pass approximately through the center of the smoke puff, due regard being given to minor protuberances on the cloud.

The time scale for the surface shot was again obtained from data on the number of frames exposed during a known time interval. On the underground shot a timing-marker generator was available for recording precise timing on the film.

It was necessary to correct the measured material velocity for obliquity on the surface shot, but on the underground shot the camera lines of sight were perpendicular to the blast line and no obliquity correction was made. Wind correction was made for both shots.

The remainder of the analysis followed the pattern described for Operation Buster.

4.4 RESULTS

The error in range is ±1 per cent except for the case of those puffs recorded by the 24-in.-lens camera; these ranges may be in error by ±50 ft since in order to extend the field of view vertically to cover the expected burst heights the ground range markers were no longer visible on the film. Since the smoke bombs burst after they pass the peak of their trajectory and since they are not aerodynamically designed "shells," the projectile falls off to one side of its vertical flight path before it bursts. The timing, and hence the material-velocity, error is again ±15 per cent for the surface-shot data but is better than ±5 per cent for the underground data, for which precise timing was available. Error in the meteorological data is the prime reason for this latter high figure. In Table 4.1 the results obtained for both the surface and underground shots are summarized.

The data on smoke puffs beyond the 4-psi region are doubtful. The reasons for this are that the higher resolution achieved by the 24-in. camera (which covers puffs in this region) shows diffuse cloud edges and that the lower pressures do not accelerate all the smoke particles evenly, owing to density variations within the cloud. The net result is that it is extremely difficult to deduce a reliable material velocity from the displacement-time curve.

Figures 4.5 to 4.28 are the displacement-time curves plotted from measurements on the traced contour plots. Unlike Operation Buster the peak excursion and part of the negative-phase excursion have not been plotted owing to the fact that the smoke puffs begin to lose their shape after being displaced by the shock wave.

Figure 4.29 presents material velocity as a function of distance from ground zero. Figure 4.30 is a graph of peak overpressure vs distance from ground zero.

Figures 4.31 and 4.32 illustrate the records obtained with the smoke-puff technique; Fig. 4.31 shows zero time, and Fig. 4.32 shows the location of the shock wave (by refraction) and the motion of the smoke puffs behind the shock front.

CHAPTER 5

TIME-OF-ARRIVAL, DUST, AND SHOCK-VELOCITY DATA

5.1 TIME OF ARRIVAL

A frame count from the sharp indication on the film at zero time to the time that the smoke first begins to move, together with the camera speed, gives a measurement of the time of arrival. This information for Operation Jangle is shown in Fig. 5.1.

5.2 DUST

On the Operation Buster films it is clearly evident that a dust or smoke cloud is produced by thermal radiation well in advance of the arrival of the shock wave. Figures 5.2 and 5.3 illustrate this effect.

Figure 5.2 shows the JATO cloud at 20 msec after zero time (Shot D), and Fig. 5.3 shows the preshock dust raised in the same area at about 1800 msec (or 200 msec before shock arrival). Figure 3.15 has already illustrated the preshock dust on Shot B.

Figure 5.4 indicates the measured rate of rise on Shot C at a range of about 3800 ft from ground zero. This rate is approximately 9 ft/sec and is probably smoke from the asphalt surface.

Figure 5.5, for Shot B at about 1900 ft from ground zero, again illustrates the smoke effect with a rise rate of 15 ft/sec. In addition, dust clouds over the desert area were apparently rising at 49 ft/sec. From these velocities it seems probable that the smoke is raised by diffusion and the dust by the "explosion" of air trapped within the dust particles; both phenomena are directly due to thermal radiation from the nuclear detonation. The rate of rise of dust due to the passage of the shock wave is seen to exceed the rise rate prior to shock arrival.

5.3 SHOCK VELOCITY

On the Operation Jangle films the progress of the shock wave could be discerned by refraction phenomena which produced an image of the shock front on the film. Figure 5.6 shows the shock front to the right of the right-hand rocket trail. Note that the phenomenon of preshock dust is not present on the underground shot. An attempt was made to obtain pressure-distance data from measurements of shock velocity. Although the shock-velocity method is subject to a much greater error than the material-velocity method, calculated pressure points fell within the range covered by the limits of error of the two methods.

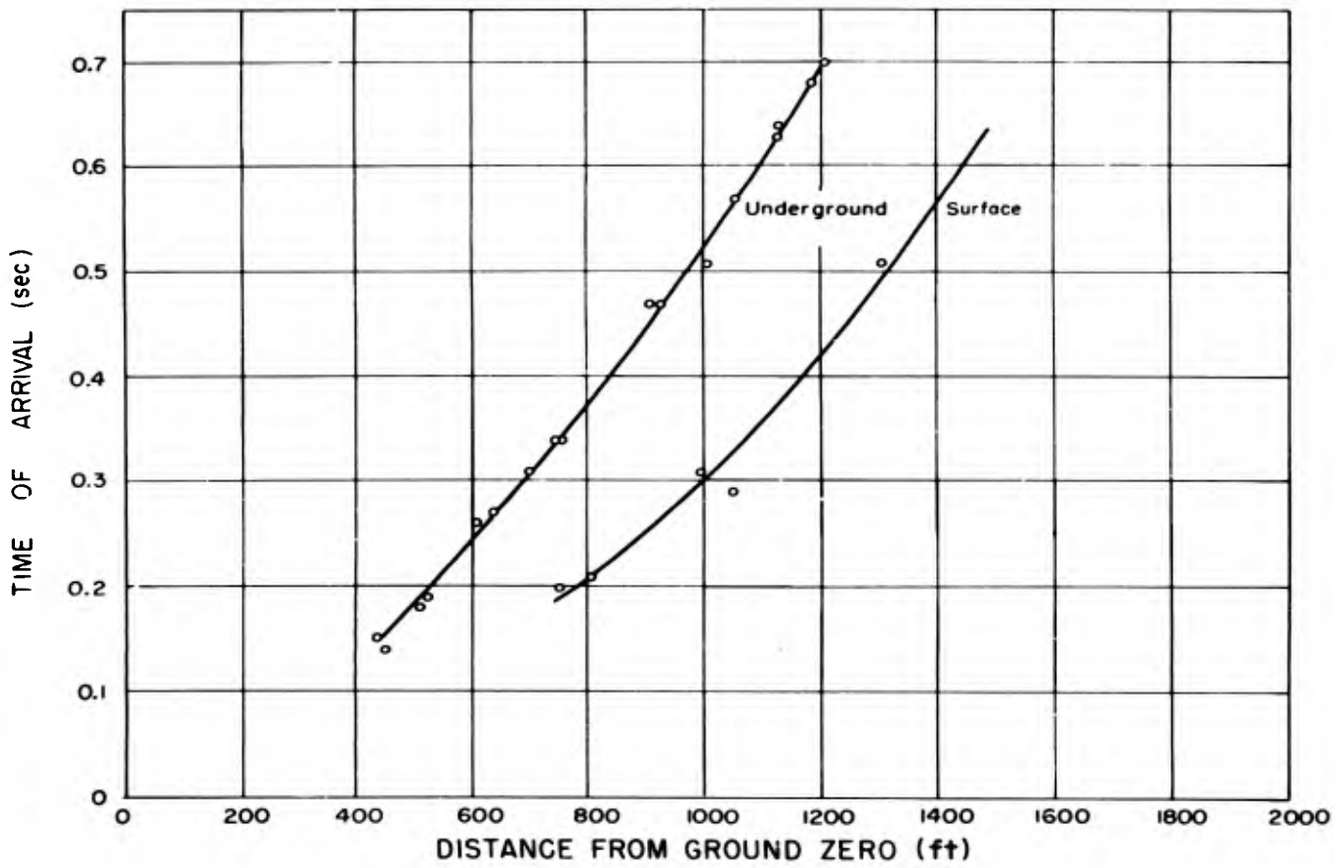

Fig. 5.1—Time of arrival vs distance from ground zero, Operation Jangle shots.

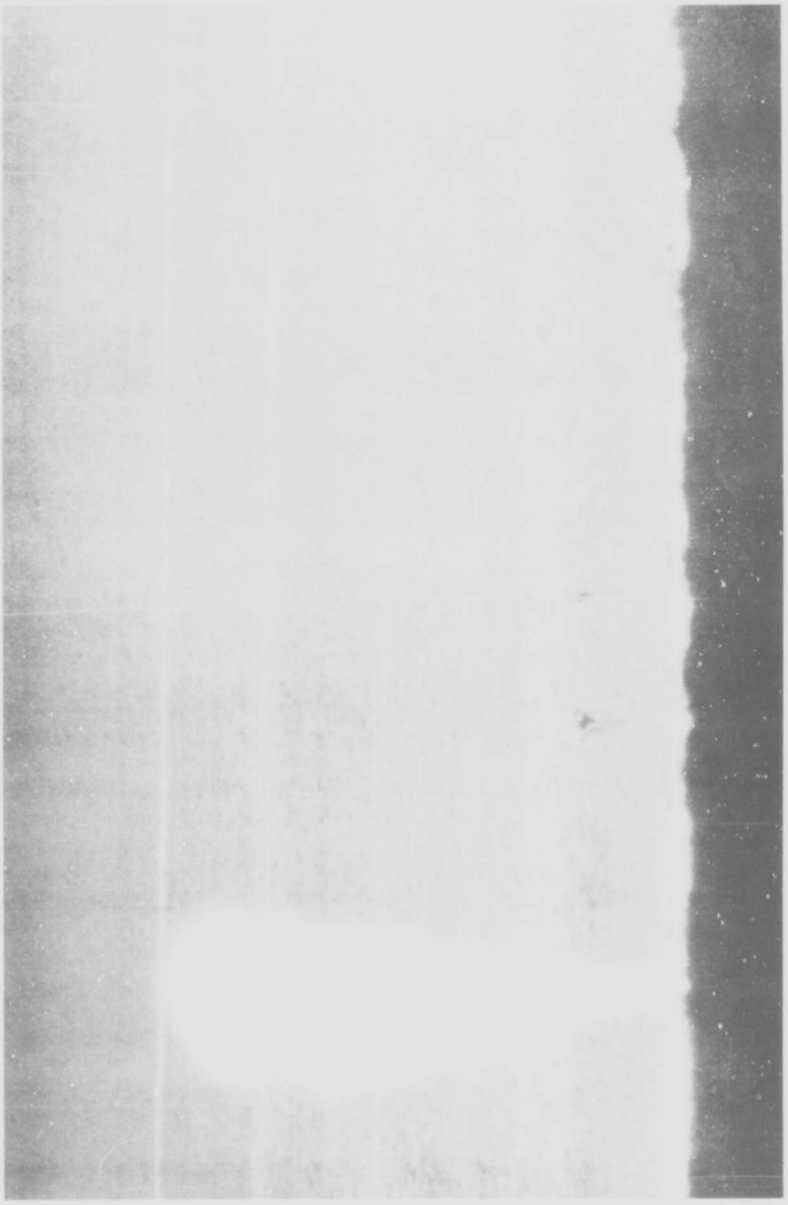

Fig 5.2—JATO at 20 msec after zero time, Shot D, 3950 ft from ground zero.

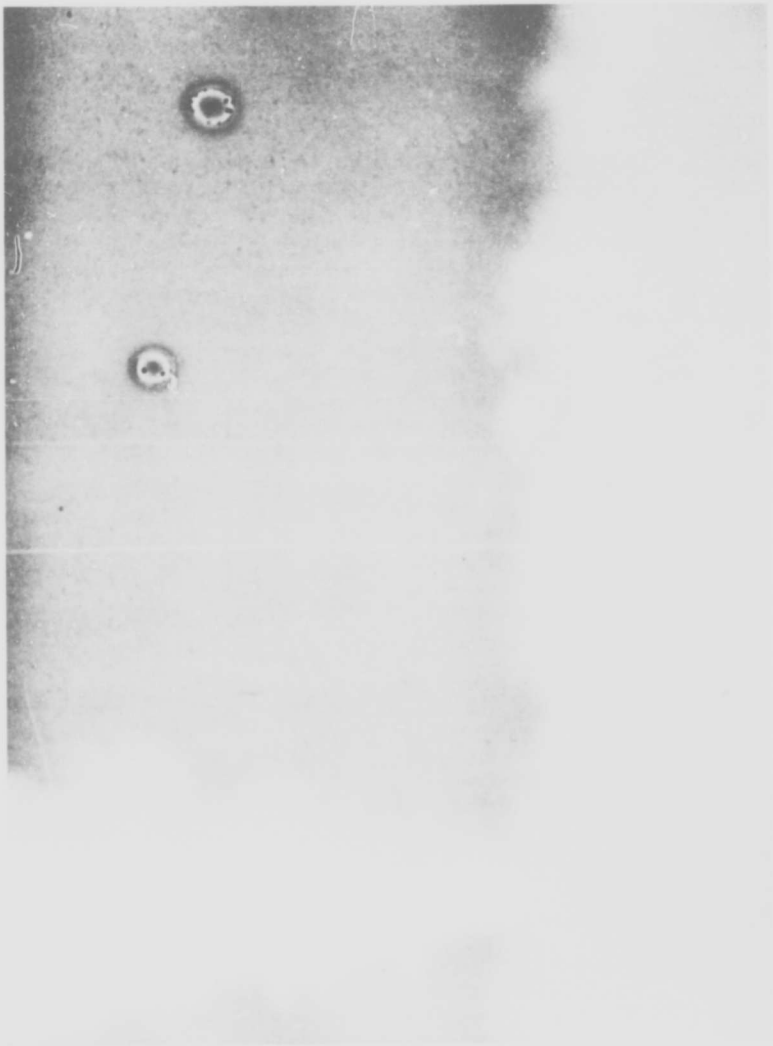

Fig. 5.3—JATO at 1800 msec after zero time (200 msec before shock arrival), preshock dust. Shot D, 3950 ft from ground zero.

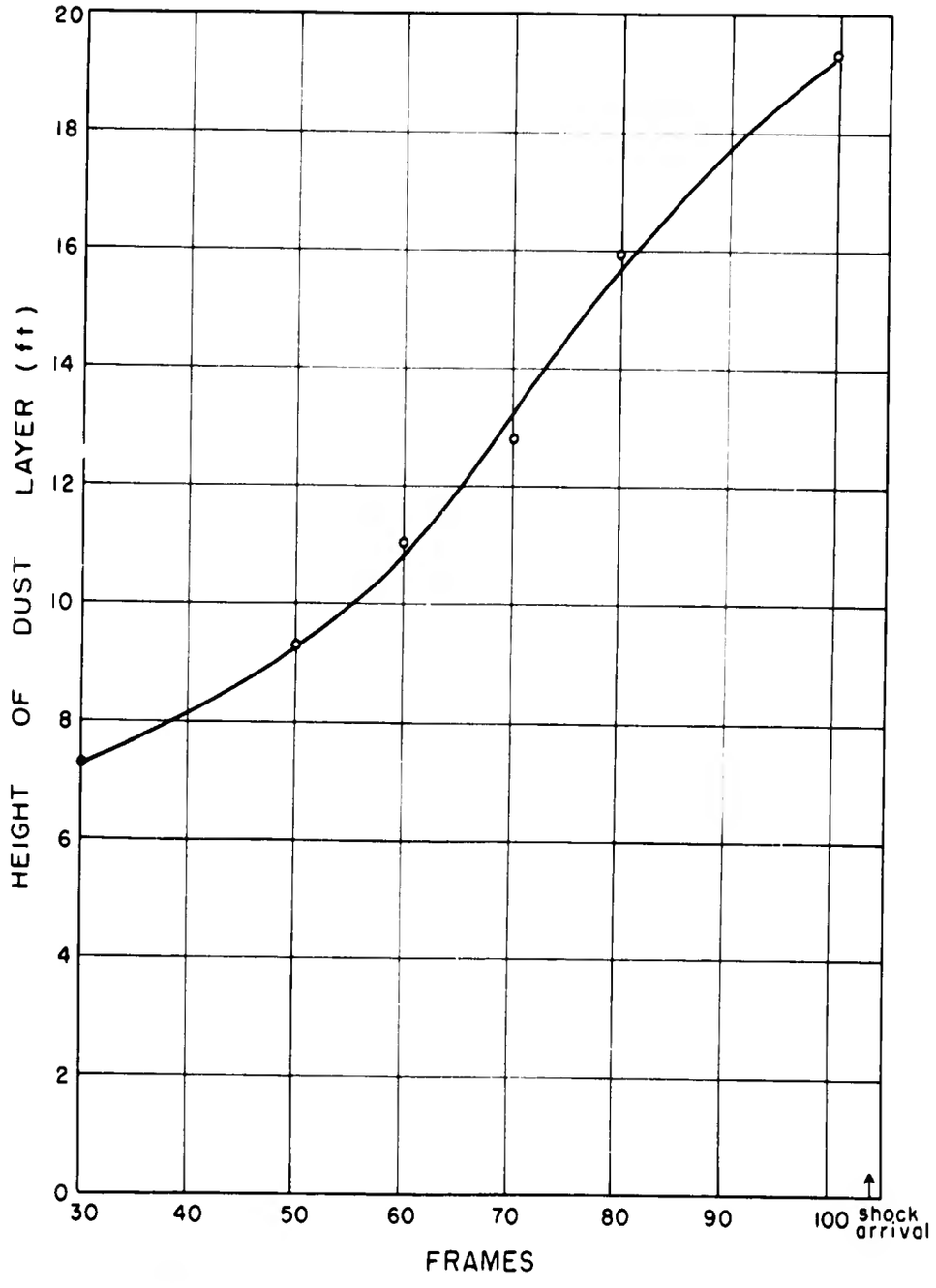

Fig. 5.4—Shot C, preshock smoke, 3810 ft from ground zero. Multiply frames by 19.95 to convert to milliseconds.

SECRET

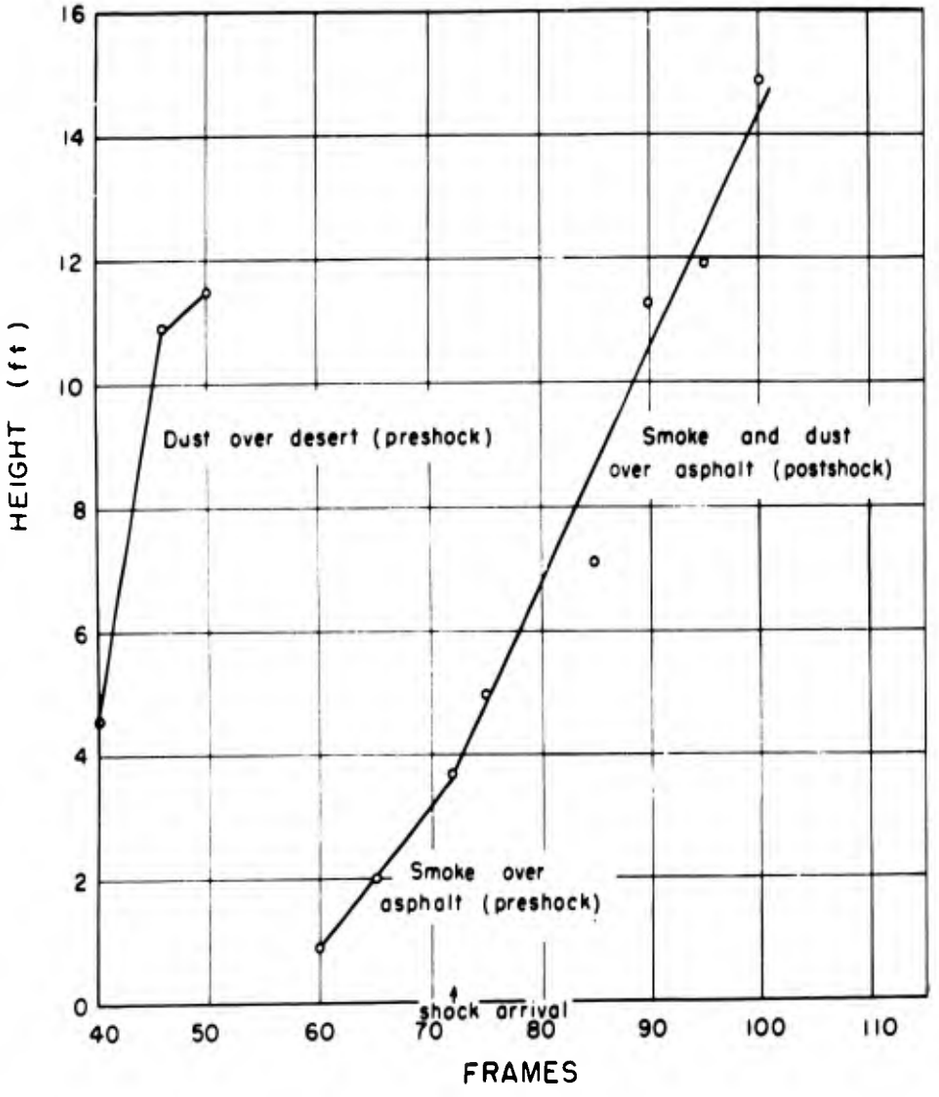

Fig. 5.5—Shot B, preshock and postshock dust and smoke, 1890 ft from ground zero. Multiply frames by 14.35 to convert to milliseconds.

Fig. 5.6—Shock front by refraction. Operation Jangle underground shot.

CHAPTER 6

CONCLUSIONS AND RECOMMENDATIONS

6.1 GENERAL

The feasibility of using material-velocity measurements as a method for determining peak pressures and other hydrodynamic data associated with nuclear explosions has been demonstrated on Operations Buster and Jangle. Two methods of smoke production have been used, each method being successful although it now appears that the smoke-bomb technique is preferable for measuring pressures well away from ground influences. The use of JATO units is desirable for tracking the triple point from its formation to an altitude of the order of 100 ft.

6.2 RECOMMENDATIONS

For future operations at the Nevada Proving Grounds the use of present smoke bombs and JATO units is satisfactory; for possible use at Eniwetok, where photographic ranges are greatly increased, a larger volume of smoke will be necessary in order to produce a readable image on the film.

Other photographic recommendations include the use of camera filters to reduce the intensity of fireball illumination, thereby allowing the use of the material-velocity method at points closer to ground zero. A camera located at an angle of about 30° to the mortar line would enable a more definite establishment of the space coordinates of the bursting smoke bomb. The Operation Buster-Jangle cameras at approximately 90° to the mortar line would establish the burst points in range from ground zero and elevation only. The proposed additional camera would provide a refinement for future use of the method. Although some data were obtained from the 24-in. camera, it has been mentioned that these data were subject to doubt since accurate ranges of the smoke puffs were not known. It is therefore imperative that the camera see reference ground markers as well as the smoke puff. This requirement means a compromise on space resolution since the vertical field of view is necessarily limited to include both the smoke burst at a height of 200 to 300 ft and a ground reference. Furthermore, resolution has a definite upper limit. It is true that in low-velocity regions high resolution is desirable, but at the same time this high resolution reveals the diffuse edge of the smoke puff, making it difficult to deduce an accurate displacement-time graph. The 12-in. camera produced very good results. The 24-in. lens now appears to be a trifle in excess of the desired and necessary resolution.

APPENDIX A

METEOROLOGICAL DATA

Meteorological observations made prior to shot time provide, primarily, values of temperature and pressure at ground zero.

A.1 TEMPERATURE

The temperature observations for each shot are listed in Table A.1.

Table A.1 — TEMPERATURE DATA

Shot	Altitude, ft	Temperature, °C	Method
B	0	11.4	Extrapolation from C.P. data
	Burst height	9.8	Extrapolation from C.P. data
	0	5.0	Wiresonde
	3	5.0	Wiresonde
	91	4.5	Wiresonde
	200	8.5	Wiresonde
	290	11.1	Wiresonde
C	0	5.3	Extrapolation from C.P. data
	Burst height	11.2	Extrapolation from C.P. data
	0	2.5	Wiresonde
	100	8.5	Wiresonde
	300	9.5	Wiresonde
D	0	15.5	Extrapolation from C.P. data
	Burst height	12.0	Extrapolation from C.P. data
	0 (0630)	10.6	Wiresonde
	0 (0645)	11.5	Wiresonde
	0 (0652)	13.7	Wiresonde
	0 (0700)	14.5	Wiresonde
	0 (0712)	15.0	Wiresonde
	3	7.0	Wiresonde
	10	8.0	Wiresonde
	100	11.2	Wiresonde
	200	11.5	Wiresonde
	275	11.0	Wiresonde
Surface	0	1.0	Wiresonde
Underground	0	14.5	Wiresonde

A.2 PRESSURE

Ambient-pressure measurements at the surface are listed in Table A.2.

Table A.2—AMBIENT-PRESSURE DATA

Shot	P_0, psi
B	12.7
C	12.55
D	12.7
Surface	12.65
Underground	12.65

A.3 WIND

Surface-wind direction and velocity are listed in Table A.3.

Table A.3—SURFACE-WIND DATA

Shot	Direction,°	Velocity, knots
B	320	09
C	360	05
D	340	02
Surface	190	02
Underground	180	02

SECRET

APPENDIX B

METHOD CHARACTERISTICS

B.1 JATO UNIT

The Model 14AS-1000 D-4 (Mark 2, Mod 3) JATO, manufactured by Aerojet and used in the Operation Buster experiment, has the following characteristics:

Fuel composition, %	
Potassium perchlorate	70
Asphalt	20
SAE No. 10 oil	10
Burning time, sec	14 (dependent on temperature)

In the field, two 45-volt dry cells in parallel provided ignition power.

The cone of smoke produced by a JATO unit is approximately 20° wide and 150 ft high, as shown in Fig. B.1. The rate of growth of the smoke column is shown in Fig. B.2.

Disadvantages of the JATO method will probably limit its use in the future to measurements of the triple-point path, from its inception up to about 100 ft. Since the exhaust velocity is extremely high just above the nozzle, a vertical velocity component makes the interpretation of the true motion due to the shock wave rather difficult in this lower region. The vertical component becomes negligible in the higher reaches of the cloud. The smoke density is not known low in the plume but is presumably rather high, resulting in a measurement of material velocity slightly lower than the true velocity. Higher in the cloud the smoke density has been reduced by expansion to about 10^{-4} g/cm^3. The continuous production of smoke further complicates the film analysis. It is not certain that the same group of smoke particles from frame to frame is being followed.

B.2 SMOKE BOMB

The smoke bombs used in Operation Jangle were purchased from Bermite Powder Company, Los Angeles, Calif., and are a nonprecision fireworks item sold under the name of Flash Salute. The propellant and bursting charge are contained in a paper-wrapped canister, 3 in. in diameter and 4 in. high. After being placed in a mortar they are normally fired by hand-lighting the fuse. Electric squibs were used to allow remote firing; the power source for the squib was a 67½-volt dry cell.

Fired at approximately −5 sec, the bursting charge had a 4- to 5-sec time of flight. After bursting, a 10-ft-diameter smoke puff was produced in about 10 msec. Cohesion is quite good, the outline of the puff remaining fairly constant for up to 5 sec.

The density is believed to be lower than that of the JATO smoke thereby giving a better measurement of velocity. After bursting there are no appreciable velocity components other than that produced by the blast wave, and there is no continued smoke production. These advantages over the JATO unit indicate the use of this method in future experiments.

Fig. B.1 —JATO cone of smoke.

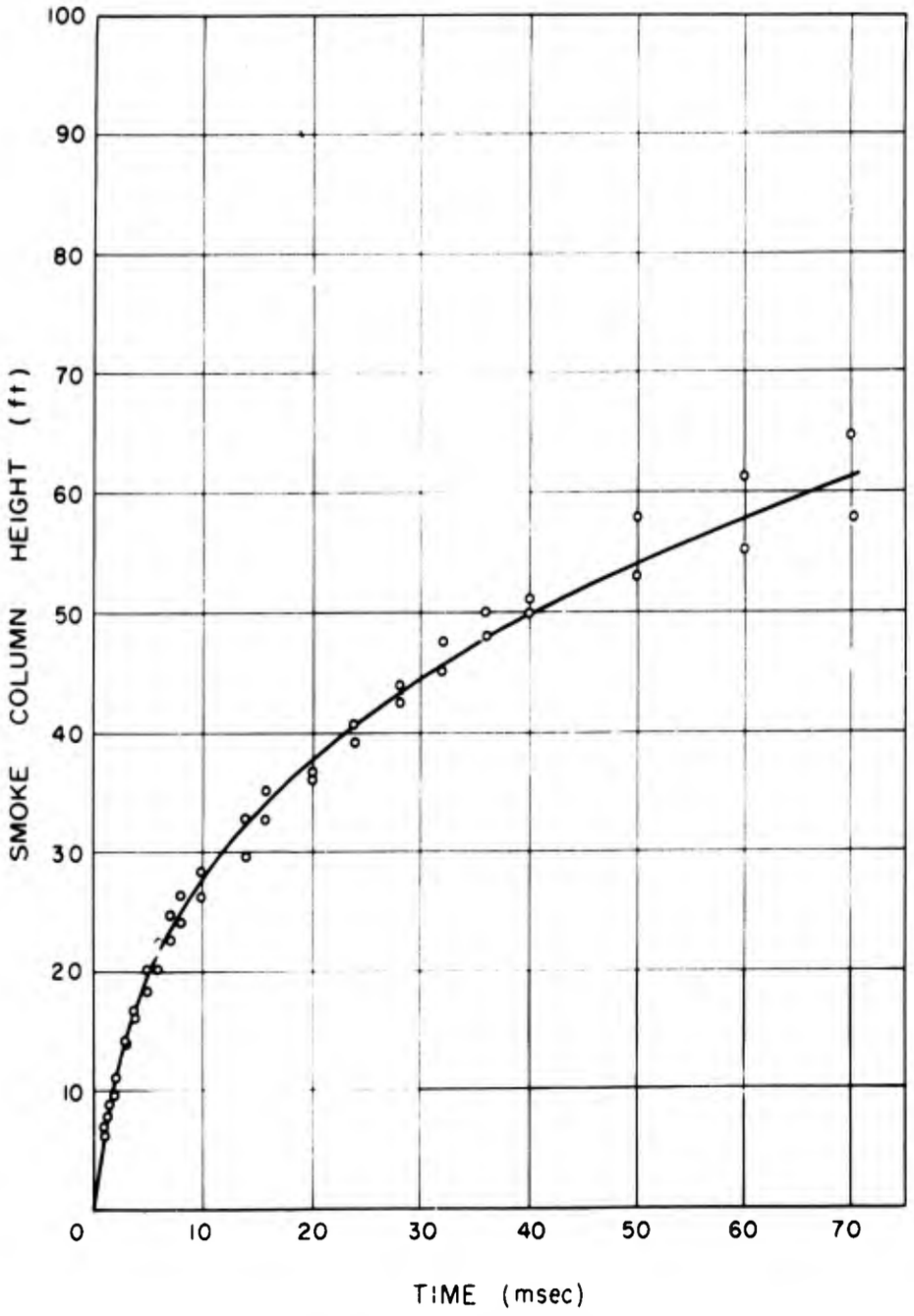

Fig. B.2—Rate of growth of JATO smoke column.

SECRET

Part IV

PIN SYSTEM OF MEASURING TIME OF ARRIVAL OF AN UNDERGROUND SHOCK WAVE, OPERATION JANGLE

by

Robert W. Newman

SECRET

CHAPTER 1

INTRODUCTION

1.1 PURPOSE

The pin system was designed to detect two distinct, but possibly simultaneous, phenomena in the ground. These phenomena were (1) the arrival of a pressure wave along a series of points in the ground, and (2) the arrival of a highly ionizing front at the same points. It was proposed that the phenomena might be separate; thus two types of pickup, one pressure sensitive and the other heat sensitive, were designed.

For the Operation Jangle underground shot, a third measurement was desirable: the arrival of the pressure wave along a line at a lesser depth than the centerline.

1.2 RESULTS

Both Operation Jangle shots gave no records which were readable or identifiable. The surface-shot records indicate that pickup along the cable caused one scope to go off scale and remain off scale and caused a blanking of trace on the other scope during the time a record might have come in. Also, the mixing box, in which all the signals were gathered and transmitted, probably was subjected to radiation great enough to destroy the electrical properties of some of the components.

The underground-shot equipment was redesigned as a result of the surface-shot experience, but still other troubles caused loss of records. Analysis of the film seems to indicate that the initial pulse, due to electromagnetic phenomena associated with the bomb explosion, swamped the amplifiers to such a degree that they remained nonconducting during the period of interest. Late signals show that the recovery time of the amplifier was of the order of 12 msec, at which time the mixing box, with amplifiers, was destroyed.

CHAPTER 2

EQUIPMENT

2.1 GENERAL

The basic equipment designed to receive and record the time of arrival of the shock wave was as follows: The shock was picked up by a pressure-sensitive closure pin or by an ionization closure pin; the shorting of both types discharged a condenser across a small resistance. Signals from individual pins were mixed and then transmitted by coaxial cable to the Y axis of an oscilloscope which was sweeping at 5000 cps. The scope was photographed by a high-speed continuous-film shutterless camera. Figure 2.1 is a block diagram of the underground-shot equipment.

In order to increase probability of recording a readable record, several devices were installed in the system. These were a thyratron unit, a relay box for applying voltages, a line amplifier (underground shot only), a camera relay control board, and a fiducial cable (underground shot only).

2.2 PICKUP UNITS

The pressure-sensitive device was an Amphenol connector PL-274 with Amphenol cap 75-CCC-1, modified as shown in Fig. 2.2. A brass insert was used in the connector as an anvil and conductor with which the closure screw in the cap made contact to establish the electrical circuit. This type of pin was thoroughly tested in underground high-explosive shots at Los Alamos and was found to be reliable and fast-closing at medium and high pressures. On the surface shot, all pins were set to close at about 2.5 psi; however, because of possible shorting of these pins before zero time, e.g., by static ground pressures, the underground-shot pins were set to close at pressures between 20 and 50 psi. Upon final check at H−18 hr for the underground shot, no pins were found to be shorted. The pins were mounted in plastic mounts and were protected by a small screen. On the underground shot the pins were lowered into position by the cables, RG-54A/U modified, leading back to the mixing box. On the surface shot the pins were pushed into position with a special tool.

On each shot the mixing box, the point at which all individual cables were connected, was farther from ground zero than the most remote pin. All pin cables were 70 ft long in order that the delays in these cables would be equal.

2.3 THYRATRON DELAY BOXES

The purpose of the thyratron delay box, Fig. 2.3, was to delay charging of the pins until after the very high initial burst of ionizing radiation had subsided. It was calculated that from 3 to 5 meters of earth would shield a pin sufficiently to keep this ionization from totally discharging a pin hooked directly to the pin box. On the surface shot, one full row of pins was

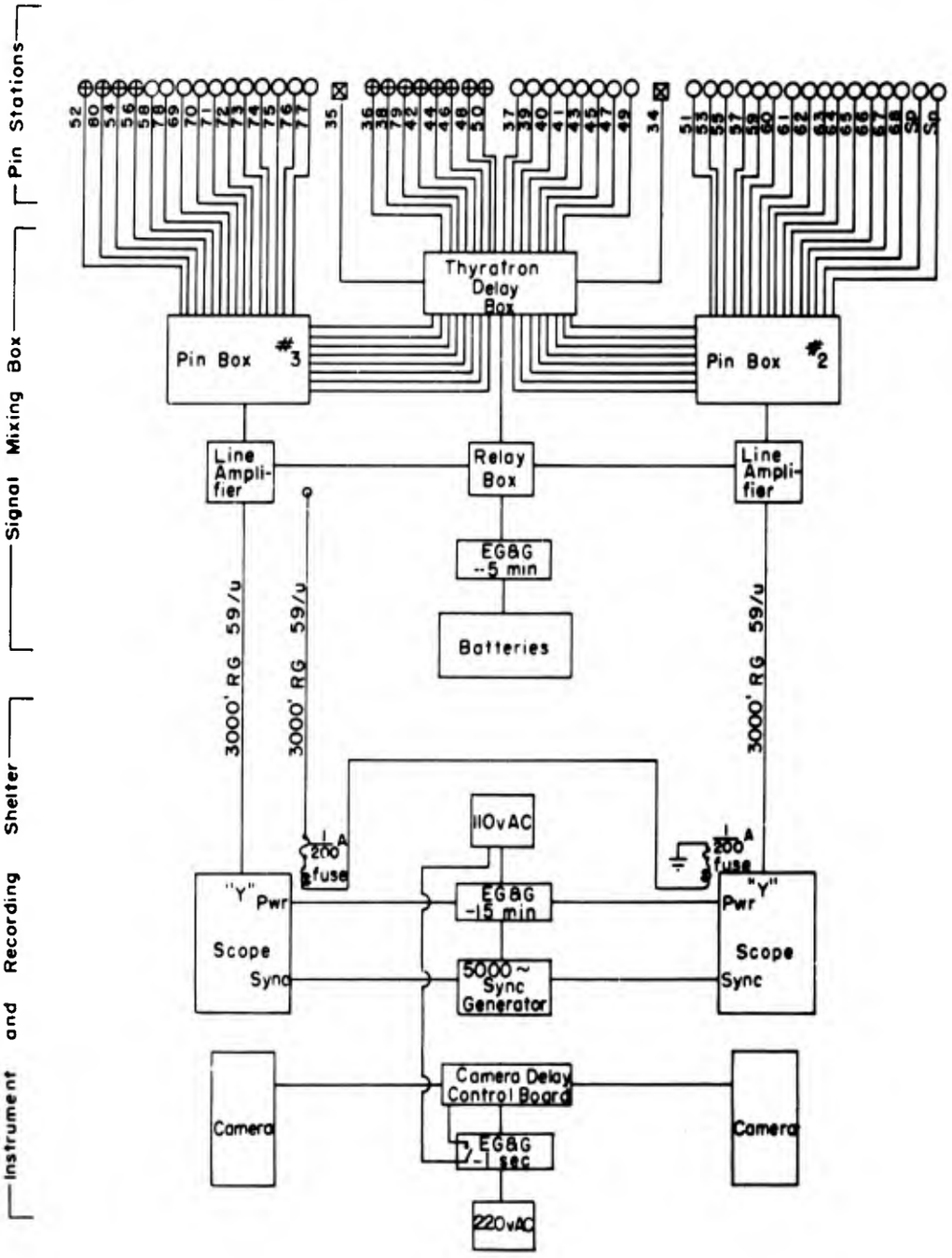

Fig. 2 1—Block diagram of the pin system. Operation Jangle underground shot. ○, pressure closure pin. ⊕, ionization closure pin. ⊠, fiducial pin.

SECRET

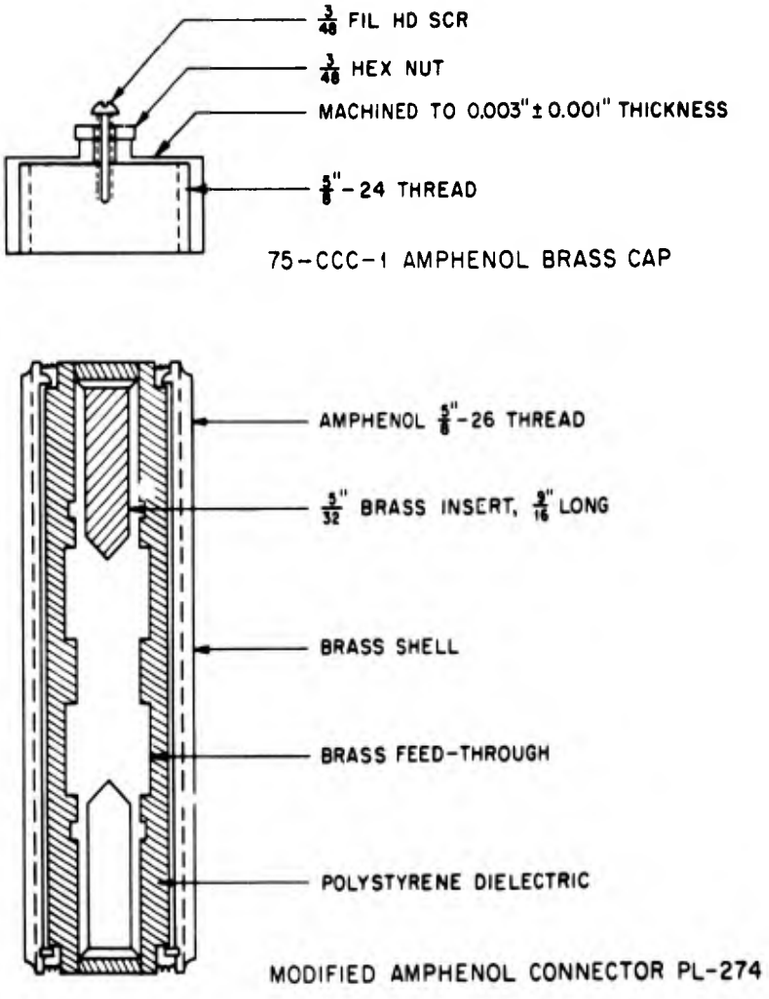

Fig. 2.2—Cross section of a pressure closure pin, expanded.

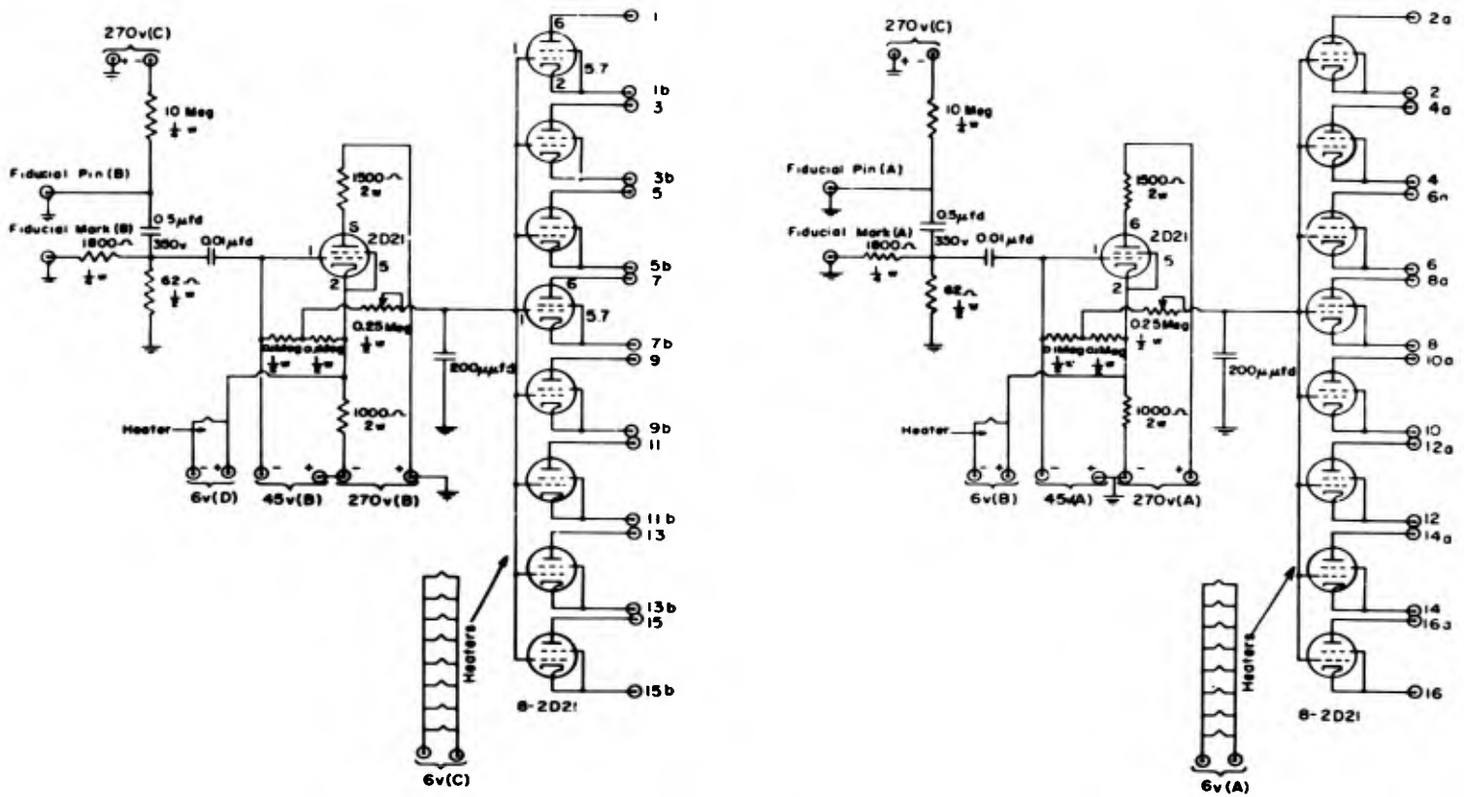

Fig. 2.3—Thyratron delay box.

connected to the delay box, and a second row was connected directly to the pin box. On the underground shot the nearest eight-pin stations were all connected to the delay box, and the remaining pins were connected directly to the pin box. The individual pins connected to the thyratron delay box were fed through separate thyratrons to the pin box, connection being made with 5-ft lengths of RG-54A/U.

The delay-box operation was as follows: An initial pulse from the charged fiducial pins, shorted by pressure or a highly ionized disturbance, caused the controlling thyratron to conduct and to remain conducting. The voltage of the biasing circuit at the individual pin thyratrons, initially at −45 volts below cathode potential, built up across the variable and fixed resistors, charging the biasing condenser. When sufficient charge was built up in the biasing circuit, all thyratrons were capable of firing. However, the circuit across the thyratrons was open, and thus no current flowed. When an individual switch closed, the associated thyratron circuit was completed, and the condenser to which the thyratron was coupled discharged, producing a pulse on the output line at the pin box. The pins connected directly to the pin box were simply shorted to discharge their condensers and give the same type of output signal.

2.4 RELAY BOX

The thyratron delay boxes and the line amplifiers were turned on by the EG&G −5 min control signal, which closed a series of relays in the relay box (see Fig. 2.4). The relay box, once actuated, remained electrically latched until it was destroyed. An extra relay was added for the amplifiers, but the circuit was otherwise as shown in Fig. 2.4.

2.5 PIN CHARGING

Pins were charged alternately positive and negative with equal charges. Positively charged pin condensers were hooked to thyratron plates, and negatively charged pin condensers were hooked to cathodes. All pins of like sign from a single box discharged differently valued R-C circuits to aid in identification of pulses. The pin-box circuit is shown in Fig. 2.5.

2.6 AMPLIFICATION

On the surface shot, pulses from the pin boxes were fed through 3000 ft of RG-8/U into the Y amplifier of the recording scopes and were amplified by a factor of about 8. On the underground shot the pulses were fed into a line amplifier, Fig. 2.6, at the pin box and were transmitted to the plates of the scopes through 3000 ft of RG-59/U. This amplifier was specially designed to take the pulses, positive or negative, from the pin boxes and amplify them by a factor of 6. The amplifier was used in an attempt to override signals induced in the 3000-ft cable by electromagnetic effects. All lines to scopes were terminated in their characteristic impedance.

2.7 OSCILLOSCOPE

The scope used was an unmodified Du Mont Model 241 with a blue screen. An external 5000-cycle pulse generator, Fig. 2.7, triggered the sweep, which was continuous. The sweep was approximately 3 in. long and was set at maximum intensity. In all cases, pulse heights were approximately $\frac{3}{4}$ in. high and were typical R-C decays. The scopes and the 5000-cycle generator were turned on 15 min before zero time. A constant voltage transformer was used for the oscilloscope, and a 5000-cycle power was used to eliminate line surge at zero time.

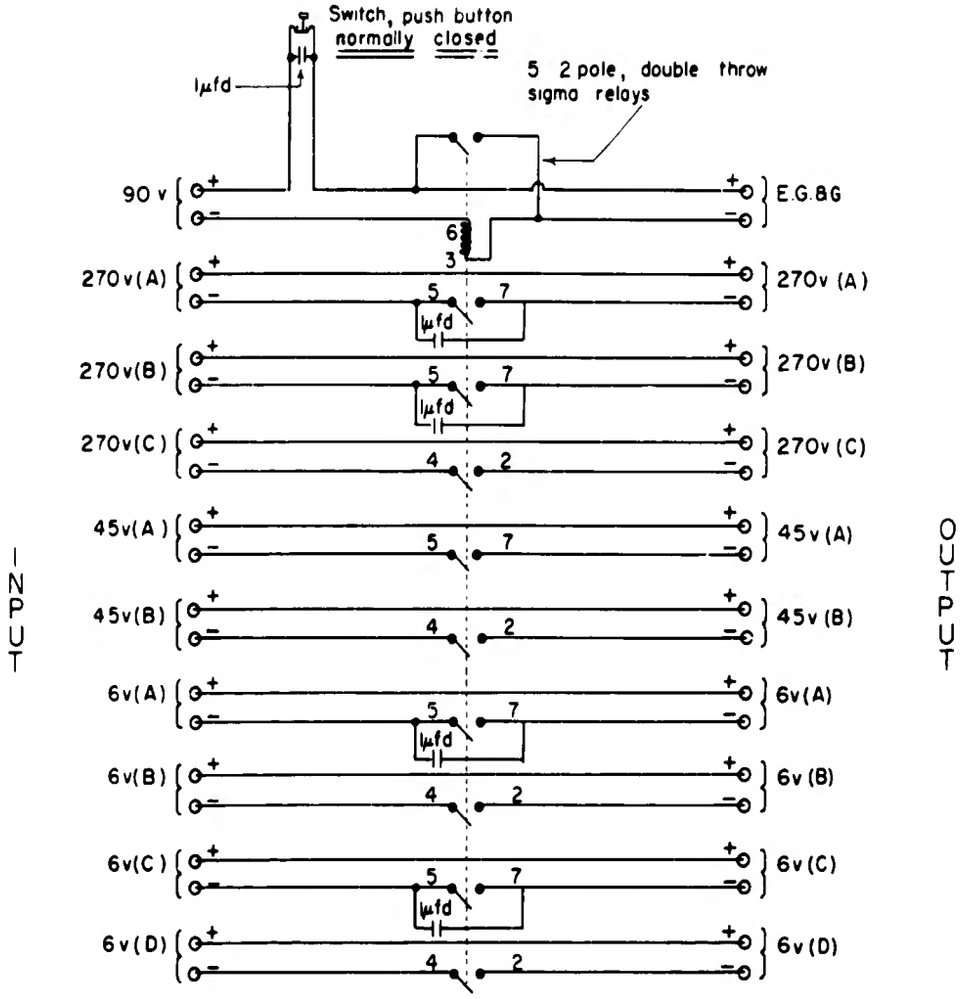

Fig. 2.4—Relay box.

SECRET

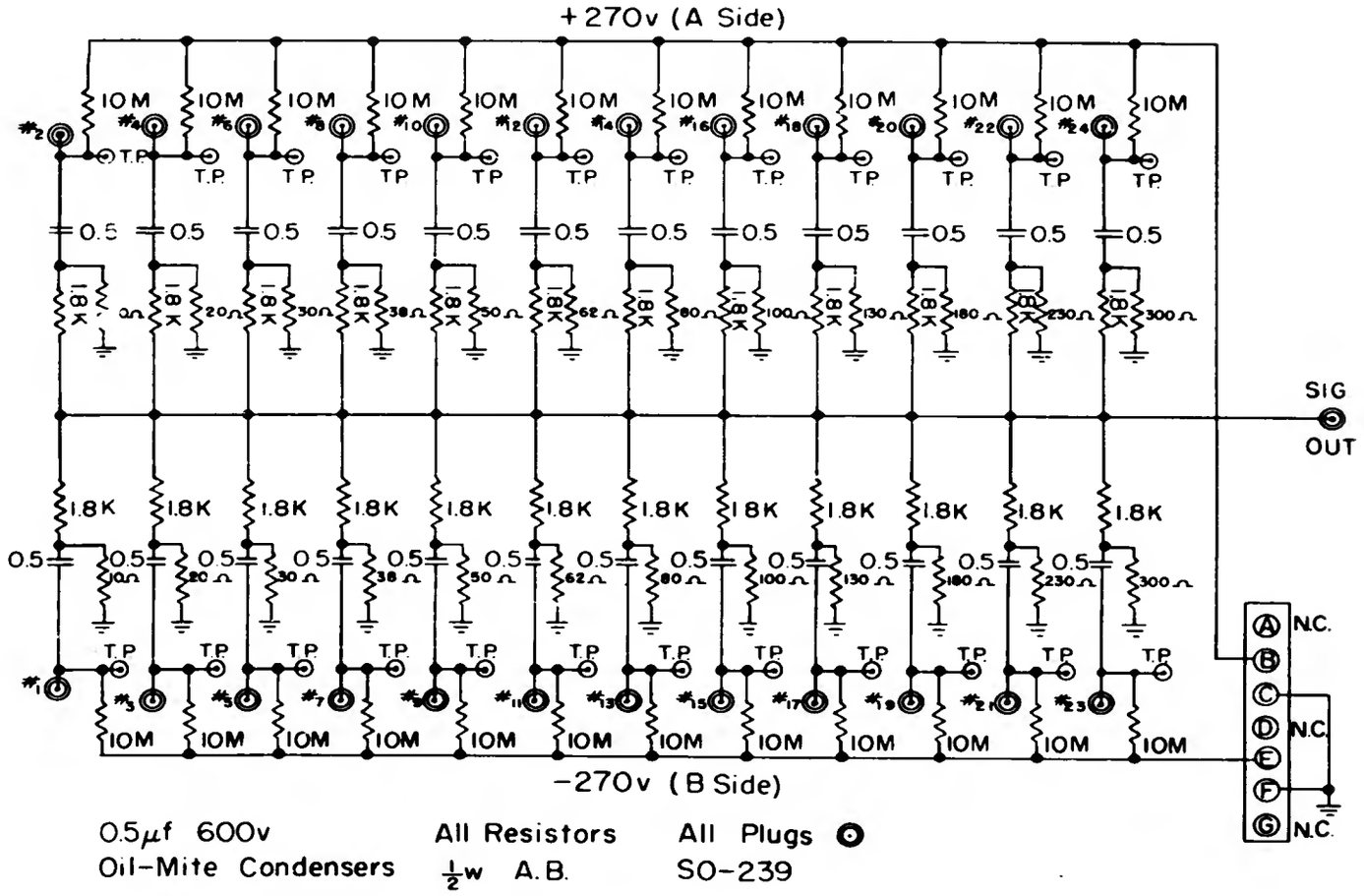

Fig. 2.5—Pin box.

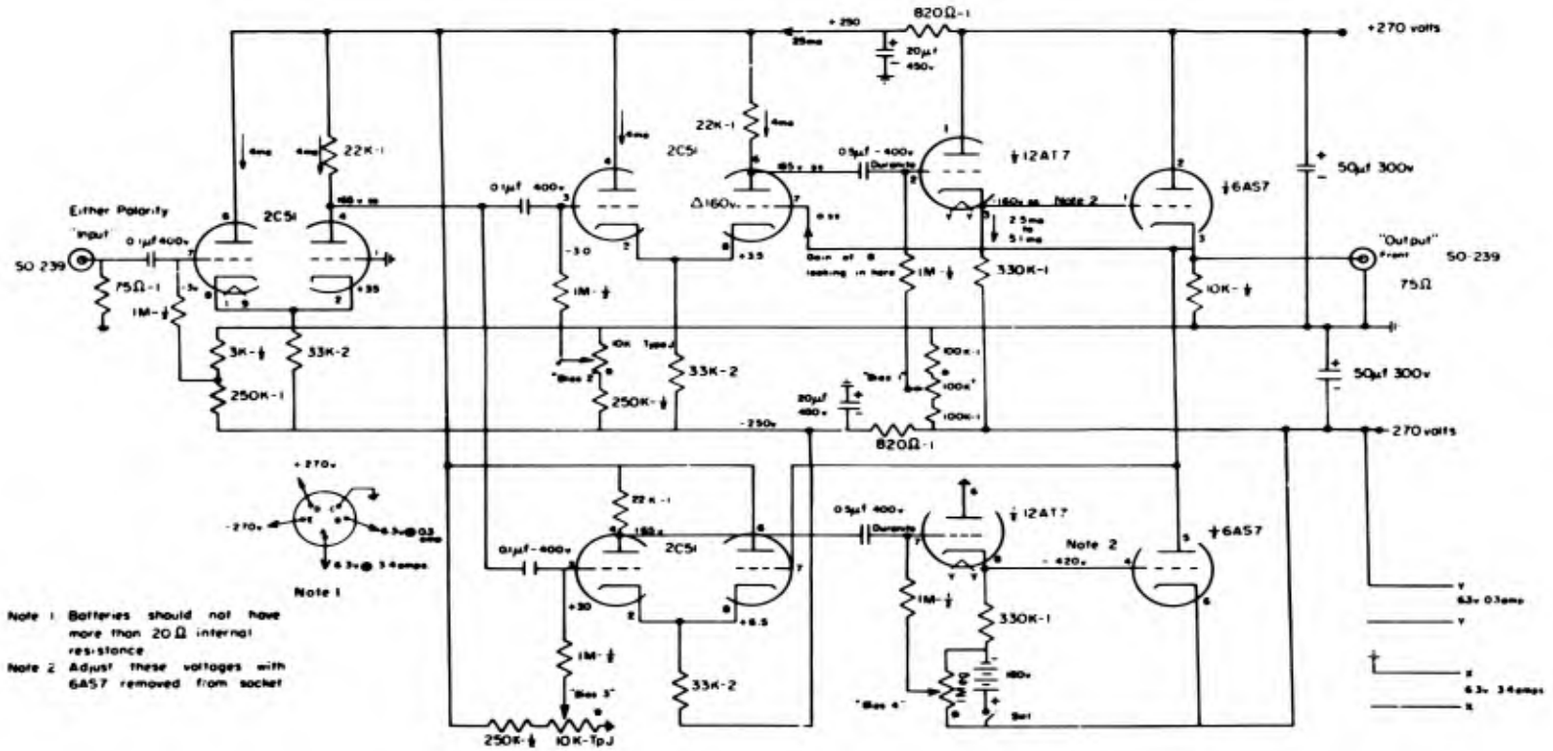

Note 1: Batteries should not have more than 20 Ω internal resistance

Note 2: Adjust these voltages with 6AS7 removed from socket

Fig. 2.6—The 75-ohm line amplifier.

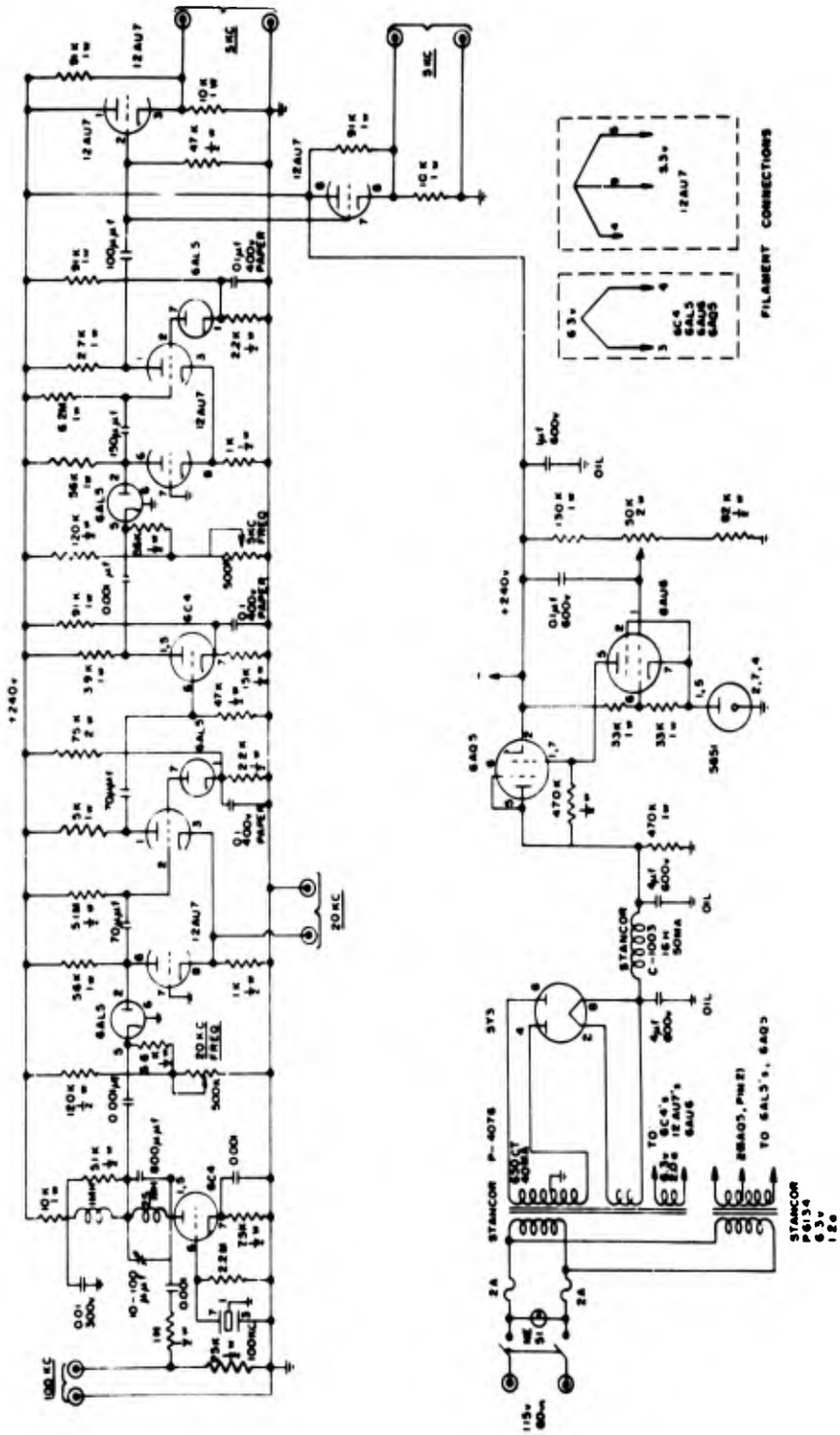

Fig. 2.7 — A 5-kc pulse generator.

SECRET

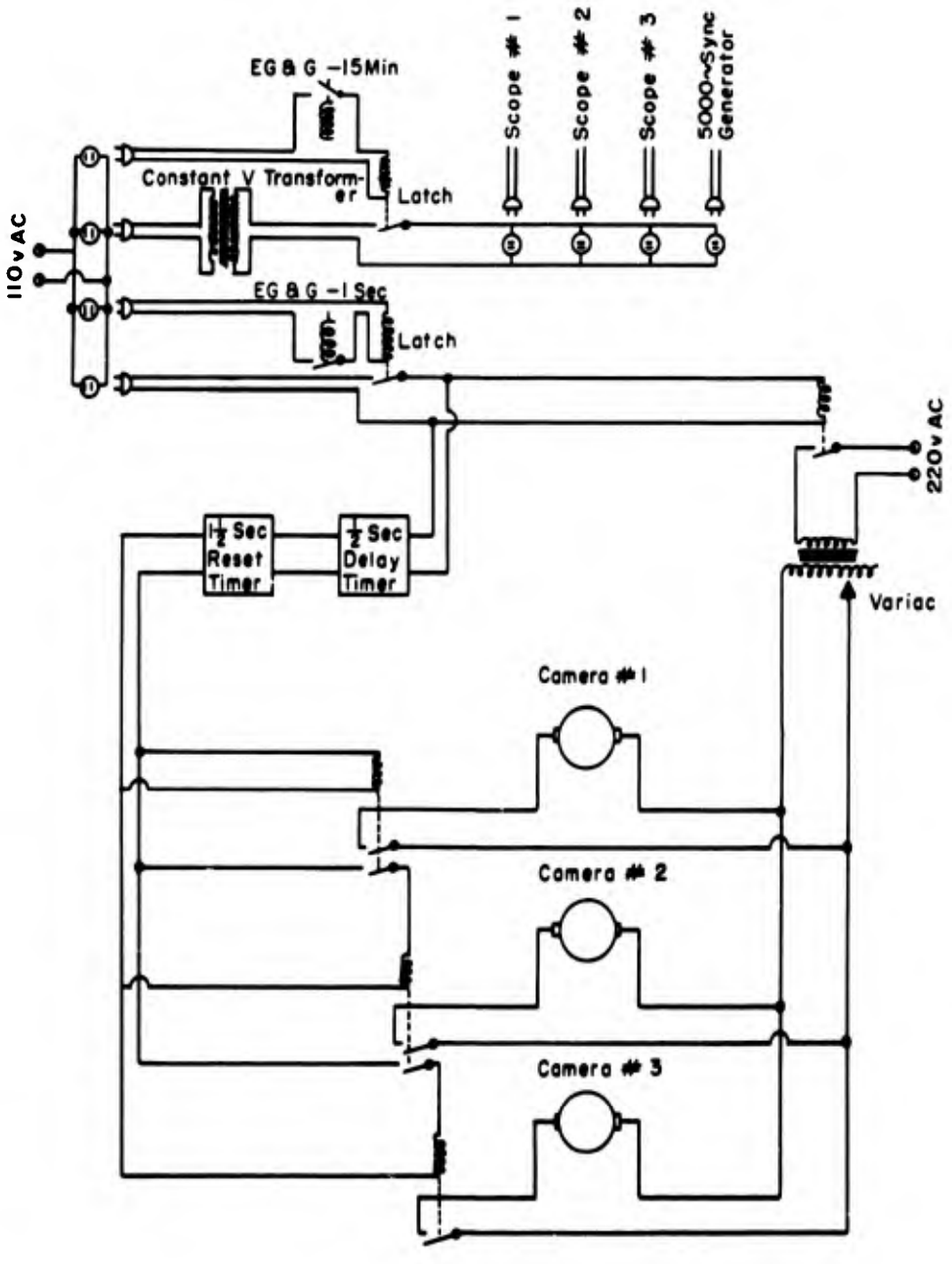

Fig. 2.8—Diagram of the recording-equipment wiring.

SECRET

2.8 CAMERAS

The cameras used were General Radio Model 651AE oscilloscope recording cameras with either f/1.5 or f/2 lenses. A control system for delaying the start of the cameras and for cutting them off was built so that the control device started at −1 sec and the cameras at approximately $-\frac{1}{2}$ sec. The cameras turned off at approximately +1 sec from zero time. The three cameras were started through a series of relays to reduce the power drop due to starting surge of the cameras. Latch relays were built into the circuit to ensure positive closure of relays during the recording interval. The camera power was fed from a Variac set at approximately 290 volts alternating current; maximum camera speed was between 80 and 100 ft/sec.

2.9 FILM

The film used was Kodak Linagraph Panchromatic (35 mm, 100-ft roll). Film was loaded in complete darkness. The only light for exposure came from the oscilloscope plates. A standard National Bureau of Standards focusing chart was used in focusing. After exposure the films were developed between 15 and 20 min in new D-19 developer.

2.10 RECORDING SHELTER

A diagram of the apparatus in the recording shelter is shown in Fig. 2.8. Two of the cameras were used to obtain the pin network records, and the third camera [identical as to scope, scope settings (except gain), and type of camera] was for recording of the resistance network pulses. The resistance method is described in Part V of this report.

CHAPTER 3

INSTALLATION OF PINS

3.1 SURFACE-SHOT INSTALLATION

Pin stations were placed in the ground at intervals of 18 in. along a vertical line through bomb center. The initial station was 18 in. below ground surface directly under the bomb. Ten stations were placed along this line; a fiducial station, above ground, was placed 6 ft from bomb center, and an added station was placed at a point 6 ft from the lower station (Station 10) on a horizontal line from that station. The cables were led back underground to a mixing box which was covered with approximately $3\frac{1}{2}$ ft of earth.

At each station, except the fiducial station, one pressure-type pin, one ionization-type pin, and one resistor lead were installed. Two pin boxes, one with a thyratron delay unit in the circuit, were used. Alternate pressure and ionization pins were connected to a single pin box for one line of pins; the remaining ionization and pressure pins were hooked to the thyratron delay box and then to the second pin box. Pins of each line were charged alternately positive and negative. Output leads from the two pin boxes were led back to separate scopes.

3.2 UNDERGROUND-SHOT INSTALLATION

The installation, Fig. 3.1, consisted of five rows of stations placed so that 24 stations were in a horizontal plane through bomb zero (17-ft depth) and 10 stations were in a horizontal plane 12 ft above the zero plane (5-ft depth). The pins were spaced so that the difference in distance from zero of any two adjacent stations in a plane was 18 in. The first deep pin was 4 in. from the outside of the metal caisson. The first shallow pin was at a distance of 25-ft slant range from zero. The first 14 stations had identical pin and resistor installations as for the surface-shot stations. The remaining stations had only one pressure-type pin at each station.

All ionization pins in the deep row and the pressure pins in the shallow row were mixed at one pin box. All deep pressure pins were connected to the second pin box. The first station contained two fiducial pins and a resistor lead only. The next eight pins in each line were fed through the thyratron delay box to the pin boxes. The remaining pins were hooked directly to the pin boxes. Signals were fed into the amplifiers before being transmitted to the recording shelter.

Pins, installed in specially designed mounts, were installed through 2-in. pipes sunk vertically. All cables were buried 2 ft to protect them from air shock. The mixing box was lined with steel, and the entire box, a 4-ft cube, was covered with a 2-ft mound of earth.

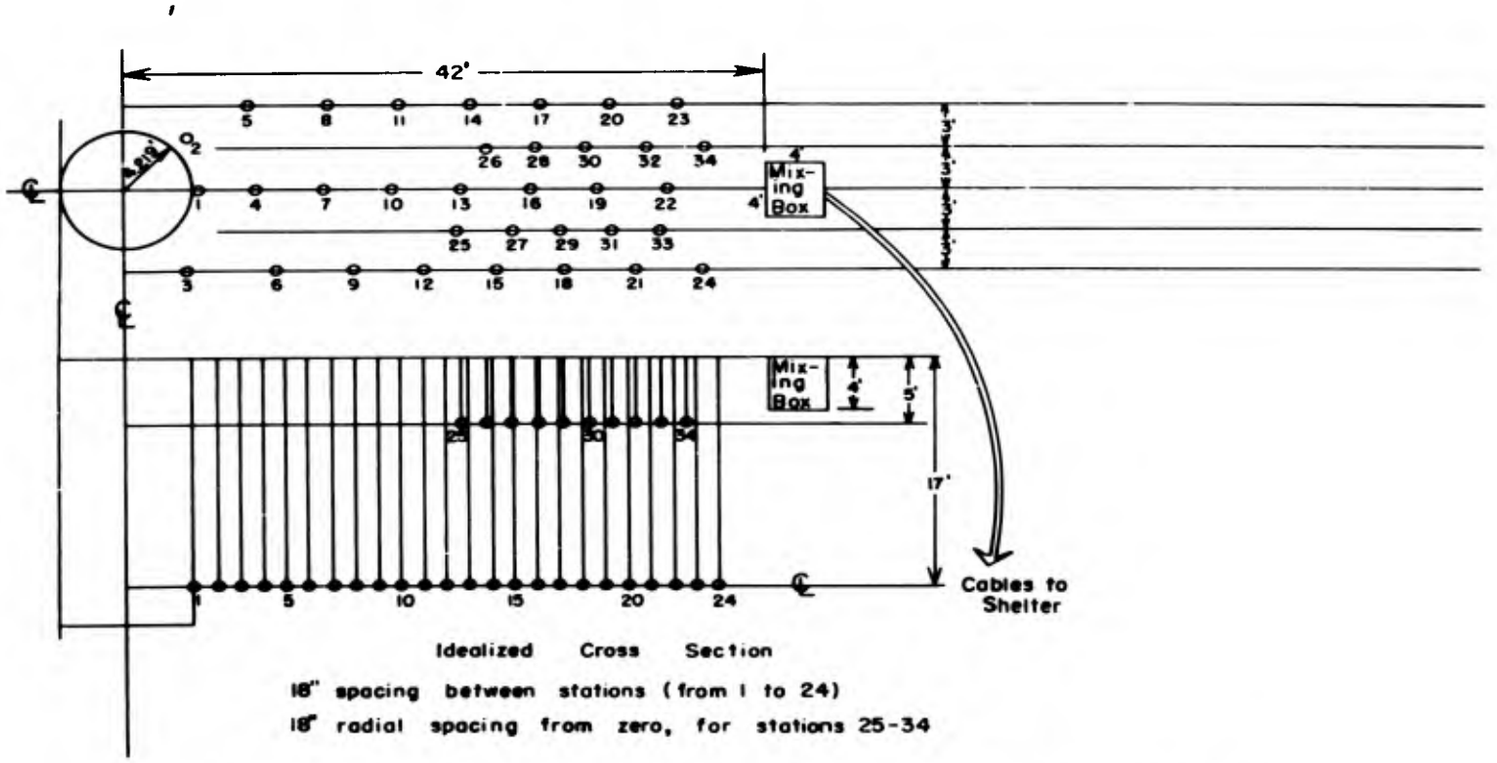

Fig. 3.1—Cross section showing pin installation, Operation Jangle underground shot. Spacing between Stations 1 to 24, 18 in.; radial spacing from zero for Stations 25 to 34, 18 in. Stations 1 and 2: two fiducial pins and one resistor lead. Stations 2 to 10 (less Station 5, which was not used): two pins and one resistor lead. Stations 11 to 15: two pins and one resistor lead. Stations 16 to 34: one pressure pin. Whenever two pins are used, one is a pressure pin and the other an ionization pin. Stations 1 to 10, 17-ft installation pipes. Stations 11 to 24, 15-ft installation pipes. Stations 25 to 34, 5-ft installation pipes.

CHAPTER 4

CONCLUSIONS AND RECOMMENDATIONS

4.1 DISCUSSION

As mentioned in Sec. 1.2 of this part, it seems probable that the initial high-level signal swamped the amplifiers on the underground shot. Closure of all pins due to ionization is very improbable since similar instruments in the resistance method were not shorted. Furthermore, shorting of pins of equal voltages and reversed polarities would send out a null signal, not the large positive signal noted on the record.

It was noted that one amplifier reversed the polarity of signals induced into it. The signals seen at the scopes were both positive, indicating that the amplifier was swamped by a large signal of positive polarity which passed through without becoming lost in the amplifier circuit. The amplifier, which would normally reverse polarity of a signal, shows signs of having tried and failed to negate the positive pulse. During the time between the initial and final pulses on the record no signals were received at the scope. Since it is improbable that all pins were initially shorted, this would indicate a definite failure in the amplifier.

The failure in the system for the surface shot was undoubtedly due to ionizing radiation which destroyed the electrical properties of batteries and condensers in the mixing box. No signal was received other than a large overdriving pulse. If any of the pins had been in operating condition, the signals of the pin farthest out should have been visible on the record. No signals were detectable.

4.2 RECOMMENDATIONS

A similar system is believed feasible with the following modifications: All signals to one scope should be of like signs. No pins, except fiducial pins, should have less than $2\frac{1}{2}$ meters of earth shielding. Clippers should control the size of an initial signal along lines which may be affected by electromagnetic phenomena. No instruments, except pickups, should have less than 4 meters of earth shielding.

Part V

RESISTOR METHOD FOR DETERMINATION OF RADIUS VS TIME OF A NUCLEAR EXPLOSION IN SOIL, OPERATION JANGLE UNDERGROUND SHOT

by

Cecil G. Young, Jr.

SECRET

CHAPTER 1

INTRODUCTION

The purpose of utilizing the resistor method was twofold. Primarily it was an attempt to measure the time of arrival at known stations of the passage of the fireball and subsequent shock wave through the ground. Second, if such a system proved successful, a simplified method of velocity instrumentation at short ranges would be feasible.

The use of resistors connected in series and embedded in high explosives was successfully employed by the Sandia Corporation to determine detonation velocity. High temperatures associated with the expanding detonation front produced enough ionization to short out successive resistors and thereby produce a series of voltage steps. These signals were transmitted through a twisted-pair line to a distant oscilloscope and were photographed. A similar system suggested itself for locating as a function of time the underground shock wave and fireball from a nuclear explosion out to ranges where the front produced enough thermal ionization to short out electrical components. A difficulty in such a system was the intense gamma ionization that might cause any electronic instrument at close ranges to malfunction. In an underground test, however, the earth should provide enough shielding to protect rugged electronic instruments and reduce the radiation on close-in components. Calculations* have indicated that for a 1-kt bomb the gamma-radiation level at 3 meters through earth after about 150 μsec would be down enough to allow a dielectric to regain its insulating properties. Accordingly a modified resistor method was developed to locate an ionized shock front or ionized fireball out to a range of about 8 meters.

---

*The calculations are based on the Greenhouse results given in Greenhouse Report, Annex 1.6, Part II, Sec. 2, and on the gamma levels given in Los Alamos Scientific Laboratory Report LAMD-1087 (not available).

CHAPTER 2

INSTRUMENTATION AND FIELD TESTS

2.1 INSTRUMENTATION

2.1.1 General Plan

For the Operation Jangle surface and underground shots at the Nevada Proving Grounds, 14 resistor stations were used. On the surface shot the stations were located at 18-in. intervals on a vertical line directly below the bomb. On the underground shot they were located at 18-in. intervals at a depth of 17.5 ft on horizontal radial lines beginning at 1.37 meters from bomb zero. In both cases the signal-generating circuits were located at about 13 meters from zero and 1 meter underground. The RG-59/U coaxial cable, 3000 ft long, carried the signals to an underground recording shelter 2500 ft from the zero point. A General Radio 651AE high-speed camera photographed the signals displayed on a Du Mont 241 oscilloscope. Figure 2.1 shows the details of the layout and locations for the underground shot.

2.1.2 Design Considerations

Since the resistors were connected in series, it was necessary to ensure that the circuit would never be opened during the successive shorting of resistors. Any such interruption would remove voltages from all remaining resistors. To prevent this the resistors were at the same location as the signal-generating circuits, and center conductors of coaxial cables were connected to each resistor and terminated with the open end at the station positions. In theory this was no different from placing the resistors themselves at the station positions and running the lines out to terminals that would connect them in series. For such a system to function properly the ionized front would have to continue to short out the connecting leads after the resistors had been destroyed. If this were the case, the closest radial position of the line would determine the instant of shorting. By preventing destruction of the resistors until all measurements were recorded, any sporadic opening of the lines would not break the series current flow. An additional feature for reliability was the shorting of each resistor to ground rather than just across its terminals. This arrangement required that only the previous resistor line had to remain shorted at the instant of shorting of the next resistor. Accordingly each line consisted of a coaxial cable with the outer conductor grounded and the center conductor connected to one side of its appropriate resistor. A parallel resistor system was avoided in order to eliminate the necessity of using large resistor values. Smaller values would not be so sensitive to electromagnetic pickup.

Other provisions were made to limit the size of any signal, to vary the amplitudes for identification purposes, and to minimize attenuation by proper matching to the 3000-ft transmission cable.

Based on previous experience and pile experiments,[1] electronic equipment employing gas tubes, electrolytic capacitors, inductances, and high impedances was avoided. Low-impedance circuits with carbon resistors and mica capacitors were used whenever possible to minimize

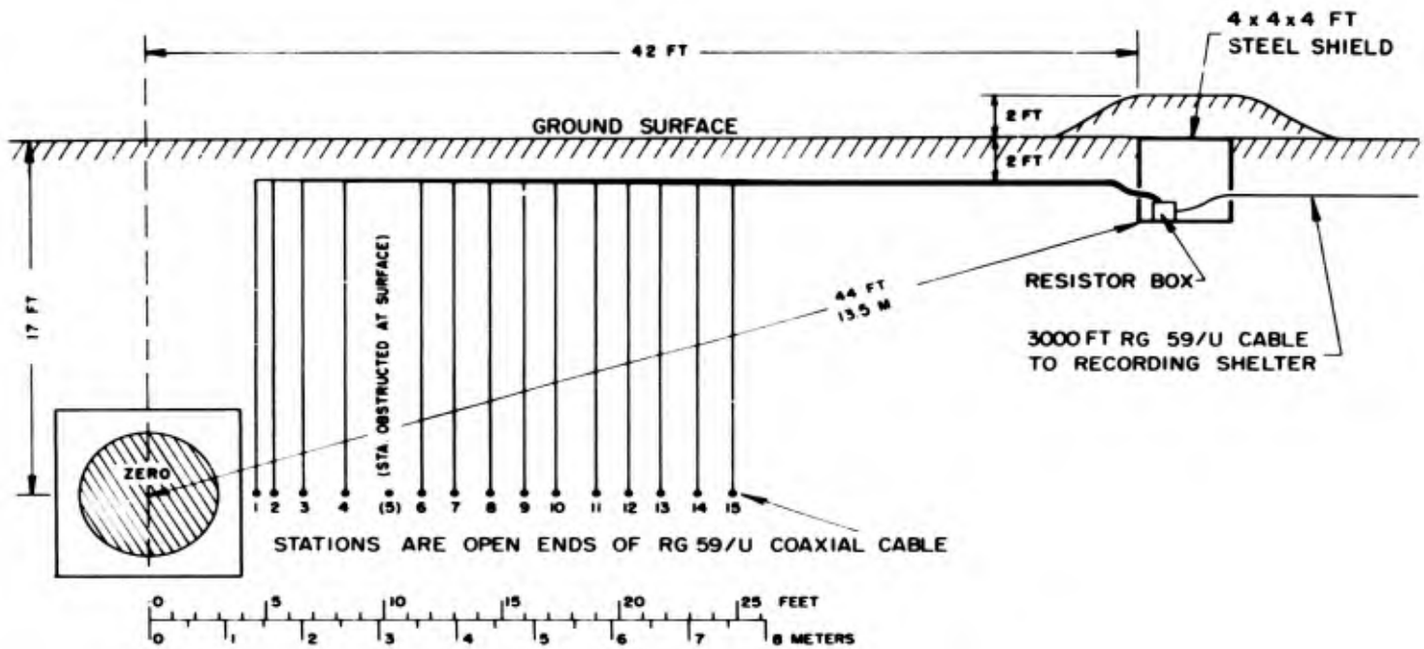

Fig. 2.1—Schematic diagram of station positions and instrumentation, resistor method, underground shot.

the effects of gamma and electromagnetic radiation.

2.1.3 Detailed System

(a) Signal-generating Circuit. Figure 2.2 shows the circuit diagram of the resistor bank and the successive components used to develop and transmit the final signal to be recorded. Resistors 1 to 14 were given values such that, when each was successively shorted to ground, the voltage across the load resistor (No. 15) was increased as shown in Table 2.1. Steps 4, 6, and 9 were increased for identification.

Table 2.1—RESISTOR-VOLTAGE STEPS

Resistor shorted	Voltage across R_{15}, volts	Step increase, volts
None	58	
1	72	14
2	84	12
3	96	12
4	123	27
5	133	10
6	162	29
7	172	10
8	184	12
9	203	19
10	214	11
11	225	11
12	236	11
13	247	11
14	258	11

The step voltages generated across R_{15} were fed to an R-C differentiator with a time constant of 30 μsec. A positive diode clipper in series with a 22½-volt battery was used to limit any large pulses resulting from electromagnetic pickup or initial shorting of many resistors. A negative diode clipper was used to remove unwanted negative signals that might be generated by intermittent removal of shorts across the resistors. A cathode follower matched the final signal to the coaxial transmission cable. For maximum transfer of signal voltage both halves of a 6AS7 triode (high transconductance) were used.

(b) Recording. Data recording was obtained with a Du Mont 241 oscilloscope with a 5BP11 tube and a General Radio 651AE high-speed camera. Signals were displayed on a horizontal sweep 200 μsec in length. Sweep flyback time was less than 10 μsec. One hundred feet of Kodak Linagraph Panchromatic 35-mm film, running at a rate of 50 ft/sec, produced a raster of successive traces approximately ⅛ in. apart. Development for 20 min in D-19 developer produced faint but readable records.

The transmission cable was terminated in a limiting and clipping circuit at the vertical (Y) amplifier of the oscilloscope. To retain a high-impedance termination for maximum voltage transfer a resistance of 1 megohm was used. A coupling capacitor of 30 μμf gave an R-C product of 30 μsec. Gain settings were adjusted to give a vertical deflection of ½ in. per 20 volts applied to the Y-input terminals.

(c) Control. Instrumentation control was initiated by the following master timing signals:

−15 min: the oscilloscope was turned on
−5 min: voltages were applied to the signal-generating-unit circuits
−1 sec: the camera control unit was actuated

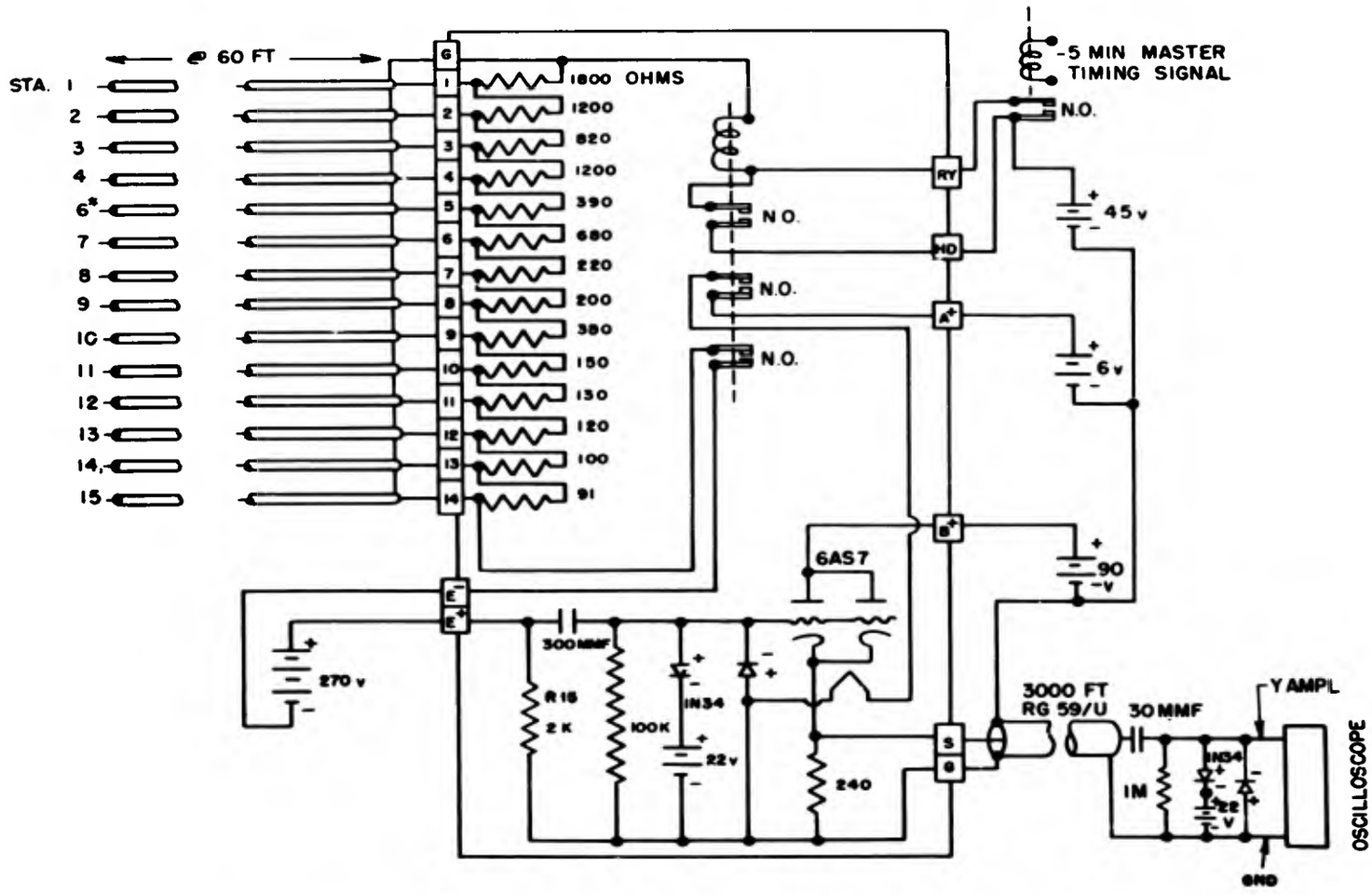

Fig. 2.2—Circuit of signal-generating unit, resistor box. Station 5 was not used because of a physical obstruction.

Hold-down relays were utilized to ensure that switches, once actuated, did not open or chatter until after zero time. A $\frac{1}{2}$-sec delay timer turned on the camera at $-\frac{1}{2}$ sec. At approximately +1 sec, all power was turned off. The control system was used jointly by this experiment and by the pressure-ionization pin experiment.

2.2 FIELD TESTS

Three field tests were made at Beta site, Los Alamos, to test various systems and to obtain experience in equipment installation and operation. Resistors were set at 0, 3, 6, and 9 in. from a buried 10-lb charge of high explosive. No evidence of shorting was recorded more than 3 in. from the charge. It was because of these poor results that 8 meters was chosen by direct scaling as the maximum range that shorting could be expected from a 1-kt bomb.

REFERENCE

1. NEPA Project, Effects of Fission Produced Radiation on Electronic Equipment, Frederic Flader, Inc., NEPA Report 624-FF-13.

CHAPTER 3

RESULTS

3.1 OPERATION JANGLE SURFACE SHOT

No data were obtained from the record on the Operation Jangle surface shot. At zero time the trace completely disappeared from the oscilloscope for 60 msec. It is suspected that a large current surge from electromagnetic phenomena was induced in the power and signal cables.

3.2 OPERATION JANGLE UNDERGROUND SHOT

3.2.1 Modifications

To avoid the blanking effect from the electromagnetic disturbance, the limiting and clipping circuit (see Sec. 2.1.3a of this part) was inserted at the input terminals to the oscilloscope. It was hoped that this would prevent any high-voltage surge on the signal cable from driving the sweep trace off the oscilloscope screen. Any low-frequency voltage surge would be differentiated by the R-C coupling. Excessive voltage amplitudes would be bypassed by the IN34 crystal diodes or, at most, would produce short spike pulses.

3.2.2 Record

Figures 3.1 and 3.2 show the time-of-arrival record. It appears as though the first three stations were shorted at zero time by gamma radiation. Stations 4 and 6 (5 was not instrumented) are barely in evidence because of some continuing initial disturbance. Stations 7 to 15 are very clear and are easily identified by their relative amplitudes. At 7.29 and 9.60 msec the record shows distinct evidence of shock arrival at the signal-generating unit. In addition to the initial noise disturbance the only other noise signal on the record appears at 735 μsec.

Fig. 3.1—Operation Jangle underground shot record, contact print.

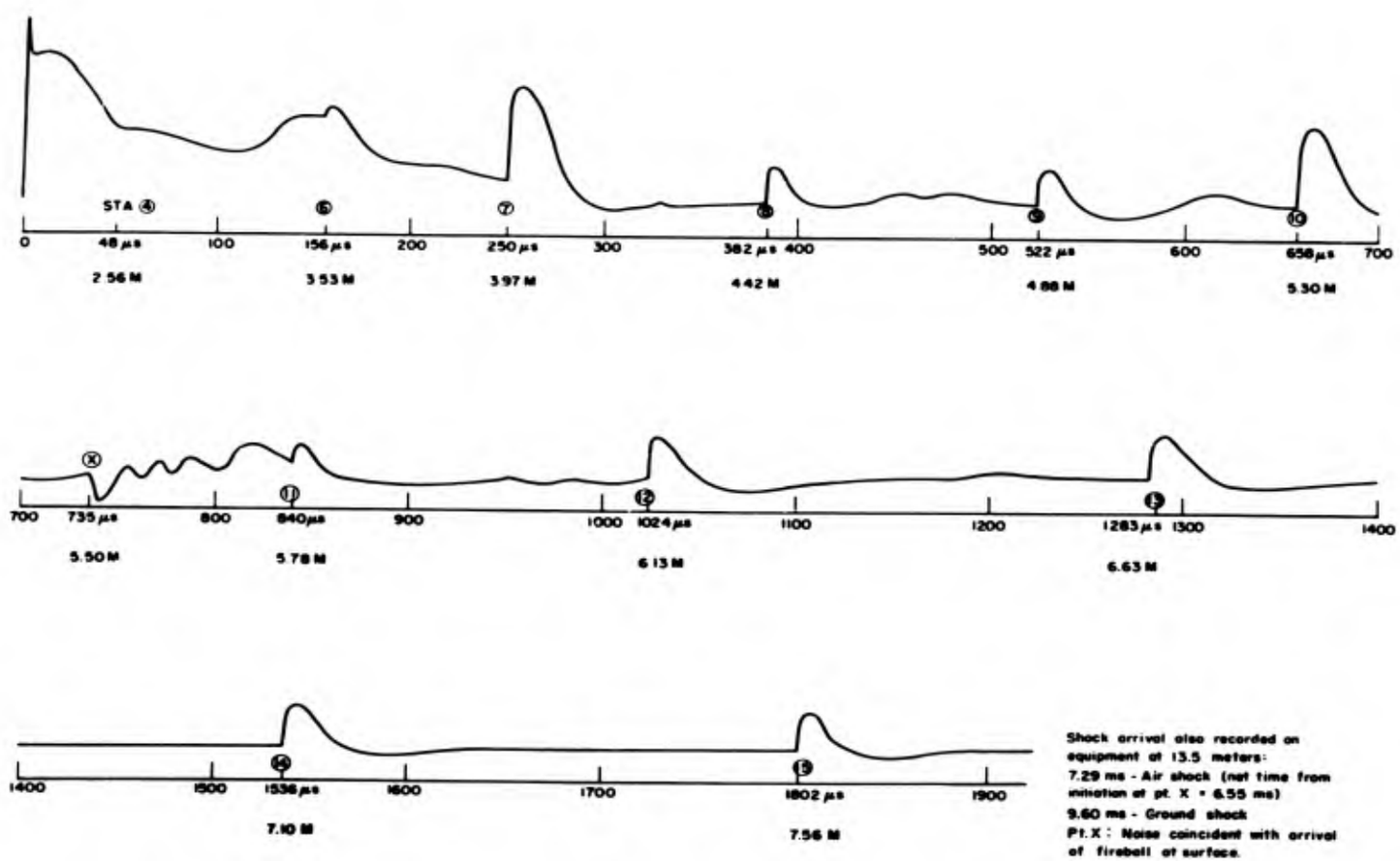

Fig. 3.2—Operation Jangle underground shot record. This is a tracing of sections of Fig. 3.1, showing time and distance for each station.

CHAPTER 4

CONCLUSIONS

4.1 COMPUTATIONS

Table 4.1 is a summary of the recorded and measured data, and the velocities are computed from these data. The distance-vs-time and the distance-vs-velocity curves are given in Figs. 4.1 and 4.2. In order to compute the velocities the slope n of the curve of log R vs log t was plotted against R. Values of n taken from the smoothed curve, Fig. 4.3, were used to obtain the velocity U from the following formulas:

$$R = ct^n$$

$$U = \frac{dR}{dt} = nct^{n-1} = \frac{nR}{t}$$

Table 4.1—DATA SUMMARY FOR OPERATION JANGLE UNDERGROUND SHOT

Station	R ± 0.05, meters	t ± 0.002, msec	n ± 0.005*	U ± 2%, meters/msec	U ± 2%, ft/sec
1†	1.37				
2†	1.63				
3†	2.01				
4	2.56	0.048	0.240	12.80	41,900
5‡	3.14				
6	3.53	0.156	0.250	5.66	18,500
7	3.97	0.250	0.273	4.33	14,200
8	4.42	0.382	0.307	3.55	11,600
9	4.88	0.522	0.325	3.04	9,950
10	5.30	0.658	0.336	2.70	8,850
11	5.78	0.840	0.345	2.37	7,750
12	6.13	1.024	0.353	2.11	6,900
13	6.63	1.283	0.362	1.86	6,100
14	7.10	1.536	0.366	1.69	5,550
15	7.56	1.802	0.370	1.55	5,100

*n is the slope of the curve of log R vs log t and is used to compute U = nR/t.
† Triggered by radiation at zero time.
‡ This station was omitted because of obstructions.

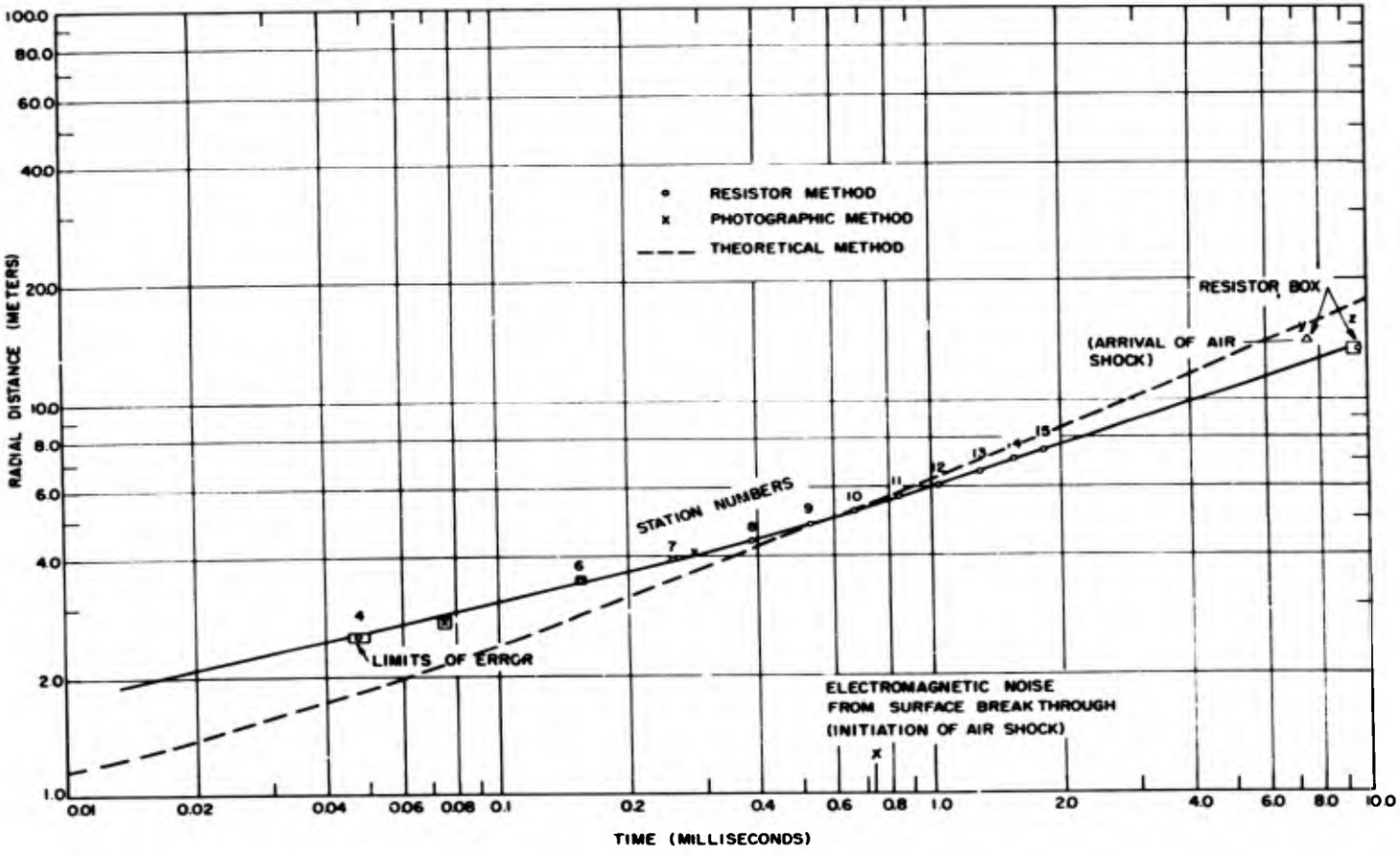

Fig. 4.1—Radial distance vs time of shock arrival, Operation Jangle underground shot. For comparison, three data points from the photographic method and a theoretical curve are included. Points x, y, and z refer to the record.

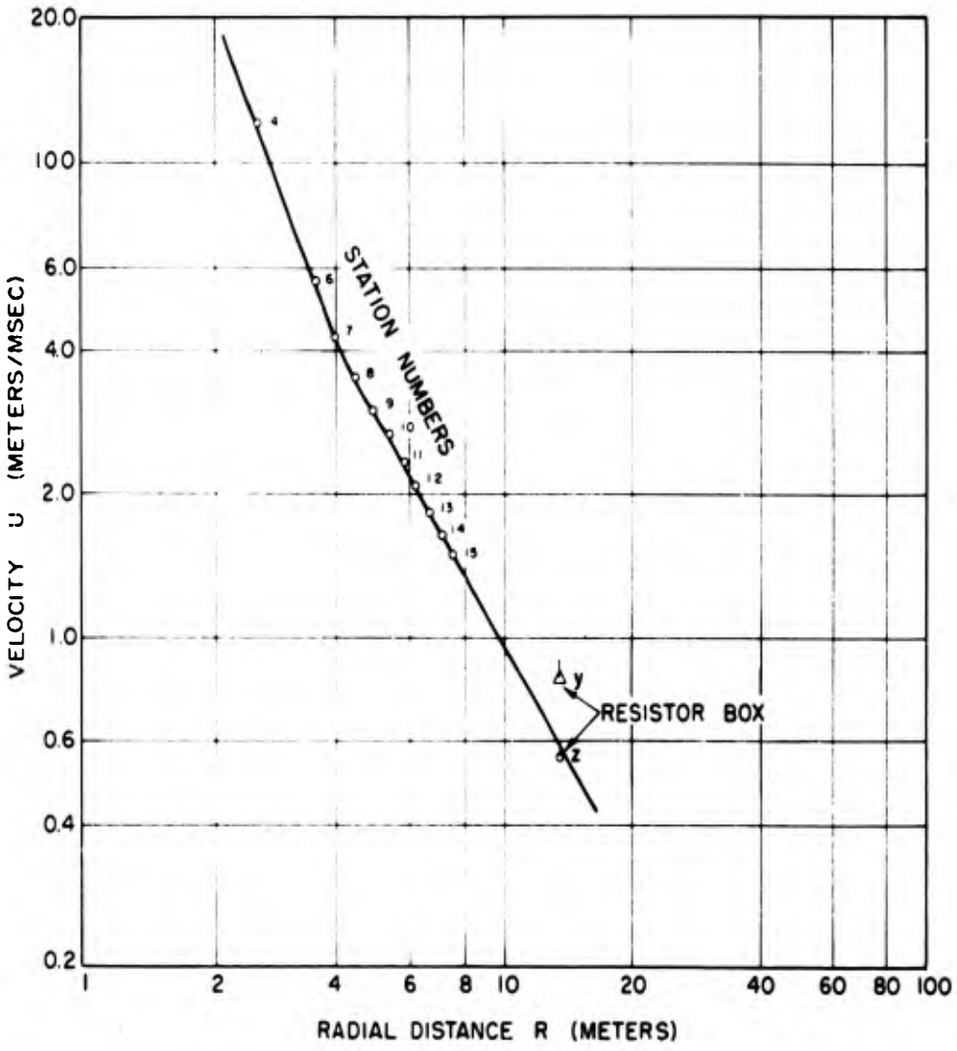

Fig. 4.2—Radial distance vs shock velocity, Operation Jangle underground shot. Points y and z are minimum values with maximum limits indicated.

SECRET

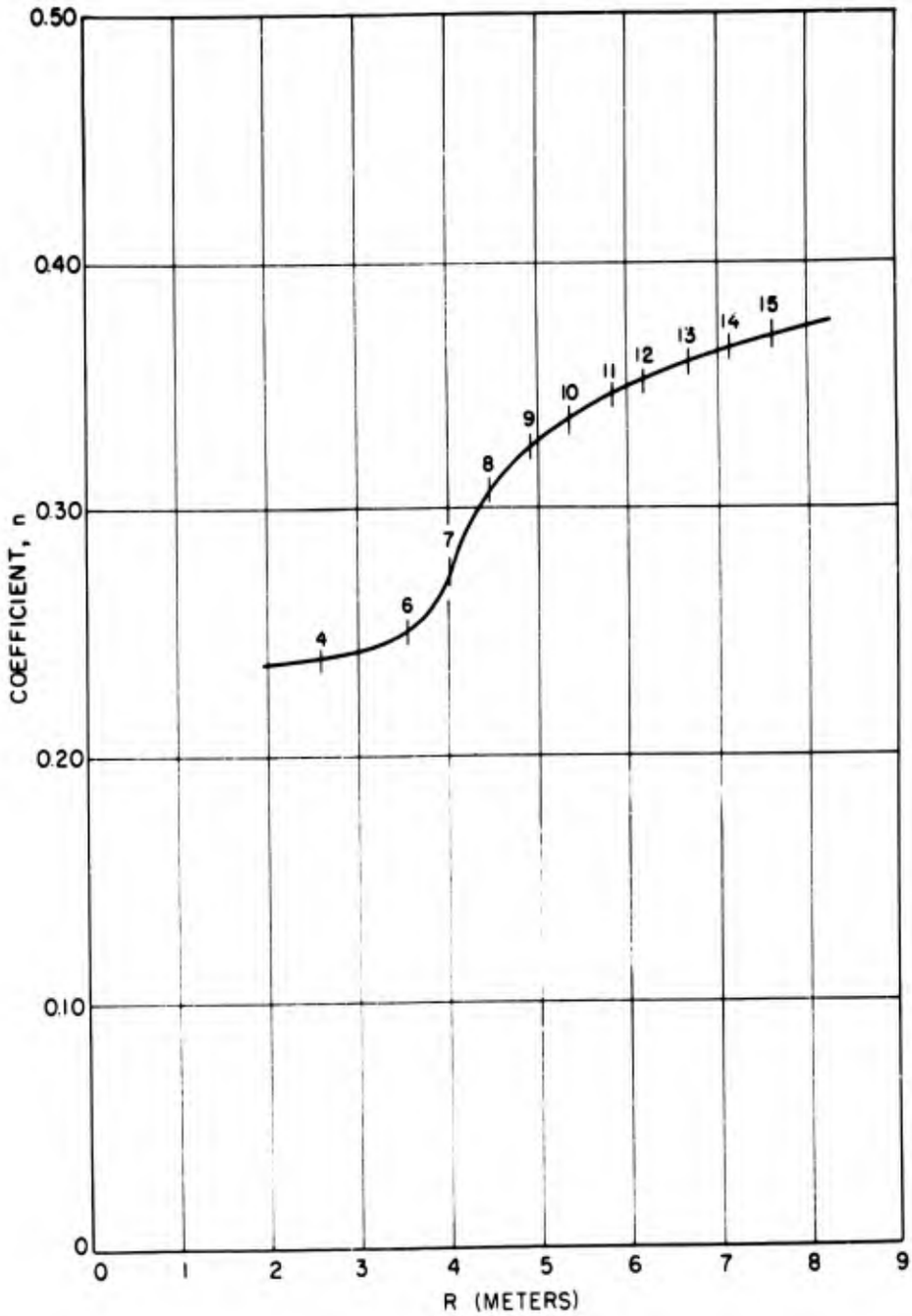

Fig. 4.3—Coefficient n as a function of radial range R, Operation Jangle underground shot. In this graph, n represents the slope of the curve of log R vs log t.

SECRET

4.2 INTERPRETATIONS

In addition to the primary data, signals at points x, y, and z gave interesting information. The noise signal, point x, at 735 μsec was suspected of being the electromagnetic disturbance associated with the fireball breaking through the ground surface. The curve of log R vs log t indicates that this occurred at the instant the fireball had traveled 18 ft horizontally. Since the bomb was 17 ft deep, the explanation seems reasonable. Except at zero time no other spurious noise was recorded. At 7.29 msec, point y, and at 9.60 msec, point z, the record showed evidence of the signal-generating unit being struck. Signal Y is characteristic of an intermittent jarring, and signal Z indicates final destruction of the unit. Using its range of 13.5 meters the curves of log R vs log t and of log R vs log U indicate that the ground shock arrived at time Z, or slightly sooner if some delay is taken into account. Time Y, also being a maximum arrival time, appears too early to fit the ground-shock curve. This could be explained as air-shock arrival. Since the unit was 1 meter underground, this would also explain why air shock would only jar the equipment whereas the ground shock would destroy it. If the speculation is correct that point x was the time of initiation of air shock, the record shows that air shock traveled 13.5 meters in 6.55 msec whereas the ground shock traveled the same distance in 9.60 msec. Figure 4.1 also shows that three data points from the photographic method are in close agreement with the resistor method.

4.3 COMPARISON WITH THEORY

The measured ground-shock velocities agree fairly closely with the predicted velocities as calculated by F. B. Porzel; the dotted curve in Fig. 4.1 shows the theoretical graph of log R vs log t. Measured velocities are increasingly higher than computed velocities at radial distances less than 3 meters and are slightly lower at greater distances. Lack of knowledge of the soil constituents at the Nevada Proving Grounds accounts for much of the discrepancy. In view of the assumptions necessary in the theoretical calculations, the agreement is considered excellent.

CHAPTER 5

RECOMMENDATIONS

These recommendations are suggested for future underground measurements for a 1-kt bomb. For greater yields, the values should be increased according to the appropriate scaling laws.

1. Stations closer than 3 meters are sensitive to gamma radiation and can be used only to record zero time.

2. There was no evidence of intermittent shorting at 75 meters, the maximum range investigated. This suggests that additional stations could be installed at greater ranges with good results.

3. If more than 14 stations are desired, the maximum requirement for voltage and resistor values can be kept low by using two or more separate systems coupled together into a common transmission line.

4. Electromagnetic noise picked up by transmission and power cable may be reduced by (a) using heavier shielded cable such as RG-5/U, (b) using a balanced line with neither side grounded, and (c) using batteries for oscilloscope power.

5. Clearer records might be obtained by increasing the oscilloscope intensity voltage and by using film developer SD-19A instead of D-19.

DISTRIBUTION

	Copy
ARMY ACTIVITIES	
Chief of Ordnance	1–3
Chief Chemical Officer	4–7
Chief of Engineers	8–10
Quartermaster General	11–15
Chief of Transportation	16–17
Chief Signal Officer	18–20
Surgeon General	21–23
Provost Marshal General	24–26
Chief, Army Field Forces	27–30
President, Army Field Forces Board No. 1, Fort Bragg	31
President, Army Field Forces Board No. 2, Fort Knox	32
President, Army Field Forces Board No. 3, Fort Benning	33
President, Army Field Forces Board No. 4, Fort Bliss	34
Commandant, Infantry School, Fort Benning	35–36
Commandant, Armored School, Fort Knox	37–38
President, Artillery School Board, Fort Sill	39–40
Commandant, AA&GM Branch, Artillery School, Fort Bliss	41–42
Commandant, Army War College	43–44
Commandant, Command and General Staff College, Fort Leavenworth	45–46
Commandant, Army General School, Fort Riley	47
Commanding General, First Army, Governor's Island	48–49
Commanding General, Second Army, Fort George G. Meade	50–51
Commanding General, Third Army, Fort McPherson	52–53
Commanding General, Fourth Army, Fort Sam Houston	54–55
Commanding General, Fifth Army, Chicago	56–57
Commanding General, Sixth Army, Presidio of San Francisco	58–59
Commander-in-Chief, European Command	60–61
Commander-in-Chief, Far East	62–63
Commanding General, U. S. Army, Pacific	64–65
Commanding General, U. S. Army, Caribbean	66–67
Commanding General, U. S. Army, Alaska	68–69
Operations Research Office (Johns Hopkins University)	70–72
Commanding Officer, Ballistic Research Laboratories	73–74
Commanding Officer, Engineer Research and Development Laboratory	75
Commanding Officer, Signal Corps Engineering Laboratory, Fort Monmouth	76–77
Commanding Officer, Evans Signal Laboratory	78–79
Commanding General, Army Chemical Center, Chemical and Radiological Laboratory	80–81
Assistant Chief of Staff, G-1	82

NAVY ACTIVITIES

AIR FORCE ACTIVITIES

[redacted]

AEC, Oak Ridge, Tenn., A31943

UNCLASSIFIED